Optimisation of Flow Distribution for Pipe Pullback in Horizontal Directional Drilling

by

J. Saliba

to obtain the degree of Master of Science
at the Delft University of Technology,
to be defended publicly on Thursday 13th June 2019 at 10:00 AM.

Student number:	4627903	
Project duration:	May 25, 2018 – May 14, 2019	
Thesis committee:	Prof. dr. ir. C. Poelma,	TU Delft, supervisor
	Dr. ir. M. J. B. M. Pourquie,	TU Delft, co-supervisor
	Dr. ir. G. H. Keetels,	TU Delft

P&E Report number: 2975

An electronic version of this thesis is available at http://repository.tudelft.nl/.

TU Delft

Acknowledgements

This project would not have been possible without the help of many people.

I would like to thank my supervisors Prof. dr. ir. Christian Poelma and Dr.ir. Mathieu Pourquie for their academic and technical support during the work of this project. Both have been very helpful with their insights into the science and engineering of fluid mechanics and the taming of the wild, rampant, majestic mustang that is OpenFOAM.

I also want to thank Visser & Smit Hanab, especially Ir. Siddarth Rajkumar, for providing me with the help and information needed for this research and of course for the opportunity to work with them.

I thank my family and relatives back home on Gozo for their encouragement throughout these two years of studying at TU Delft.

I thank all my friends at 3ME and at TU Delft for their collaboration and for sharing their knowledge with me.

Finally, I want to express my great gratitude to Eve, for her constant inspiration and motivation during the writing of this thesis and the creation of this booklet.

J. Saliba
Delft, June 2019

Abstract

Horizontal Directional Drilling permits the creation of tunnels which pass beneath rivers and canals to allow the passing of services from one side to the other. The final stage of this process involves lining the tunnel with a plastic or steel pipe. The pipe is pulled inside into the borehole using the same drilling rig that was used to bore the tunnel. For the case of a plastic High Density Polyethylene (HDPE) pipe, issues of buoyancy may arise during this pullback process since the tunnel is pre-filled with drilling mud which now primarily acts as a lubricant. This presents a problem since with this buoyancy, the pipe is lifted up to brush against the tunnel wall, creating issues with the pullback process because of the added pulling resistance. There is the possibility of cutting slots in the pipe wall at the front end of the pipe in order to allow in drilling mud so as to ballast and offset this buoyancy. The drilling fluid is a suspension of bentonite in water and is characterised as a non-Newtonian shear-thinning Herschel-Bulkley fluid, which possesses a finite yield stress.

This study aimed to find whether the current slot proportions used for a given borehole diameter, pipe diameter and pipe thickness are sufficient for allowing in drilling mud to ballast the pipe. This was a case where the multiphase flow given by the interaction of air and drilling mud can be simulated using CFD. OpenFOAM is used for this purpose to first simulate the current practice.

The multiphase solver interFoam together with the non-Newtonian Herschel-Bulkley and air model was validated for a series of cases before the main simulations were run. These validations included the Marsh Funnel test and the Slump test. These are two kinds of workability tests used for cement pastes and drilling muds. Cement pastes and drilling muds are characterized as three-parameter Herschel-Bulkley fluids and the physical setups of the Marsh Funnel and Slump tests were replicated in computational space. The flow time of the Marsh funnel test and the slump diameter from the CFD simulations were compared with experimental data from literature thus validating the model in OpenFOAM.

The main simulation setup recreates the situation of an HDPE pipe concentric with the borehole, with the axis of the domain at an angle to the horizontal. There is drilling mud above the slot at time t = 0s. The drilling mud comes into the domain from the annulus from below the slot. The simulations showed that the flow into the slot initially came in from both the drilling mud above the slot and from the inlet. After the volume of drilling mud above the slot is almost drained completely through into the inner pipe, the mud level inside the pipe starts to become comparable that outside the pipe and both interfaces rise upwards at approximately the same pace.

Subsequently, certain parameters were changed from the first benchmark case in order to see what is the effect of these individual variables. The effects of a lower drilling mud yield stress, a longer pipe slot, lower drilling mud density, a different slot aperture shape, increased flow and a steeper angle of pipe penetration were all tested in the simulation campaign.

The idea is that with better and faster filling, less pipe buoyancy results. An extension of this idea is that the difference between mud levels inside and outside the pipe should be kept to a minimum. That is why the aim is to increase the flow rate through the slot in the pipe.

The results show that increasing the slot length by 30% from the current practice increases the throughput of drilling mud by 10%. The results also show that an elliptical slot profile has a neutral effect and decreasing the yield stress of the drilling mud has a slightly beneficial effect.

Contents

Nomenclature

CFD	Computational fluid dynamics
HDD	Horizontal directional drilling
HDPE	High density Polyethylene
PIMPLE	Pressure-Implicit Method for Pressure Linked Equations
PRCI	Pipeline Research Council International
SIMPLE	Semi-Implicit Method for Pressure Linked Equations
$[]_0$	yield state
$[]_1$	first
$[]_2$	second
$[]_b$	body
$[]_f$	face
$[]_g$	gas
$[]_i$	inner
$[]_l$	liquid
$[]_n$	normal
$[]_o$	outer
$[]_p$	plug
$[]_w$	wall
$[]_{ann}$	annular
$[]_{mod}$	modified
$[]_{plug}$	plug
$[]_{shear}$	shear
δ	stabilization constant
$\dot{\gamma}$	strain rate
γ	phase fraction
κ	diameter ratio
ρ	density
θ	angle
A	area
d	distance

f	force
g	acceleration due to gravity
Hb	Herschel-Bulkley number
K	Consistency index
L	Length
m	inverse flow behaviour index
n	flow behaviour index
p	pressure
Q	flow rate
R	Radius
Re	Reynolds number
T	deviatoric viscous stress tensor
U	velocity
v	velocity
Z	Stability criterion

1 Introduction

1.1. Introduction to Horizontal Directional Drilling

Horizontal Directional Drilling originated from petroleum engineering in the 1970s and formed into its current state by combining with methods utilised in the utilities and water well industries. Horizontal Directional Drilling is now a well-established technology which creates horizontal boreholes underground along a predefined trajectory. Once this borehole is complete, a conduit or pipe is pulled into the bore. This allows utilities to be passed through this pipe. Horizontal Directional Drilling (HDD) is one of several trenchless technologies, which as the name implies, require no excavations to make trenches to route utilities between two points such as two points on each side of a canal, river or motorway. Figure 1.1 shows the primary HDD markets which shows that almost a quarter of all projects are commissioned by telecommunications companies.

HDD projects are classified into three categories according to the diameter of the product pipe used. For Mini-HDD the diameters of the product pipe go up to 0.3m. For Maxi-HDD the range is between 0.6 and 1.5m diameter. Midi-HDD product pipe diameters are between 0.3 and 0.6m. For this study, the diameter of the HDPE pipe is over 0.6m and thus it is classified as Maxi-HDD.

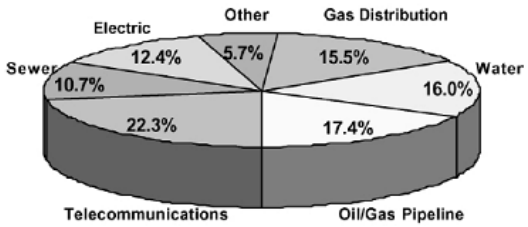

Figure 1.1: Primary Horizontal Directional Drilling markets. Taken from [13].

1.2. Materials involved in Horizontal Directional Drilling

Horizontal Directional Drilling rig machines which carry out these operations provide the thrust or pulling force – depending on the direction of action – for cutting out the borehole. The process consists of three phases: pilot hole drilling, reaming and product pipe pullback as shown in Figure 1.2. The first stage makes the permanent trajectory which the borehole will have. The drill bit enters the ground at an angle of 8° to 18° during the pilot hole drilling stage. During drilling, the drill bit path is directed using methods which employ electromagnetism or optical methods. The subsequent stage of reaming serves to widen the pilot bore to the final diameter. This may be done in more than one pass of the reamer.

All throughout these two operations, drilling fluid (also known as drilling mud), flows out from the drill bit or reamer. This serves to transport the cuttings away from the location of drilling and cool down the drill bit among other secondary functions. Drilling mud is a suspension of a naturally-occurring mixture of clay minerals - called bentonite - in water.

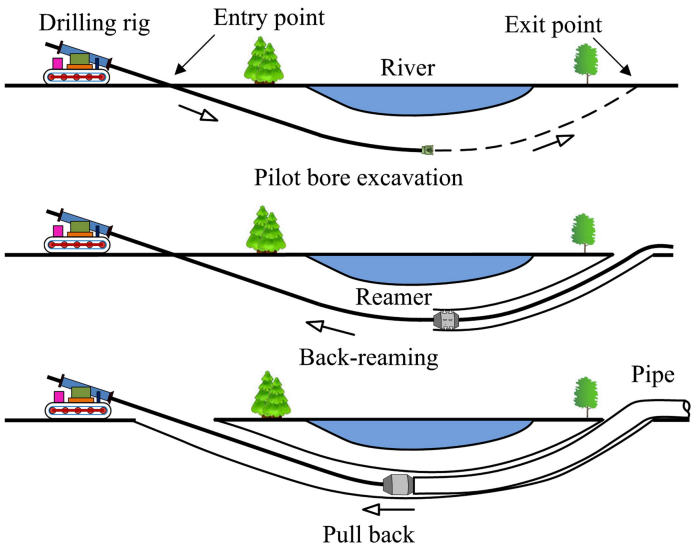

Figure 1.2: Schematic of Horizontal Directional Drilling's three main stages. Taken from [71].

For the final stage of product pipe pullback – known simply as 'pullback' – the traction provided by the drill rig is now used to pull the product pipe into its permanent position, inside the borehole. The product pipe may be made from thermoplastic polymer such as High Density Polyethylene (HDPE) or ductile iron or steel.

1.3. The Pullback Stage and Ballasting

In the final stage of pullback, the conduit or product pipe is pulled into the borehole which is pre-filled with drilling fluid. A pullhead which is connected to the front end of the product pipe serves to connect the pipe to the drill string which will pull the pipe in position. The pullhead itself is connected to a swivel to prevent the transmission of rotation from the drill string to the product pipe. Between the pullhead and the drill string a reamer is also used which ensures that the hole remains open and unobstructed. The reamer also contains a nozzle which delivers more drilling fluid which will replenish the fluid displaced from the progressive immersion of the pulled pipe into the hole. This extra drilling mud comes from the mud pump on the drilling rig side. The mud pump's secondary function is to recycle and polish re-used drilling mud. The pullback stage is complete when the reamer, swivel and pullhead emerge at the drill rig side of the borehole.

The pullback process entails overcoming resistance to motion inside the borehole which is composed of various different components or contributors. The estimation of the total of these resistances thus is crucial for the successful completion of this process. One of these components is the resistance force between the pipe and borehole wall.

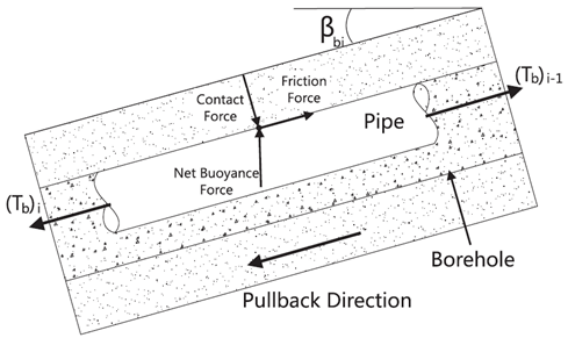

Figure 1.3: Schematic of the force of buoyancy causing the product pipe to brush against the wall of the borehole. Taken from [15].

The cause attributed to the friction between the ground inside the borehole and the product pipe due to contact is the buoyancy force which props up the product pipe against the upper arc of the borehole wall. A schematic of this phenomenon is shown in Figure 1.3. This occurrence is mitigated in practice by means of 'ballasting' whereby the product pipe is filled with water to compensate for this tendency of the pipe to

float and rub against the borehole wall. This ballasting can be done by either filling the pipe from the free end with water or by passively filling it with drilling fluid by allowing it inside the interior of the product pipe. The drilling fluid comes into the pipe from the surrounding space in the borehole. This entry is done through holes in the wall of the product pipe itself at the pulled end, just behind the attached pullhead. For the purposes of this project, this action will be called "passive ballasting". No formal description of this method in literature has yet been found.

There are industry standards such as ASTM F1962 "Standard Guide for Use of Maxi-Horizontal Directional Drilling for Placement of Polyethylene Pipe or Conduit Under Obstacles, Including River Crossings" [9] which provides estimates of the force needed to pull in a product pipe. The estimates predict an increase of the pulling force by 60% if the pipe brushes along the borehole wall for the entirety of its length.

1.4. Problem Definition: Passive Ballasting

The above method of ballasting which allows the drilling mud to flow inside the inner bore is used for product pipes made from HDPE. The method used by drilling contractors in the Netherlands in order to achieve passive ballasting is by welding an additional pipe section of similar wall thickness-to-diameter ratio as the product pipe between the pullhead and the product pipe. This extra pipe section would have slots cut in its wall every 2 feet and be positioned 90° rotationally away from the previous slot. This is to ensure that at least one slot is unconstricted and allows in drilling mud for passive ballasting. An example of this method can be seen in Figure 1.4 taken from an HDD drilling contractor in the Netherlands. An HPDE pipe of an outside diameter of 80cm is comprised of four sections that are welded together. Each section of the new fused pipe has a slot of 38cm length and 9cm width. These sections were welded together in such a way that each centreline of the slot would be at 90° from the ones next to it.

Figure 1.4: Custom made pipe section with slots of length comparable to the inner diameter of the pipe and width comparable to the pipe wall thickness. Slots are circled in red. Picture taken by author in the yard of a Dutch HDD contractor.

Drilling contractors that use this method of passive ballasting also have to keep track of the displaced drilling mud that comes out of the borehole as the pipe is lowered in. They are faced with a problem during this operation. There is a tendency that when too much drilling mud is displaced during the pulling in of the product pipe, it becomes more difficult to pull in the pipe, with the process becoming irregular with several undesirable pauses. This led to the belief that incomplete or at least insufficient passive ballasting action is the cause of these difficulties which arise.

The pressure required to force the drilling mud through the slots is coming from two sources: the hydrostatic pressure head of drilling mud which goes above the slot as the pipe is pulled into the borehole and the flow of replenishing drilling mud which comes from the reamer's nozzle ahead of the pullhead.

If there is any insufficient passive ballasting this could come from incomplete filling of the pipe during the initial phase of the pipe being pulled in the borehole when the pipe is still at an inclination parallel to the borehole. It is during this time that the hydrostatic pressure head above the slot is at a minimum because the slot has still only travelled a comparatively small distance into the borehole.

The aim is to find the timescale of passive filling of the pipe during this initial stage of pullback and thus obtain an indication of the flow rates of drilling mud in through the slot in the pipe. Subsequently we can also increase or decrease any of the most easily changeable factors in the pullback operation to see whether there can be room for improvement of the current practice.

With the availability of Computational fluid dynamics (CFD) one can explore the phenomena occurring during pullback with the same rigour as in physical testing and experiments. One can better understand the effect of various parameters on the physics of the drilling mud entering the pipe slot without constructing any test rigs. In this particular case, this would be challenging given the restrictions imposed by simultaneous tunneling and fluid rheology.

The objectives of this study are:

1. To set up a simulation using Computational Fluid Dynamics (CFD) which captures the most relevant geometry and rheology of the initial moments of pullback - the entry stage with the pipe inclined at an angle to the horizontal.
2. To obtain a quantitative measure of the timescale of filling of the pipe by passive ballasting.
3. To determine if there are any parameters or variables which allow any room for optimisation and also can be easily changed from the current practice to improve the pullback performance.

1.5. CFD with OpenFOAM

OpenFOAM was used extensively as a CFD tool in this study. OpenFOAM (Open source Field Operation And Manipulation) is an open source software package (written in the programming language C++) developed by Henry Weller that lends itself particularly well to solving (differential) comparisons in simulations of physical processes related to: fluid dynamics, combustion processes, tensors, rheology, thermodynamics, turbulence models, chemical kinetics and heat radiation [53].

1.6. Methodology

To investigate the behaviour of the drilling mud as it enters the slot, a literature survey is first needed to establish which parameters are relevant to this study.

The literature survey also served to determine the geometry and proportions of the solid walls involved in pipe pullback and the rheological characteristics of the drilling mud. Furthermore since this thesis includes the use of CFD, part of the literature survey addressed physical tests and experiments from civil engineering literature and also the numerical methods used in OpenFOAM by the solver `interFoam`.

Literature about physical tests on multiphase air and Herschel-Bulkley fluid flows were needed so that these can be replicated in CFD to validate the multiphase flows also present in the main simulation campaign.

During the validation stage, CFD simulations which aimed to replicate either the flow times or slump diameters of cement pastes.

After the validation phase a deeper understanding of OpenFOAM's implementation of the multiphase solver `interFoam` coupled with OpenFOAM's native Herschel-Bulkley fluid model was achieved.

The next phase of the main simulation campaign required decisions to be made regarding how the computational domain is going to be set up. This meant deciding which rheological parameters the standard drilling mud is going to possess and the domain geometry which can capture best the phenomena during the first few seconds of pipe pullback.

The first main simulation aimed to replicate a typical pullback condition where the pullhead and pipe are still concentric with the borehole and drilling mud is being pumped from ahead of the swivel. The borehole is pre-filled with drilling mud. This first main simulation is taken to be the benchmark and subsequent simulations will have a single parameter changed in order to see what its effect on the inner pipe filling time is. These parameters included the angle of entry, the yield stress of the drilling mud, the length of the slot, the density of the drilling mud and the shape of the aperture of the slot.

Finally the results from every simulation are compared to determine the effect of the changed parameters on the pipe filling time.

1.7. Report Structure

Chapter 2 will give a literature survey of all the relevant topics to this project: the rheology of drilling muds; the methods available for simulating non-Newtonian multiphase fluid mechanics; the physical tests and ex-

periments available from other studies to be used as validation cases and past studies into using CFD for investigating pipe pullback in HDD. Chapter 3 will present the results of the validation tests carried out before the main simulations. Chapter 4 will outline the modelling methods and the simulation setup used for this study. Chapter 5 will present the results and a discussion about their interpretation. Chapter 6 will give some conclusions and recommendations for future work. Finally appendices are available to detail the files used in OpenFOAM for the main simulations used for this study.

2

Literature Review

Horizontal Directional Drilling as a complete operation has been thus far studied mostly from the perspective of petroleum engineering applications because of the initial drilling stage aspect. For the scope of this study, specifically for the final operation of pipe pullback, the focus of previous research was oriented towards upgrading and obtaining better understandings of the estimate of the pipe pullback force loads required. This is only partially related to passive ballasting. There are currently no references to any action similar to passive ballasting or its performance in literature.

The literature reviewed for this project served to establish what are the conditions found in HDD pullback conditions; the characteristics of the materials used - mainly the drilling fluid; and for the fluid dynamics simulations in OpenFOAM - the finite volume methods and solvers available for use and their mechanics.

2.1. HDD Pullback Conditions

The conditions during pipe pullback from a practical perspective relate to the geometrical, kinematic and rheological parameters found during the operation. There are three aspects which are the most relevant to this study as they will provide the initial and boundary conditions of the simulations.

Najafi [49] suggests that entry angle with which the pipe descends into the ground should be between 8° and 20° to the horizontal. The exit angle on the other hand should be less than 10°.

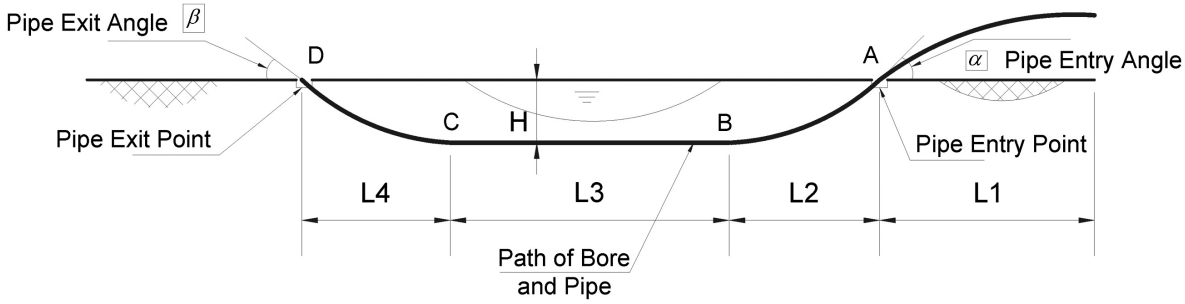

Figure 2.1: Typical HDD installation bore geometry. Taken from ASTM F1962-11 [9].

With regards to the pullback rate, in the two on-field cases recorded by Rabiei et al. [59], the pullback rate was 12cm/s for two cases where the borehole diameters were around 0.8m and 1.2m.

Different sources such as Polak and Lasheen [57], Faghih et al. [30], Rabiei et al. [58] and Shu et al. [66] suggest that the pipe diameter should be 66% of the swivel reamer diameter which is ahead of the pipe.

The studies by Polak and Chu [56] and Cheng and Polak [22] and also Baumert and Allouche [15] and Baumert et al. [16] aimed to provide a deeper understanding of the mechanics of the resistance experienced by the rig during pipe pullback. They aimed to pursue the characterization of the pulling force needed as being due to seven components: (1) Weight friction between pipe and ground; (2) Weight friction between pipe and borehole; (3) Pipe weight and buoyancy; (4) Fluid drag friction; (5) Friction at the tunnel bend; (6) Friction due to the pipe's stiffness; (7) Resistances exerted on drilling string. This is a very detailed analysis of the total resistance force due to pullback and the aims of these studies is also always to compare their detailed

analysis to a more simplistic and conservative calculation procedure offered by the Pipeline Research Council International (PRCI) [43], NEN 3650 [4] and ASTM F 1962 [9]. The latest review by Cai et al. [21] concluded that the pullback force required for an HDPE pipe is overestimated by all three standards. The conclusion was that the fluid drag component accounts for 6% of the total resistance. The contribution of the friction caused by buoyancy was included in the major fraction of 79% that also includes the friction at the tunnel bend, but there is no mention of the specific fraction of the buoyancy's contribution to this proportion. Therefore, the contribution by friction due to the buoyancy is assumed to be appreciable.

In spite of this, analyses into the fluidic drag component of the resistance were relevant to this project because they are the only studies which looked into how the drilling fluid behaves inside the annulus region in the volume between the outside pipe and the ground wall of the borehole. They also provided more details into other relevant parameters like angle of inclination and the relative velocity of the pipe to the borehole wall.

The study of the fluid drag experienced by the pipe during pullback by Faghih et al. [30] and Rabiei et al. [58] and Shu et al. [66] reveals the changes in the direction of the flow of the drilling fluid as the pipe moves through the borehole. The fluid discharges from the reamer and will fill and surround the borehole and will either come out of the entry point or the exit point of the drill string at the topsoil surface, whichever path presents the least resistance. This is shown in Figure 2.2. What is shown in this figure is also the predominant drilling mud velocity profile at each stage of the pullback.

The work by Rabiei et al. [60] tries to establish the hydrokinetic pressure and fluid drag changes during pipe pullback by using the finite volume method. While the study concluded that indeed the PRCI methods for pullback overestimate the fluid drag component and the hydrokinetic pressure, it also showed that the rheological characterization model for the drilling fluid also is of importance.

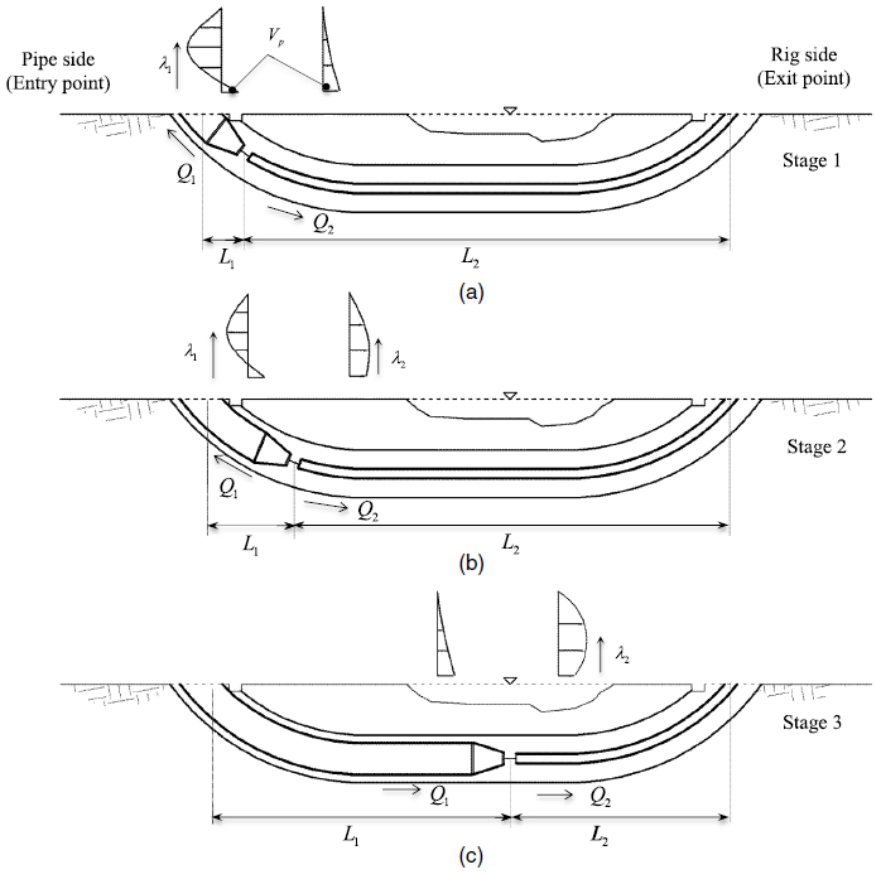

Figure 2.2: The splitting of the drilling fluid flow into two directions and the trend towards flow direction preference as the pullhead moves through the borehole during pullback. Rabiei et al. [61]]

2.2. The Drilling Fluid as a Non-Newtonian Fluid

Non-Newtonian fluids are liquids which do not follow Newton's law of viscosity. Newtonian fluids exhibit a shearing stress linearly proportional to the subjected rate of shearing strain. This law describes the constitutive equation of the liquid and thus the property of viscosity. In the case of a non-Newtonian liquid, the shearing stress does not display a linear relationship with shearing strain rate. An introduction to the concept of non-Newtonian fluid dynamics in industrial engineering applications is given in Chhabra and Richardson [23].

Non-Newtonian liquids' apparent viscosity might increase with strain rate as with shear thickening or dilatant liquids or alternatively decrease as with shear thinning liquids also called pseudoplastics. Both shear thinning and thickening fluids start shearing upon an imposed stress even if infinitesimally small, yet there is another class of liquids which are Bingham plastics which require a finite shear stress before they start shearing. Upon increasing the stress the shearing rate will increase linearly with the stress. Herschel-Bulkley fluids which are also called yield pseudoplastic fluids display shear thinning with increase in stress as described in the paper by Herschel and Bulkley [41].

The drilling fluid or mud used in civil and petroleum engineering applications has been mostly characterised in research as a Herschel-Bulkley fluid as detailed in Hemphill et al. [40]. The one-dimensional equation for the shear stress τ for a Herschel-Bulkley fluid is given by:

$$\tau = \tau_0 + K\dot{\gamma}^n \tag{2.1}$$

Where, τ_0 is the yield stress, K is the fluid consistency index, $\dot{\gamma}$ is the shearing rate and n is the fluid behaviour index. The latter is less than 1 since the drilling mud is a shear-thinning liquid.

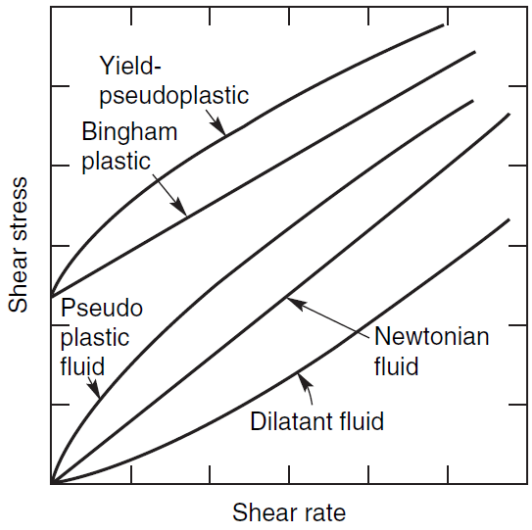

Figure 2.3: Newtonian and Non-Newtonian fluids. Herschel-Bulkley fluids are also called yield pseudoplastic fluids. Taken from Chhabra and Richardson [23]

The drilling fluid or mud used in HDD applications is a suspension of water and bentonite by 5 to 10% by weight of the latter component.

Bentonite is a type of clay known as montmorillonite that swells in volume with the addition of water. The type used in drilling applications is sodium bentonite as opposed to calcium bentonite. Certain projects for HDD require the addition of polymers to the bentonite suspension so that it can increase the fluid consistency index and yield stress in order to achieve better borehole structural stability, increased transport of drill cuttings and also cutting settling retardation [49].

Bentonite suspensions also exhibit thixotropic behaviour, where the rheological characteristics of the fluid consistency index and the fluid behaviour index become time-dependent [17]. For the scope of this study, the time scales for any appreciable change in the rheology were taken to be greater than the time scales which relate to the transport of drilling fluid and therefore the effect of thixotropy was taken to be minimal.

Talmon and Huisman [68] conducted a study to investigate the falling velocity of particles in a drilling fluid. The secondary aspect of this study which was used was the range of values for the three rheological parameters of τ_0, K and n given for various samples of drilling fluids for various mass concentrations of ben-

tonite. This provided the information needed to assess what a typical drilling mud suspension's rheological parameters are if characterized as a yield pseudoplastic for a particular mass concentration of bentonite. These parameters could later be used as constants in the fluid flow simulations.

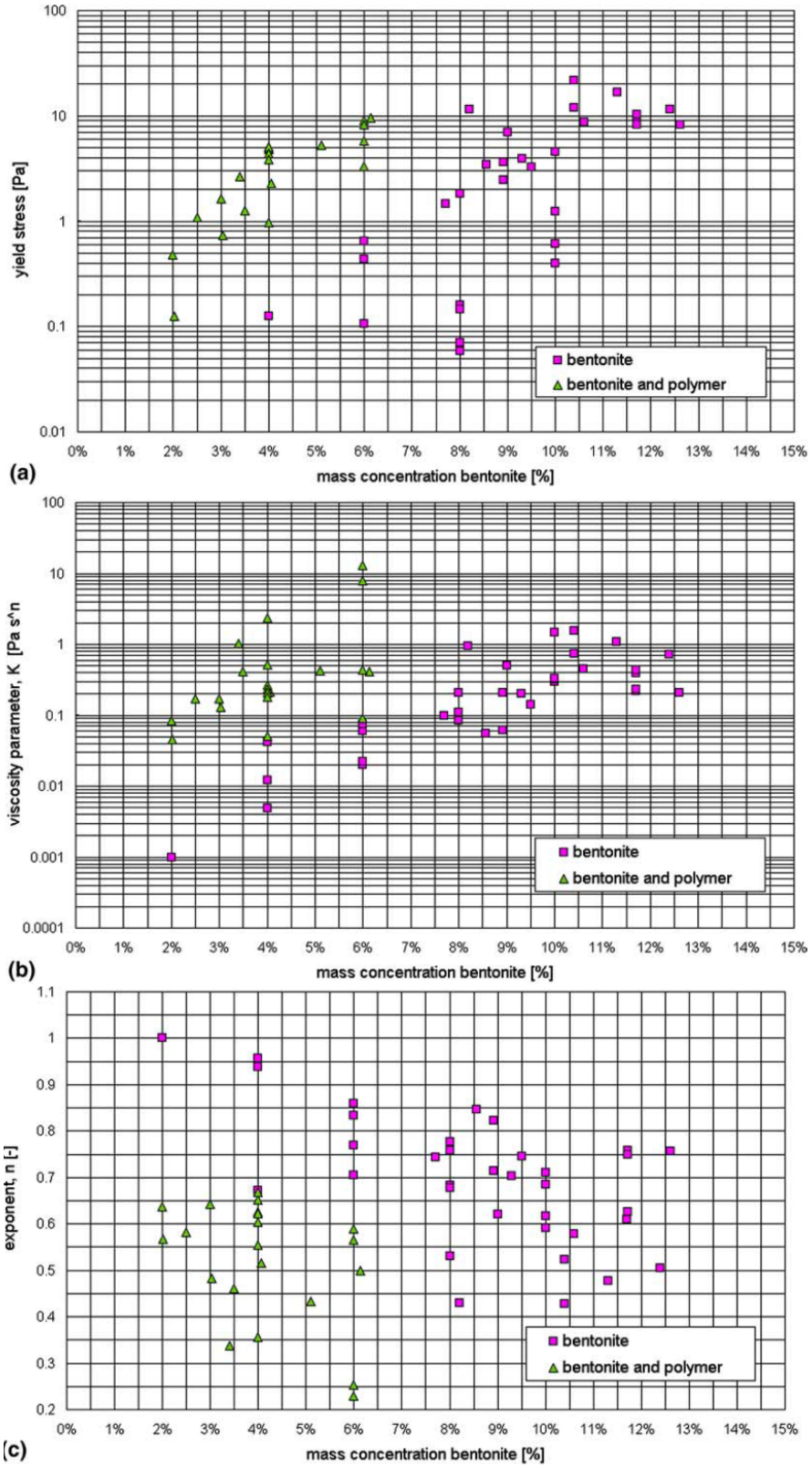

Figure 2.4: Compilation of numerical values of the three Herschel-Bulkley parameters of bentonite drilling fluids from Talmon and Huisman [68]

2.2.1. Herschel-Bulkley Fluid Pipe Flow and Annulus Flow

The simplest configuration for internal flow for a non-Newtonian fluid is that of a laminar Hagen-Poiseuille flow case, where the applied pressure gradient drives the flow through the pipe. In the case of a Herschel-Bulkley fluid the possibility could arise where even though the fluid is moving though the duct, there is a region of unsheared, unyielded fluid which moves along the axis of the duct as a plug.

In literature there is also mentioned the use of a 'Herschel-Bulkley number' or 'yield number' in order to describe the relative importance of yield stress on the plug formation balanced against the sheared flow region [51],[70]. This would be reflected in the ratio between the diameter of the unsheared plug and the total duct diameter. In general the Herschel-Bulkley number is given by the following:

$$Hb = \frac{\tau_0}{K} \frac{1}{(du/dy)^n} \tag{2.2}$$

The shearing rate can be approximated by (U/R) for the case of a cylindrical duct and thus the expression can be of the form:

$$Hb = \frac{\tau_0}{K} \frac{R^n}{U_0^n} \tag{2.3}$$

Since the flow of drilling fluid which comes out from the reamer flows in the space between the two cylindrical walls of the borehole and the outer surface of the pipe this can be considered to be an annulus flow. In reality this configuration may be for the most part with the axes of cylinders will not be aligned and thus there is eccentricity in the annulus. For the case of a horizontal annulus flow where the axes are concentric, there is once again the possibility that if the influence of the sheared region is sufficiently low, there can be a ring-shaped annulus of unsheared drilling fluid in the duct moving at constant velocity which would be also the maximum velocity in the cross-section. In that case the Herschel-Bulkley number takes the form of:

$$Hb = \frac{\tau_0}{K} \frac{(R_2 - R_1)^n}{U_0^n} \tag{2.4}$$

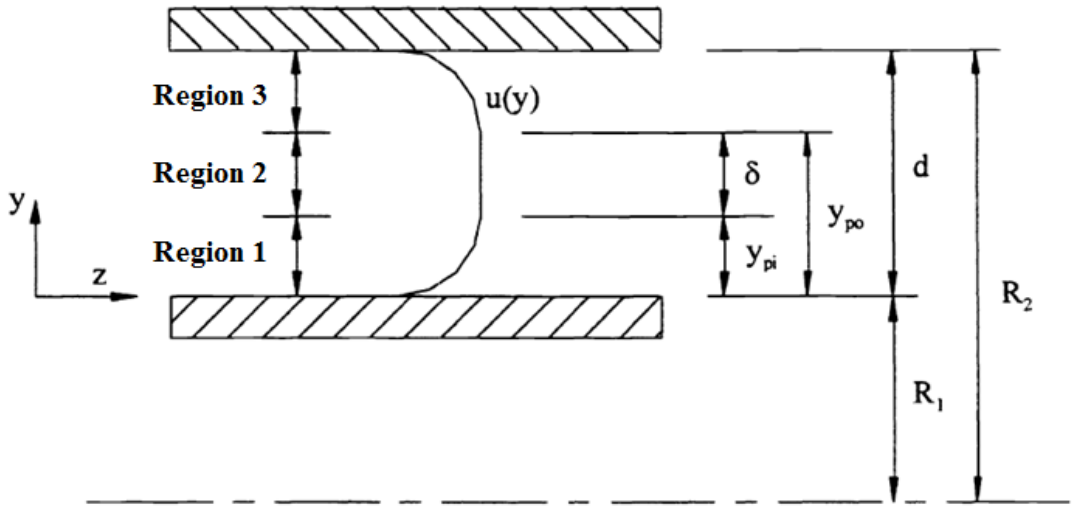

Figure 2.5: Typical velocity profile through a concentric annulus duct in the presence of a linear pressure gradient. Taken from [70]

For the case of a central plug flowing between the annulus' walls, the duct is separated into three regions: (1) the lower sheared region touching the inner wall, (2) the plug region and (3) the upper yielded region touching the outer annulus wall. This is shown schematically in Figure 2.5. The velocity profiles inside the annulus for each of the 3 regions are respectively given by:

$$u_1(y) = \frac{n}{n+1}\Big(-\frac{\Delta P}{KL}\Big)^{\frac{1}{n}}\Big[\Big(\frac{d-\delta}{2}\Big)^{\frac{n+1}{n}} - \Big(\frac{d-\delta}{2} - y\Big)^{\frac{n+1}{n}}\Big] \tag{2.5}$$

$$u_2(y) = \frac{n}{n+1}\Big(-\frac{\Delta P}{KL}\Big)^{\frac{1}{n}}\Big(\frac{d-\delta}{2}\Big)^{\frac{n+1}{n}} \tag{2.6}$$

$$u_3(y) = \frac{n}{n+1}\Big(-\frac{\Delta P}{KL}\Big)^{\frac{1}{n}}\Big[\Big(\frac{d-\delta}{2}\Big)^{\frac{n+1}{n}} - \Big(y - \frac{d+\delta}{2}\Big)^{\frac{n+1}{n}}\Big] \tag{2.7}$$

These profiles are equivalent to the case of Hagen-Poiseuille flow between two parallel plates, also called a rectangular slot. The requirement for a high degree of accuracy for which a parallel plate velocity profile represents an annulus velocity profile would be that the ratio between the inner and outer radius of the annulus, R_1/R_2 be greater than 0.3 [19].

2.2.2. Laminar and Turbulent Flow of Herschel-Bulkley Fluid

As with all fluids, the regime of the flow depends on the relative influence of the viscous and the inertial forces at play. For Newtonian fluid flows, the relative importance of these forces is embodied in the Reynolds number. For pipe flow the consensus is that laminar flow in cylindrical pipes ceases at a Reynolds number of 2100 which is the critical Reynolds number. For time-independent fluids this critical number changes depending on type and extent of non-Newtonian behaviour. Slatter [67] elaborated on the laminar-turbulent transition of Herschel-Bulkley fluids by working on mineral slurries in pipes. The author builds his case on the fact that the viscous and inertial influences in the fluid are determined only by the region of the fluid which is subjected to shearing deformation and thus omitted that region of the volumetric flow rate which is associated to the unyielded plug of material at the centre of the duct. This lead to the formulation of a modified Reynolds number [67], [23]:

$$Re_{mod} = \frac{8\rho V_{ann}^2}{\tau_0 + K\Big(\frac{8V_{ann}}{D_{shear}}\Big)^n} \tag{2.8}$$

where

$$V_{ann} = \frac{Q - Q_{plug}}{\pi(R^2 - R_p^2)} \tag{2.9}$$

and

$$D_{shear} = 2(R - R_p) \tag{2.10}$$

Even for a Herschel-Bulkley fluid laminar conditions end at $Re_{mod} = 2100$ [23]. The yield stress and flow behaviour index n have an increasingly greater role in affecting the onset of the transition point which becomes ever more delayed. This is because these parameters have a stabilizing effect [33], [34].

The transition to turbulent flow for a Herschel-Bulkley fluid in an annulus with concentric cylinders has been the subject of a few studies. Desouky [26] were the first to propose a model for the transition to turbulence for Herschel-Bulkley fluids in a pipe. The concept was extended to annular geometry.

Founargiotakis et al. [32] and Kelessidis et al. [46] used parameteric correlations to predict the friction factors for a given Reynolds number for laminar, transitional and turbulent regimes for annulus flow of Herschel-Bulkley fluids.

Ryan and Johnson [65] presents a dimensionless stability parameter which is the ratio of the turbulent energy production to the rate of work done by the viscous stresses. This is for normal cylindrical pipe flow. They claim for a Newtonian fluid, transition starts when this parameter reaches a value of 808. This parameter is defined as:

$$Z = \left|\frac{R\rho V}{\tau_w}\frac{\partial V}{\partial r}\right| \tag{2.11}$$

where R is the pipe radius, V the mean axial fluid velocity and τ_w the wall shear stress.

In the same vein, Hanks [38] presented a stability criterion for concentric annuli. At 404 the transition to turbulence occurs. This value is claimed to also be true for non-Newtonian fluids in Hanks [38] but Gucuyener and Mehmetoglu [36] said that this is not the case for yield stress fluids. The form of Hanks [38] criterion was:

$$K = \left| \frac{\rho V \times w}{\nabla \cdot T} \right| \tag{2.12}$$

where K is the stability criterion, w is the vorticity vector $\nabla \times v$. T is the deviatoric stress tensor. Erge et al. [28] modified the stability criterion of Ryan and Johnson [65] to concentric and eccentric annulus flow. The experiments they conducted involved using a long annular test section and a wide range of flow rates. Laponite was used as a Herschel-Bulkley fluid in this study. Their own version of this modified stability criterion was now given by:

$$Z = \left| \frac{R_H \rho V}{\tau_w} \frac{\partial V}{\partial r} \right| \tag{2.13}$$

where

$$R_H = R_o - R_i \tag{2.14}$$

The Reynolds number was defined as:

$$Re = \frac{12 \rho V^2}{\tau_W} \tag{2.15}$$

As found in Ahmed and Miska 2009 [6].
Erge et al. [28] also made use of the yield or Herschel-Bulkley number. In this case it was given by:

$$Hb = \frac{\tau_0}{\tau_w} \tag{2.16}$$

Erge et al. [28] worked to find out various relations including that between the flow behaviour index n and the critical Reynolds number. As shown in Figure 2.6, the critical Reynolds number is between 2500 and 3000. This applies for a concentric annulus, where the diameter ratio is between 0.5 and 0.7 - which is what would be found for Maxi-HDD.

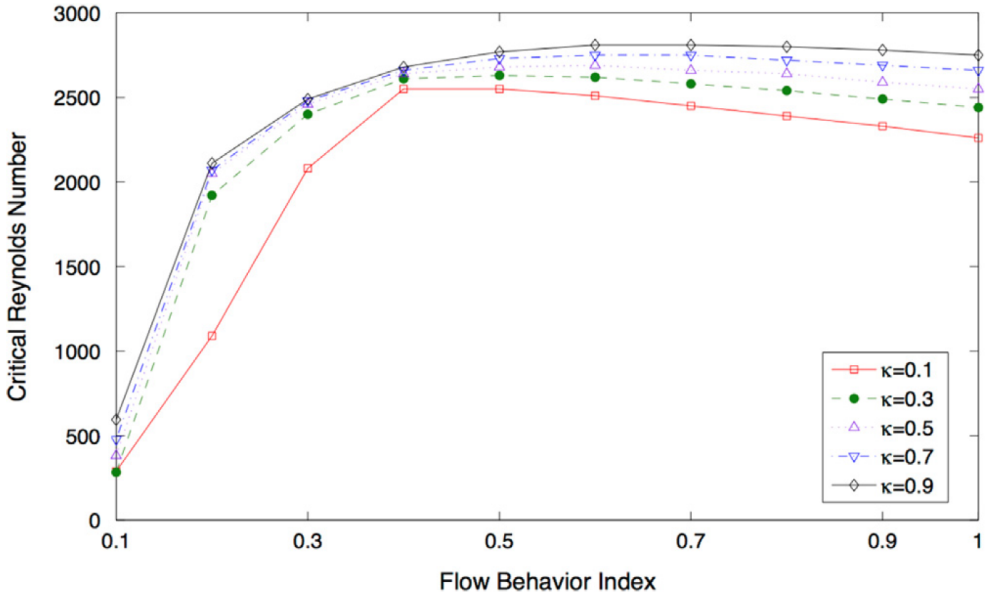

Figure 2.6: The variation of the critical Reynolds number for increasing flow behaviour index n. The results are shown for various diameter ratios, κ. Taken from Erge et al. [28].

2.3. Physical Tests and Numerical Simulations

There is a wide range of experimental data related to the flow of Herschel-Bulkley liquids. The types of experiments which were relevant for this study involved internal flows with no free surface and free surface flows where the case can be considered as a multiphase flow with the two phases being the non-Newtonian liquid and air. The measurements from the considered experimental studies were used to validate the finite volume method for Herschel-Bulkley fluid multiphase flow before running the main simulations. The method used

predominantly for these simulations is the Volume of Fluid method which will be introduced later on in this chapter.

There have also been several numerical simulation studies which attempted to predict the behaviour of liquids treated as Herschel-Bulkley fluids which are not only limited to drilling fluids but also certain cement pastes, concrete and water suspensions of clay materials such as kaolinite.

In the case of fresh cement suspensions, the approach to validate the numerical model implemented to predict the behaviour of the fluid has been the same as this study. Cremonesi et al. [25], Bouvet et al. [20] and Ferrara et al. [31] all modelled the cement paste as a non-Newtonian fluid and tried to use standard and established industrial consistency tests to validate their simulations. These consistency tests come in the form of the Marsh Funnel test and the slump test. All three studies used both of these tests for comparison with the results from the simulations however the rheological model implemented in their case was the Bingham Plastic model. Referring to Figure 2.7 we can see the work done by [25] in simulating the flow through a Marsh funnel. The paste was modelled as a Bingham Plastic which is equivalent to a Herschel-Bulkley fluid with a flow behaviour index n of 1. The darker regions in the computational domain shown indicate the unyielded regions of the fluid.

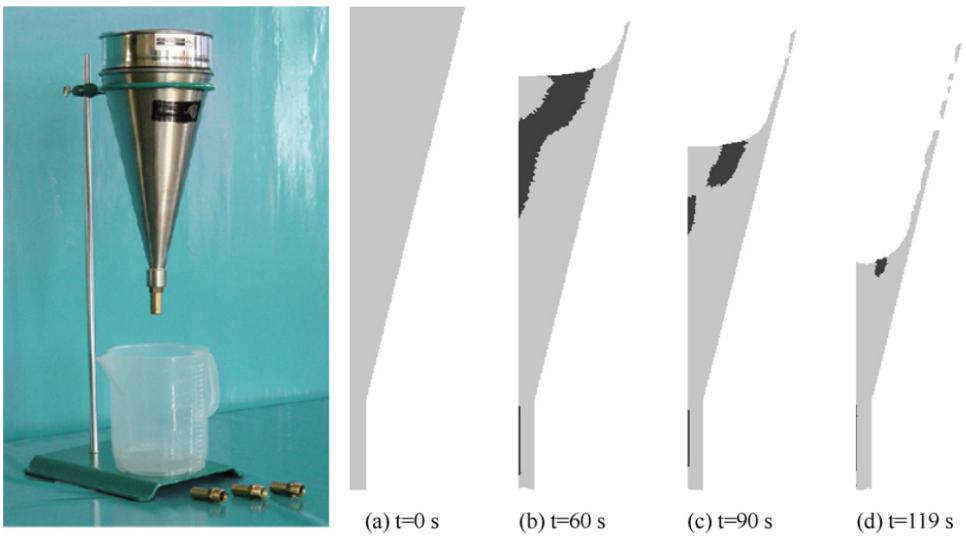

Figure 2.7: (Left) The Marsh Funnel test setup with standard funnel and graduated container underneath. (Right) The corresponding CFD multiphase flow simulation carried out by Cremonesi et al. [25] in order to validate the rheological model. The fluid was modelled asa Bingham Plastic. The darker regions of the figure on the right indicate the unyielded regions.

2.3.1. Pipe Flow

There have been numerous studies about the Hagen-Poiseuille flow of non-Newtonian liquids in cylindrical ducts such as Escudier and Presti [29] and Park et al. [54]. Benslimane et al. [18] in particular studied the laminar, transitional and turbulent pipe flow of bentonite suspensions which were used as drilling fluids. One key result is the mean axial velocity profile plot for the laminar regime. The four parameters of density, yield stress, flow behaviour index and consistency index taken from this study were used for the preliminary validation test for a Hagen-Poiseuille flow finite volume method simulation for a steady flow case. The results from this study can be seen in Figure 2.8.

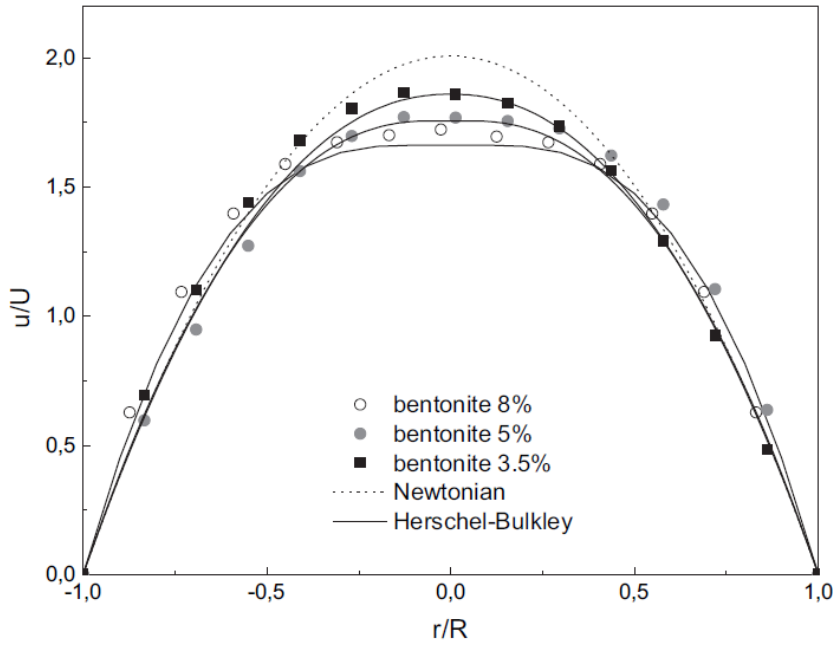

Figure 2.8: Mean axial laminar velocity profiles of drilling fluid flowing through a round duct. The velocity is nomalized with the maximum plug velocity and the radial distance is non-dimensionalised. Taken from Benslimane et al. [18]

2.3.2. Marsh Funnel tests

The Marsh Funnel test is a standard effective viscosity test for drilling fluid used on the project site. One quart or litre of drilling mud is poured in the funnel and the time for all the fluid to come out is timed. The industrial standards which describe the measurement procedure for a drilling fluid and the dimensions of the Marsh funnel are DIN 4127 [10] and also the API RP 13B-1 [5].

For the case of cement pastes and grouts, the standards EN 445 NF P18-358 [3] or EN 445 NF P18-507 [3] are used depending on the mineral admixture of the concrete. There have been studies that sought to predict the flow times of a given fluid characterized as a Herschel-Bulkley liquid by using the above mentioned standards as a basis for the analysis. This was done either through finite volume method simulations or through analytical techniques. In that way, if predicted flow times are very close to the physical reality, then that would mean that the fluid can be characterized better in terms of yield stress, consistency index and flow behaviour index by using just the simple Marsh Funnel as an instrument instead of a rheometer. Guria et al. [37] and Balhoff et al. [14] consider mostly an analytical approach to correlate the three Herschel-Bulkley parameters to the drilling fluid flowing out of the funnel and the time it takes to do so.

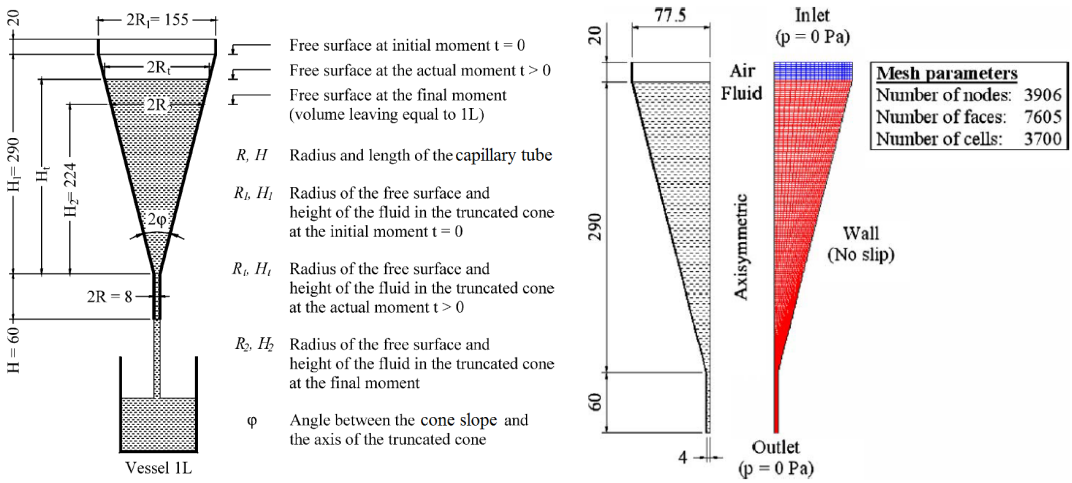

Figure 2.9: (Left) The geometry and dimensions of the Marsh Funnel used by Nguyen et al. [50] in their CFD simulations. (Right) The mesh used for the computational domain for the simulations

Nguyen et al. [50] sought to use numerical finite volume simulations with the Volume of Fluid method to predict the flow time for a given cement grout. The Marsh cone is modelled as an axisymmetric body with cylindrical coordinates. The cement grout and the air above are the two interacting yet immiscible phases present in the funnel. For each phase, the volume fraction is treated as a local variable and is calculated for every finite cell volume. As the volume fractions of each phase change with position and time, the free surface interface starts coming down and moves away from its initial position. At the same time as this is occurring, the liquid is leaving the domain through the outlet in the simulation just as one would expect in reality. The interface is marked by a thin region of cells which possess volume fraction of 0.5. A schematic with the dimensions of the Marsh Funnel and the mesh used for the simulations by Nguyen et al. [50] is shown in Figure 2.9.

Nguyen et al. [50] carried out this analysis using Fluent 6.1 and made use of the Herschel-Bulkley rheological model within Fluent which is encapsulated in the following bi-viscosity model:

$$\mu = \begin{cases} \mu_0 & \dot{\gamma} \leq \dot{\gamma}_0 \\ \frac{\tau_0 + K[\dot{\gamma}^n - (\tau_0/\mu_0)^n)]}{\dot{\gamma}} & \dot{\gamma} > \dot{\gamma}_0 \end{cases} \tag{2.17}$$

This bi-viscosity scheme is needed to ensure that at very low shear rates the viscosity does not increase by several magnitudes leading to numerical stability issues. Thus at a critical shear rate, the fluid is treated as a Newtonian fluid with a very high viscosity and the shear stress would still be very close to just off from the yield point value. A schematic of this is shown in Figure 2.10. This is the same approach used by OpenFOAM to treat the Herschel-Bulkley fluid model and is explained further at the end of this chapter.

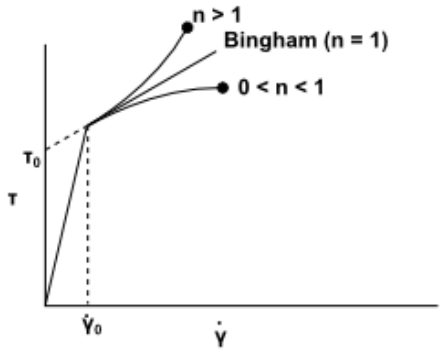

Figure 2.10: The bi-viscosity model used for the numerical simulations for Herschel-Bulkley fluids within the FLUENT CFD software. For low shearing rates, the scheme shifts to a Newtonian model. Taken from ANSYS [12]

The authors observed that after an initial brief transitory period the flow rate decreases linearly with time and therefore did not simulate for the entire time needed for one litre of the cement grout to flow out.

The authors also compared the simulated flow times with cement grouts of increasing cement content by weight. Rheometer measurements showed that as could be expected, an increase in water content decreased the yield stress, the density, and the consistency index and flow time required. With this approach the authors still had to add some systematic corrections to their simulations' flow times in order to improve the deviation from the physical flow times which differed by over 15%. This is why the authors describe their approach as "semi-analytical".

2.3.3. Slump tests

Another type of flow test which is used to test for the workability of a fluid is the slump test. It is used to assess the consistency quality of concrete or cement pastes, grouts and mortars. The test is carried out using a slump cone in the shape of a conical frustum which is open at both ends. The frustum is placed on a flat, level, smooth and impermeable surface and it is filled to the rim with the concrete mixture. The frustum is then lifted up in one rapid smooth movement and the final resting diameter of the slump of the concrete is measured. There are various variations of this test across different standards such as the ASTM C 143 [8] and the BS EN 12350-2 [7]. The final slump diameter is related to the yield stress of the tested fluid and as reported by Roussel and Roy [64], various authors have tried both analytical and numerical approaches to correlate the yield stress to the final diameter of the slump. Figure 2.11 shows an example from literature where the spread of a cement paste is measured after being released from an open conical frustum.

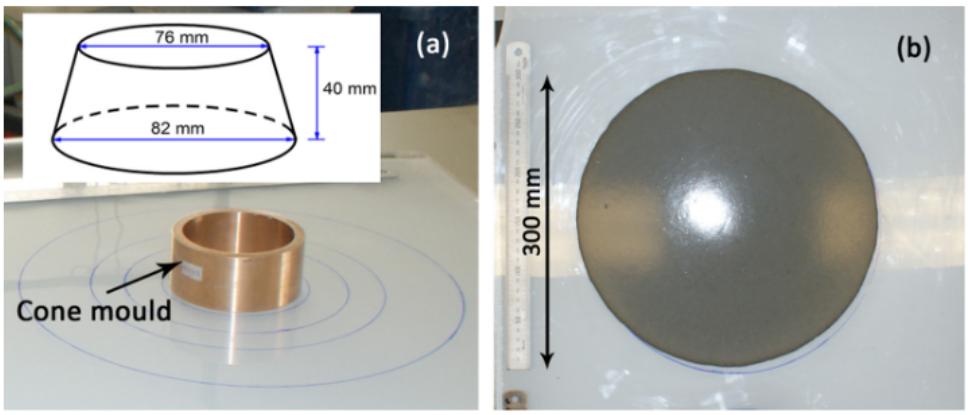

Figure 2.11: The mini-slump test. Rigid hollow frustum is filled with the tested fluid. The frustum is then lifted rapidly to allow fluid to spread. The final diameter of the spread of the fluid is measured. Taken from Lin et al. [47]

In the case of cement grouts and mortars the mini-slump cone is used. This mini-slump cone method was developed by Wedding and Kantro [69] and as such is not standardized as a procedure by any organization, but the proportions of the truncated cone have been adopted in many studies including Jayasree and Gettu [44]. The replication of the behaviour observed in the slump test has been the focus of the research of some studies which used numerical simulations in order to predict the final resting diameter and slump height. The studies mentioned above [25],[20],[31] make use of the finite volume method and the volume of fluid method to predict the final slump diameter. Figure 2.12 shows the work of Cremonesi et al. [25]. The column of cement paste is unyielded at time t = 0s. Then the column slumps to reach the final diameter at 0.22m, with all the cement reaching the yield stress of the paste again as with the initial condition. A half the time taken for the slump to reach its final diameter, the uppermost regions of the slump had already reattained the unyielded state since their shearing was low.

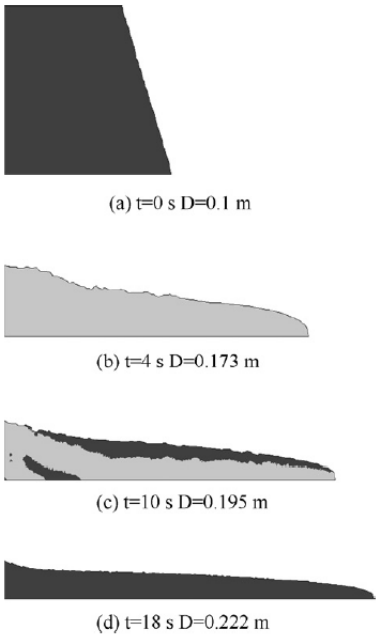

Figure 2.12: The simulated spread of a cement spread taken from [25]. The dark regions are unyielded regions. The paste was modelled as a Bingham plastic in this case.

Jayasree and Gettu [44] also implemented the Marsh funnel and Wedding and Kantro [69] slump test to assess the effect of plasticizers on cement pastes. The pastes were characterized as Herschel-Bulkley fluids with shear-thinning behaviour. Thus the experimental data for final slump diameters were used for validating the Herschel-Bulkley constitutive equation model for OpenFOAM coupled with the multiphase solver for this study.

2.3.4. Surface Tension

Up till now for the above mentioned examples of spreading flows, the assumption was that interfacial effects were treated as insignificant and the viscous effects were much more dominant. In his review paper Coussot [24] states that one reason for the fact that viscous effects are invariably taken to be dominant in yield stress flows is because we do not have decisive insight about the effective surface tension of these fluids.

For the case of suspensions it has been suggested by Roussel et al. [63] that the surface tension is simply the same as that of the interstitial fluid. The same author admits however that this argument may not hold when the components of the liquid layer along the fluid interface are unknown as what would happen with concentrated pastes.

2.3.5. Annulus Flow

Experimental data and numerical simulations found in literature pertaining to annulus flow sought to investigate the effects of eccentricity, thermal convection and the rotation of the inner cylinder since these are all effects which are found in drilling applications. Annulus flows were not used for model validation for this project but a few important points can be taken from the work of Nouar and Lebouche [52]. The authors use numerical methods to solve the continuity, momentum and energy equations for a given three-parameter Herschel-Bulkley fluid. Using the inverse of the flow behaviour index and another two non-dimensional parameters namely the relative dimension of the plug core ap and the Herschel-Bulkley number Hb the design chart below was generated which can be used for the computation of the relative dimension of the plug core.

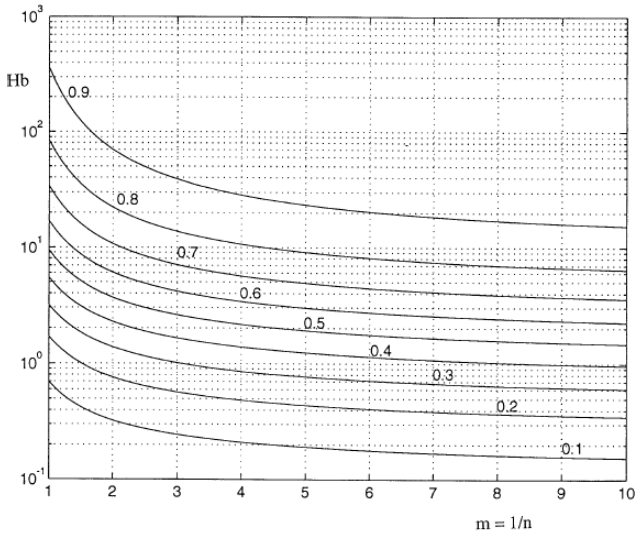

Figure 2.13: Plot of Herschel-Bulkley number against the inverse of the flow behaviour index. The numbered lines are for a given plug core relative dimension. Taken from Nouar and Lebouche [52].

What can be seen from the design chart above in Figure 2.13 is that with a relatively high value of flow behaviour index n of 0.7 as found with drilling fluids, and low flow velocities the relative plug core and thus the unsheared, unyielded region within the annulus pipe can occupy 90% of the span of the annulus.

2.4. Numerical Methods in OpenFOAM

The OpenFOAM solver used for the entirety of this study was `interFoam`, which is an incompressible, isothermal, two-phase flow solver which uses a modified version of the Volume of Fluid approach which in turn was initially proposed by Hirt and Nichols [42].

2.5. Volume of Fluid Methods

The filling process of the annulus volume in the borehole and the inner volume of the HDPE pipe is a case of a variable mass flow with a moving free surface interface. Moving boundary problems can be tackled by either Lagrangian or Eulerian algorithms depending on the reference frame selected.

Eulerian methods emphasise on points in space and the coordinate system pertaining to the fluid domain is fixed. Eulerian algorithms are robust and utilize a fixed mesh system. Fixed mesh methods in turn include

surface tracking methods, volume tracking methods and level set methods. These methods all need to utilize a so called flag variable which could be the volume fraction or the level set fraction. The volume fraction is the proportion of the finite volume cell's capacity which is occupied by one phase – usually the liquid in the case of gas-liquid simulations. Therefore the value of this volume fraction is equal to 1 if the cell is fully filled with liquid and equal to zero if fully filled with gas. The cell might also possess a volume fraction between 0 and 1 denoting partial liquid filling. It is these cells that usually contain or are situated at a gas-liquid interface. A schematic of this concept is shown in Figure 2.14.

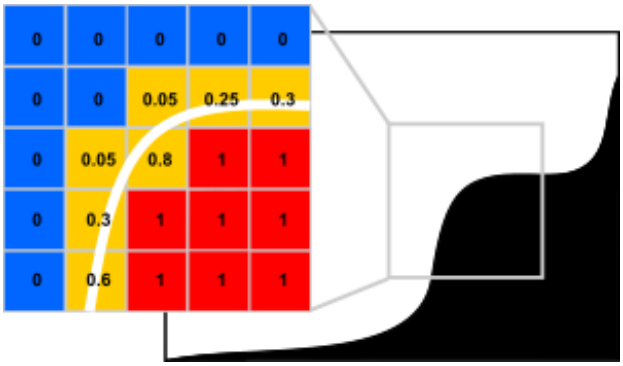

Figure 2.14: Schematic representation of the VOF method. Taken from [1]. Cells which occupy the value of 0 are completely filled with the gas phase, whilst cells filled with liquid are represented as possessing the value of 1. The interface would be represented by any number between 0 and unity.

The volume tracking method does not directly store the shape of the interface like with surface tracking methods but stores the volume fraction within each cell, and in doing so it tries to reflect the status of filling within each cell and then reconstruct the interface based on the volume fraction. There are at least four volume tracking methods in existence: MAC (Marker and Cell), FAN (Flow analysis network), SLIC (simple line interface calculation) and VOF (Volume of Fluid) [72]. The earliest version of the VOF method was already very robust. VOF later incorporated the PLIC (piecewise linear interface calculation) method which better improved the interface construction.

With the VOF method, the evolution of the interface is mapped using a discrete function γ also called an indicator function, which is the same as the volume fraction.

2.5.1. interFoam

`interFoam` uses the basic VOF algorithm but with added interface sharpening. It works only with two phases [48]. It uses a homogenous mixture approach where the parameters attributable to the two phases for example the velocity or the density, are averaged. Thus the two immiscible fluids are considered as effectively one single fluid throughout the domain. One momentum equation is solved in fact. In the conventional VOF method, the transport equation for the volume fraction or indicator function of one phase is solved simultaneously with the continuity and the momentum equations:

$$\nabla \cdot \boldsymbol{U} = 0 \tag{2.18}$$

$$\frac{\partial \gamma}{\partial t} + \nabla \cdot (\boldsymbol{U}\gamma) = 0 \tag{2.19}$$

$$\frac{\partial (\rho \boldsymbol{U})}{\partial t} + \nabla \cdot (\rho \boldsymbol{U}\boldsymbol{U}) = -\nabla p + \nabla \cdot \boldsymbol{T} + \rho \boldsymbol{f_b} \tag{2.20}$$

Where $\boldsymbol{U}$ represents the velocity field shared by both phases, γ is the volume fraction, $\boldsymbol{T}$ is the deviatoric viscous stress tensor, ρ is the density, p is the pressure, $\boldsymbol{f_b}$ are body forces per unit mass. The properties of the effective fluid are calculated as:

$$\rho = \rho_l \gamma + \rho_g (1-\gamma) \tag{2.21}$$

$$\mu = \mu_l \gamma + \mu_g (1-\gamma) \tag{2.22}$$

where ρ_l and μ_l and ρ_g and μ_g are the densities and dynamic viscosities of liquid and gas, respectively [48].

In OpenFOAM's `interFoam`, what is added on top of this is an additional term of a convective nature which comes from taking the velocity in terms of the weighted average of the respective liquid and gas velocities. The scope of this term is to sharpen the interface and narrow down the band of cells which contain a volume fraction value between 0 and 1. The equations for the two phase fractions can be expressed as:

$$\frac{\partial \gamma}{\partial t} + \nabla \cdot (\boldsymbol{U_l}\gamma) = 0 \tag{2.23}$$

$$\frac{\partial (1-\gamma)}{\partial t} + \nabla \cdot \Big[\boldsymbol{U_g}(1-\gamma)\Big] = 0 \tag{2.24}$$

The assumption is that the contribution of the liquid and gas velocities to the progression of the interface are proportional to the respective phase fraction. The velocity of the effective or fictitious fluid as a weighted average is:

$$\boldsymbol{U} = \gamma \boldsymbol{U_l} + (1-\gamma)\boldsymbol{U_g} \tag{2.25}$$

From equation (2.25) we can derive a time-dependent equation for the volume fraction γ:

$$\frac{\partial \gamma}{\partial t} + \nabla \cdot (\boldsymbol{U}\gamma) + \nabla \cdot \Big[\boldsymbol{U_r}\gamma(1-\gamma)\Big] = 0 \tag{2.26}$$

Where $\boldsymbol{U_r} = \boldsymbol{U_l} - \boldsymbol{U_g}$ is a vector of the so called 'compression velocity'.

This term is only active within the interface zone.

The compression term is effectively a relative velocity term. Its discretisation is based on the maximum velocity magnitude at the interface region and its direction is obtained from the gradient of the volume fraction:

$$U_r, f = n_f min\Big[C_\gamma \frac{|\phi|}{\boldsymbol{S}_f}, max\Big(\frac{\phi}{\boldsymbol{S}_f}\Big)\Big] \tag{2.27}$$

C_γ is a constant which controls the free surface compression and is switched off if it is set to 0; applies conservative interface compression if set to 1 and enhanced compression for values greater than 1. ϕ is the face volume flux, n_f is the face unit normal which is calculated at cell faces in the free surface region using the volume fraction gradient at cell faces,

$$n_f = \frac{(\nabla \gamma)_f}{|\nabla \gamma)_f + \delta_n|} \cdot \boldsymbol{S}_f \tag{2.28}$$

where δ_n is a stabilization constant to counteract the grid non-uniformity.

This added convection term contributes greatly to a better interface resolution and avoids the need for using the CICSAM (Compressive Interface Capturing Scheme for Arbitrary Meshes) scheme. It does use however another scheme which is MULES (Multidimensional Universal Limiter with Explicit Solution). The Courant Number Co needs to be limited to approximately 0.25 for stability in the case of the explicit MULES algorithm but with a "semi-implicit" MULES algorithm switched on in the `fvSolution` file – that is `MULESCorr` is set to yes - there is no upper bound for the Courant number for stability but the level is more determined by temporal accuracy requirements [53].

2.5.2. Herschel-Bulkley fluid model implementation in OpenFOAM

As explained above OpenFOAM also uses what effectively is a bi-viscosity model. Below a certain threshold shear stress, the model switches to a more viscous regime where the shear stress is linearly proportional to the shear rate. The user specifies 5 different parameters in the transport model in the `transportProperties` file [11].

The four usual parameters are those of density, yield stress, the fluid consistency index and the flow behaviour index. Of these, τ and k are divided by the density within the solver and result as `tau0` and `k`. The value for the density and the flow behaviour index stay the same. The bi-viscosity framework is implemented with the fifth parameter `nu0`. This parameter is dimensionally equivalent to a kinematic viscosity [11].

3

Validation Tests

This chapter presents the results from the four validation tests carried out to examine the behaviour shown by a given Herschel-Bulkley fluid under certain boundary conditions. The first test is a steady-state simulation of a Hagen-Poiseuille flow. The result from this can be compared to the analytical solution. A preliminary test parallel to the first test was used to identify the effect of the previously mentioned OpenFOAM parameter `nu0` on the flow behaviour of the fluid. The third case is that of the gravity-driven flow of a Herschel-Bulkley fluid through a Marsh funnel. The last test is that of the slump test.

3.1. Hagen-Poiseuille Flow

The objective of this test was to judge the capability of the OpenFOAM Herschel-Bulkley transport model to capture the plug flow associated with a yield stress fluid such as a drilling fluid. An adequate model would predict the radius of the plug as well as the velocity of both the plug and the sheared region of flow between the plug and the wall of the conduit.

The exact solution for Hagen-Poiseuille flow of a given Herschel-Bulkley fluid for a given ρ, τ_0, K and n is as found in [23].

$$u(r) = \frac{R}{\tau_w k^{\frac{1}{n}}} \frac{n}{n+1} \left[(\tau_w - \tau_0)^{\frac{n}{n+1}} - \left(\frac{\tau_w r}{R} - \tau_0 \right)^{\frac{n}{n+1}} \right] \tag{3.1}$$

The setup in OpenFOAM involved making use of the periodic boundary condition where the outflow is recycled into the 'inlet', emulating a very long pipe. This done within OpenFOAM using the `cyclic` boundary condition which is equivalent to the periodic one. The mesh was generated using `blockMesh` within OpenFOAM.

The experimental results of Benslimane et al. [18] were used for this test. This work details to laminar pipe flow of bentonite suspensions. These results are not essential since an analytical solution for Hagen-Poiseuille flow is readily available, yet by referring to an experimental study we can extract the correct set of parameters which will provide a plug flow regime. The results of the study with the velocity profiles for the three water-bentonite suspensions of 3.5, 5 and 8% are shown in Figure 2.8.

For this test, the 8% by weight bentonite-water suspension was considered.

Table 3.1: Parameters used for the Hagen-Poiseuille simulation campaign based on the parameters of the experiments of Benslimane et al. [18]

Parameter	Units	Value
Density	kg·m^{-3}	1050
Yield Stress	Pa	10.53
Consistency Index	Pa·s^n	0.57
Flow Behaviour Index	-	0.59
Pipe Radius	m	0.01
Volume-Averaged Flow velocity	m·s^{-1}	0.5

The solver used for this case is the SIMPLE algorithm as formulated by Patankar and Spalding [55], found

as `simpleFoam` in OpenFOAM. This offers a steady-state solution. For all tests 20,000 iterations were used and the resulting residuals were sufficiently diminished in all instances of this validation case.

Three levels of mesh refinement were used. For the first run, 50 cells were used in the radial direction, followed by 75 and then finally 100. The `simpleGrading` option for `blockMesh` for the ratio of the last cell length to the first cell length was always maintained at 0.001. Figure 3.1 shows the mesh for the Hagen-Poiseuille simulations along with the boundary conditions for this case.

The boundary conditions for the Hagen-Poiseuille case were the following:

- Zero pressure gradient at the walls.
- Periodic boundaries at the inlet and outlet.
- Axisymmetry through using the `wedge` utility.
- No slip velocity at the walls.
- Fixed average axial velocity of 0.5m/s.

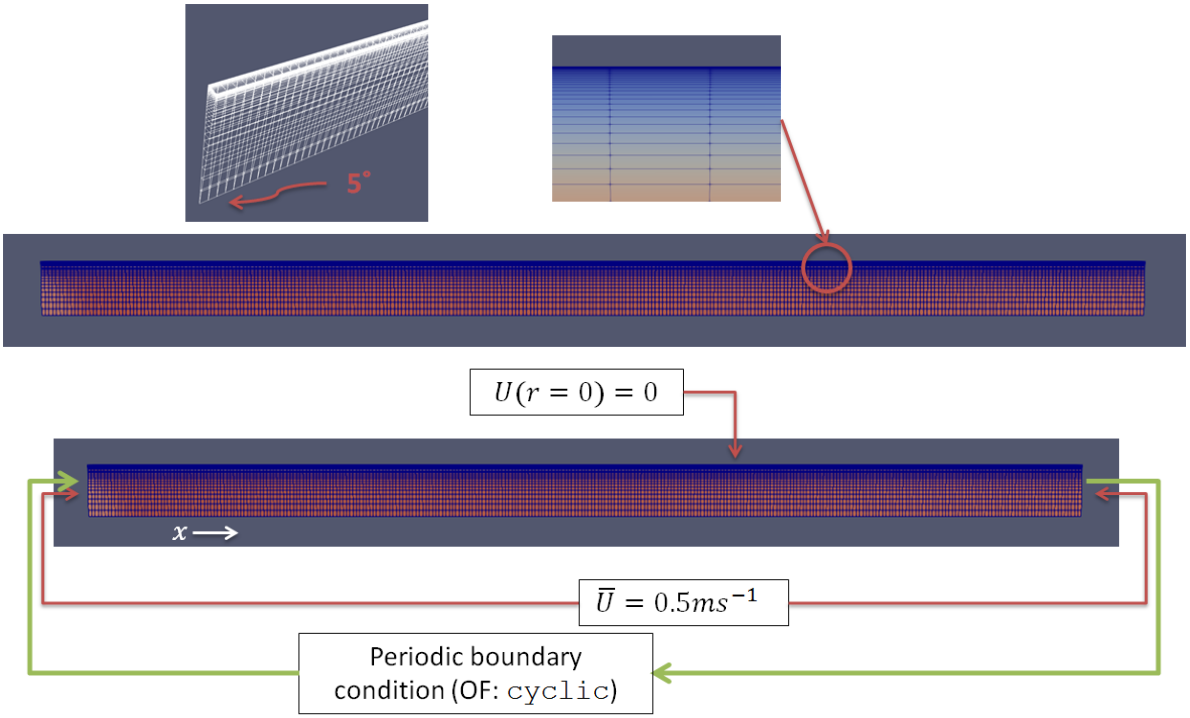

Figure 3.1: Meshing and boundary conditions for the Hagen-Poiseuille tests. [Top] The meshing used in OpenFOAM's own `blockMesh` meshing utility. Note the wedge at 5° used for axisymmetry and the grading of the mesh towards the pipe wall. [Bottom] Boundary conditions for the Hagen-Poiseuille case.

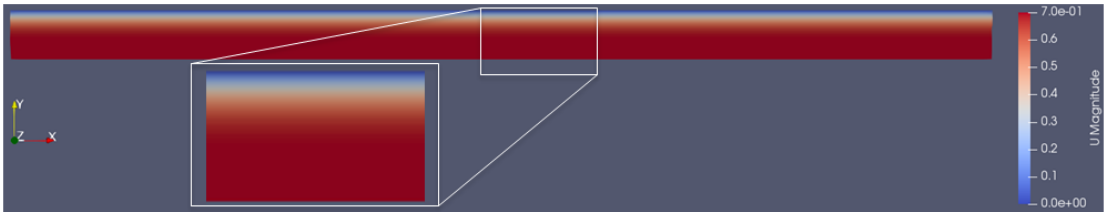

Figure 3.2: The resulting velocity along the pipe as seen on ParaView. Red indicates higher velocity. The maximum velocity is the plug velocity and at 0.7 m/s it is in close agreement with the experimental results of Benslimane et al. [18].

The results for the plug velocity and the plug radius and the wall shear stress for these the mesh refinement levels were taken from these simulations and compared with the exact solution given by equation 3.1. These

results are shown in Table 3.2 and in Figures 3.2 and 3.3. Figure 3.2 shows that the central red band is the plug region moving along the central axis at the same maximum velocity.

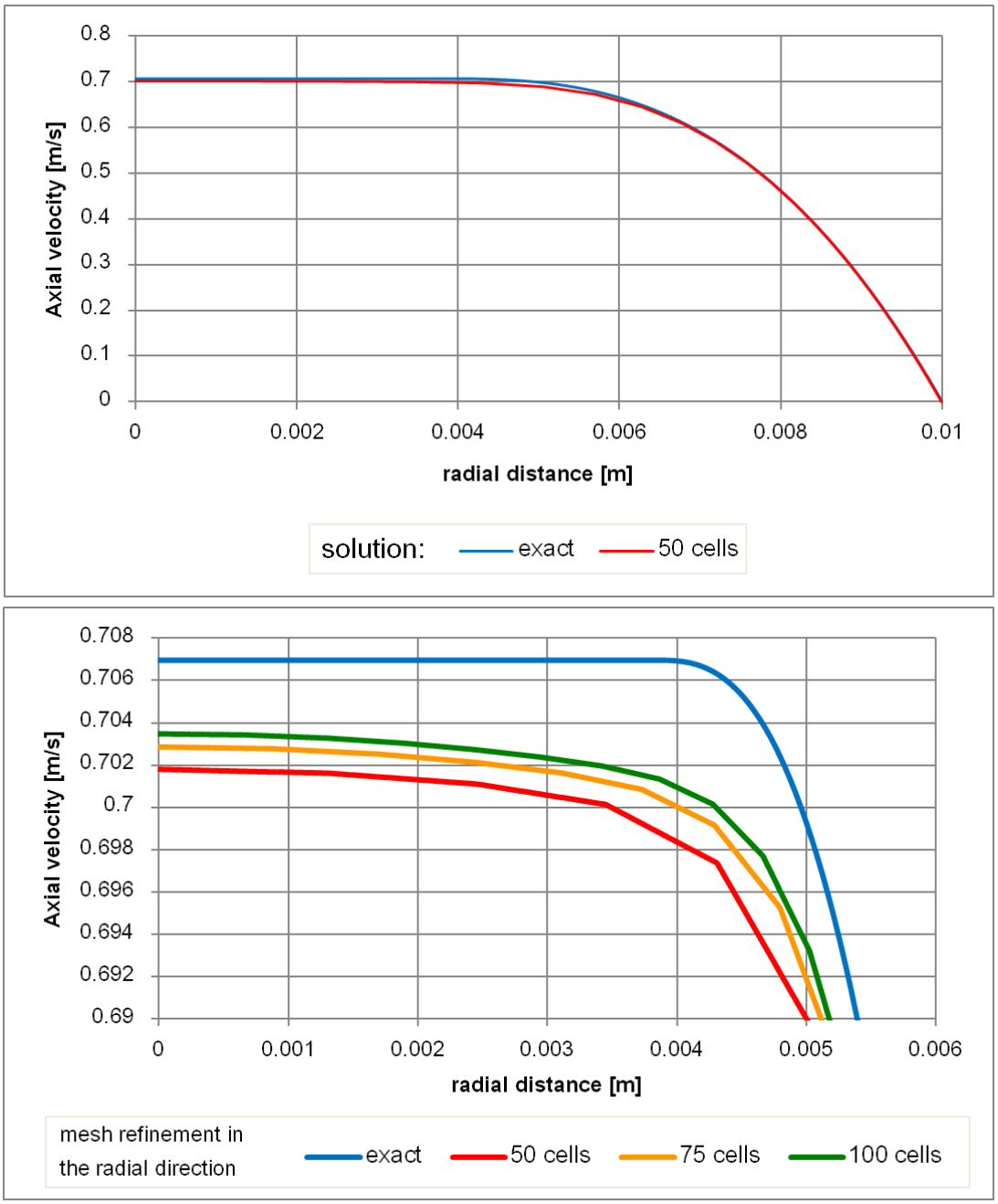

Figure 3.3: Axial velocity profile for an 8% water-bentonite suspension for the data shown in Table 3.1. [Top] 50 cells in the radial direction compared to the exact solution. [Bottom] Comparison of the plug velocity and plug radius with the exact solution for the second and third mesh refinements and also the original mesh with 50 cells in the radial direction. The rest of the plot which covers the radial position from 0.006m upwards is not shown so that the relative value of the plug velocity along with the plug radius can be seen and compared.

These results show that the solution is converged. As can be seen from Table 3.2, the percentage difference between the exact solution and the simulations diminish with increasing mesh refinement for both the plug velocity and the plug radius. In Figure 3.3 we can see the CFD solution approaching the plug velocity and the plug radius with more cells in the radial direction.

The effect of `nu0` on the steady state velocity profile of a Herschel-Bulkley fluid flowing through a cylindrical duct was checked by varying the nu0 as a multiple of `tau0` where the ratio of `nu0` to `tau0` is varied logarithmically from 10^{-4} to 10^{4}. The resulting velocity plots are shown in Figure 3.4.

Table 3.2: Results from the Hagen-Poiseuille simulations

		Plug Radius [m]			Plug velocity [m/s]			Wall Shear Stress
Mesh Size	Radial Cells	CFD	Exact	% diff	CFD	Exact	% diff	[Pa]
1	50	0.003457	0.003856	10.36	0.7018	0.7070	0.73	27.3431
2	75	0.003736	0.003856	3.11	0.7029	0.7070	0.41	27.3294
3	100	0.003876	0.003856	0.52	0.7035	0.7070	0.23	27.3217

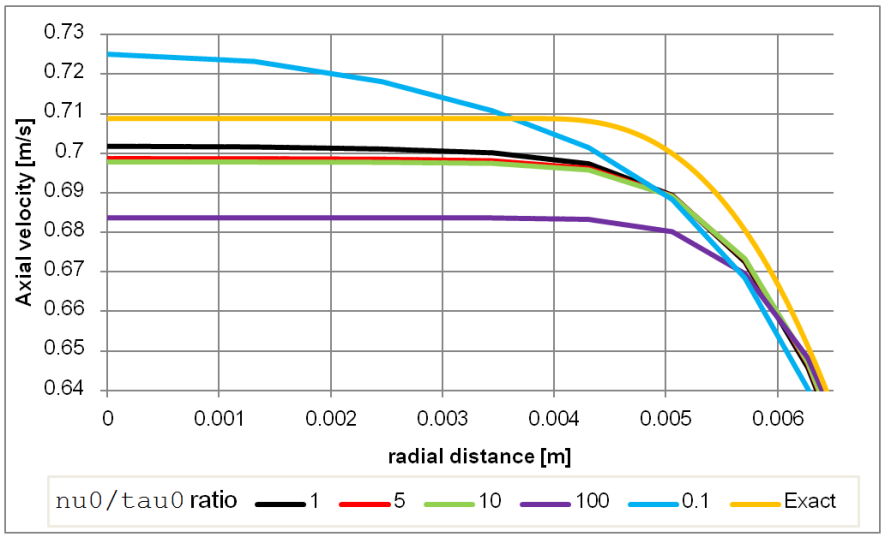

Figure 3.4: Axial velocity plot for different values of the ratio of `nu0` to `tau0`. For this case `nu0` and `tau0` have to be numerically equal so that the simulation approaches best the exact solution. The black line is the velocity plot for a `nu0` to `tau0` ratio of 1. The light orange line is the exact solution provided by equation 3.1. It can be clearly seen that for a `nu0` to `tau0` ratio of 1 this comes closest to the exact solution. The rest of the plot which covers the radial position from 0.006m upwards is not shown so that the relative value of the plug velocity along with the plug radius can be seen and compared.

The conclusion from Figure 3.4 is that the ratio between `nu0` and `tau0` should numerically be equal to 1. This is because it is with this ratio that the numerical solution from the simulation approaches best the exact solution. Therefore throughout the following simulations, `nu0` was always kept numerically equal to `tau0`.

3.2. Marsh Funnel Test

The next series of validation tests made use of the comparison between the time taken for a set amount of Herschel-Bulkley fluid to flow out of a standard Marsh Funnel and that of a corresponding case in CFD.

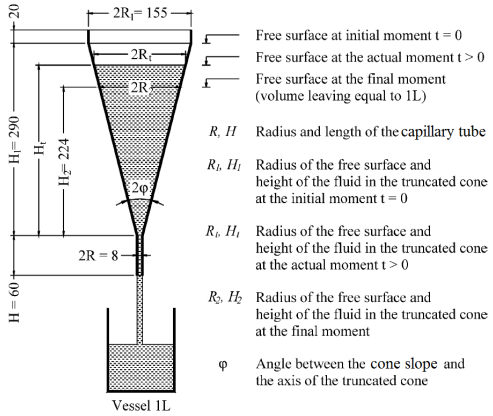

Figure 3.5: The dimensions of the Marsh Funnel as used by Nguyen et al. [50] in their study. The funnel is recreated with Gmsh as a mesh and utilizes the axisymmetry of the case to simulate the flow for only a wedge portion of the domain.

The physical test data from Nguyen et al. [50] was used for comparison with simulation results. The authors detail how they treated different grades of cement grout flowing out of the funnel as a Herschel-Bulkley

Table 3.3: Parameters for the Marsh Funnel test based on the experimental data by Nguyen et al. [50]

Parameter	Units	Value
ρ	kgm^{-3}	1873
τ_0	Pa	10.8
K	Pas^n	4.9
n	-	0.455
Flow time	s	24.1

fluid and what were the corresponding flow times for each different composition.

For this test, the No. 6 cement grout described in Nguyen et al. [50] was used which had the rheological characteristics of a Herschel-Bulkley fluid as detailed in Table 3.3.

Since this is a multiphase flow case with two separate, distinct phases with an air-fluid interface, the solver used was `interFoam`, which is by nature a transient solver. The two Courant number set for this study were always kept at 0.1, both for `maxAlphaCo` and `maxCo`. This decision is based on the values for these parameters that Raees et al. [62] and Gopala and Wachem [35] used for their respective studies, therefore with the Courant number at 0.1 it is a good starting point.

The meshing methodology for this case made use of the axisymmetry of the funnel and thus a wedge. The dimensions of the Marsh Funnel used by Nguyen et al. [50] is shown in Figure 3.5. From knowing the prescribed geometry of the funnel and the stated flow time of the cement grout it is possible to expect a defined range where the interface will be found between the time right after the opening of the tube of the funnel until the point where all the grout has left the funnel. This was also part of the study carried out by Guria et al. [37]. In spite of the fact that the real physical Marsh Funnel test requires that 1 litre of the fluid comes out of the funnel, in these CFD simulations, the simulation is carried out until the flow rate coming out of the funnel started decreasing linearly with time in order to save time. This allows us to have structured, fine meshing in the region where this interface is expected to be found and also at the outlet tube of the funnel. Then for saving on the cell count, the rest of the domain is meshed using an unstructured mesh which is comparatively coarser. This can be seen on the left portion of Figure 3.6. Four levels of progressive mesh refinement were used.

It is also important to note that for reasons that pertain to obtaining a good quality multiphase flow simulation, only hexahedral meshes were generated for all the simulation campaigns. The reason is that were they to be tetrahedral-dominant meshes, there would be issues with the tracking of the interface and spurious interface motions attributable to local incorrect directions of the interface normal.

From these simulations onwards Gmsh was used exclusively for generating meshes. Gmsh offers an intuitive script-based approach to generating 3D meshes with possibilities to control the meshing of edges, surfaces and volumes effectively [2]. First the geometry and the hexahedral-dominant mesh are created in Gmsh and then imported into OpenFOAM using the `gmshToFoam` utility.

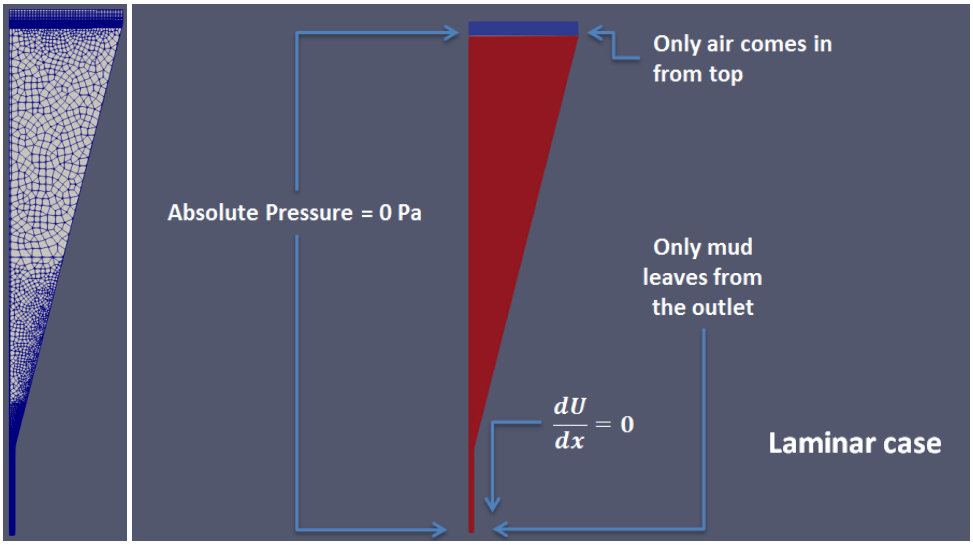

Figure 3.6: [Left] One of the meshes used for the Marsh Funnel simulations. Note the structured meshing at the top and the capillary tube area. The middle section of the cone of the funnel is unstructured. [Right] The boundary conditions used throughout the funnel simulations. Shown in red is the drilling fluid phase and in blue the air phase. Note the interface between the two phases.

The boundary conditions for the case are illustrated in the Figure 3.6. The top and bottom faces are imposed to have always air and mud respectively. This is done through the `alpha.mud` file within the `0` folder in OpenFOAM.

Furthermore, the total pressure is imposed to be atmospheric at both the top inlet and the bottom outlet. The flow at the outlet is imposed to be fully developed and hence there is no change in velocity in the axial direction downwards. Thus $\partial U/\partial x = 0$. Additionally, the flow is imposed to be laminar throughout the simulation through the `turbulenceProperties` file in the `constant` folder.

Using OpenFOAM's own command of `flowRatePatch` it is possible to keep track of the flow rate at the outlet of the funnel and know the flow rate at every time step. The aim here is to recognize when the flow rate diminishment with time has reached linearity for a sufficient period of time which indicates that the simulation can be stopped.

The flow time for 1 litre of the cement grout to flow out of the tunnel was found by using the flow rate reduction rate extracted from the plot of flow rate against time for each simulation of Figure 3.7. A linear regression fit is imposed after the flow is stabilized. This happens almost exactly after 1s has passed from t = 0. In order to corroborate this approach a further graph is plotted of the accumulated cement grout which has passed through the outlet against time as seen in Figure 3.8. This figure shows that indeed a linear trend starts after 1s of flow.

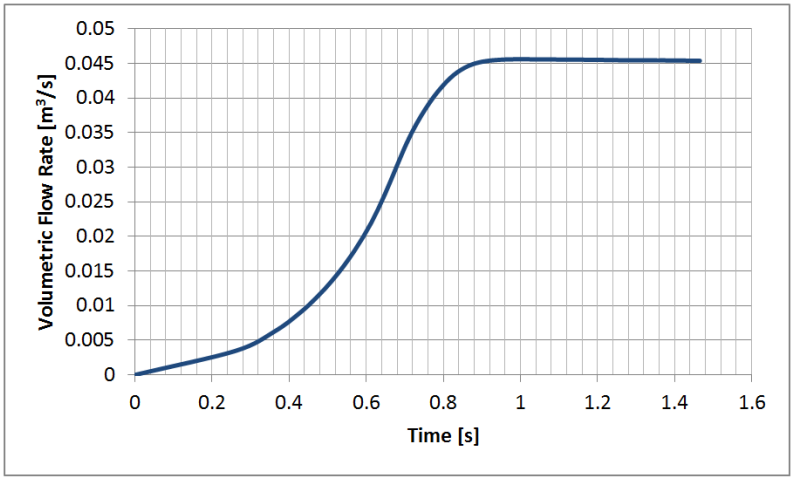

Figure 3.7: The variation of the volumetric flow rate with time for the cement paste flowing through the Marsh Funnel for the coarsest mesh level. The volumetric flow rate decreases linearly with time after approximately 1 second from t = 0.

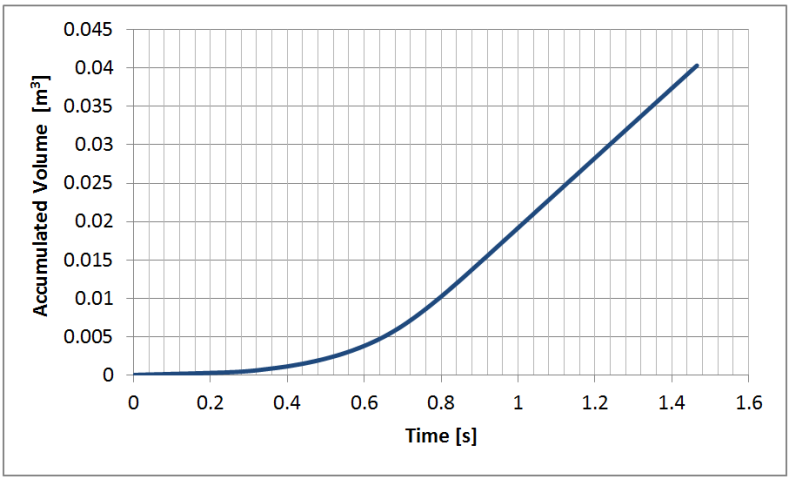

Figure 3.8: The variation of the accumulation of cement paste with time. Notice that after t = 1s one can say that the accumulation of the cement paste increases linearly with time.

From Table 3.4 here is a mismatch between the increase in the number of cells and the extrapolated flow time since there is no direct predictable relationship. However, since all flow times are in the region of 22.6

Table 3.4: Flow times in seconds for the different grades of meshes for the Marsh Funnel test simulation based on the experimental data by Nguyen et al. [50].

Mesh Size (number of cells in thousands)	Flow Time [s]
68	22.65
71	22.42
84	22.78
100	22.57

Table 3.5: Rheological Herschel-Bulkley parameters of the cement paste from Jayasree and Gettu [44] used for the mini-slump test simulation.

Parameter	Units	Value
ρ	kgm^{-3}	2395
τ_0	Pa	12.29
K	Pas^n	0.668
n	-	0.723

seconds which itself is very close to the reported time of 24.1 seconds for this cement grout.

Nguyen et al. [50] did not report any uncertainty in their experimental data. Thus, in this case the validation of this case will be taken to be sufficient because of the closeness of the simulated flow time and the experimental flow time.

3.3. Slump Test

The final round of validation test cases involved simulating the slump test, the consistency test used in civil engineering for concrete and cement pastes.

The experimental data for the slump test from Jayasree and Gettu [44] for a particular cement paste which was modelled as a shear-thinning Herschel Bulkley fluid with the rheological parameters shown in Table 3.5.

The axisymmetry of the case permitted the use of a wedge shaped mesh. The final aim of this validation test is to match closely the final diameter of the slump of paste reported by the experiments in Jayasree and Gettu [44]. For this particular paste it is stated that the final diameter of the slump is 143mm. There is no indication of the time taken for this slump diameter to be reached.

The spreading stops when the shear stress in the paste becomes equal to or smaller than the yield stress.

The geometry of the open frustum described in Jayasree and Gettu [44] is found in Figure 3.9 alongside the mesh used for the case.

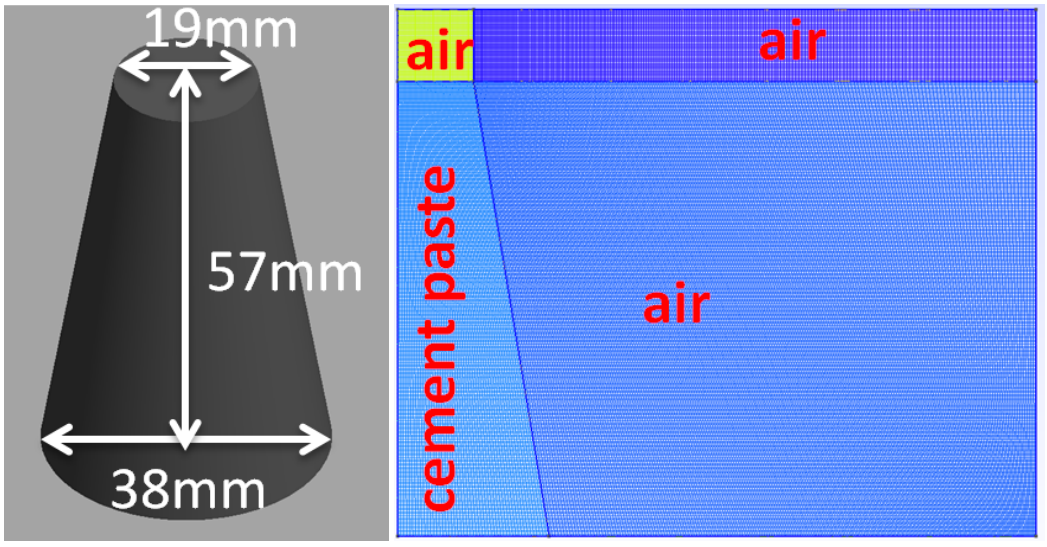

Figure 3.9: [Left] The geometry and dimensions of the open frustum described in the study of Jayasree and Gettu [44]. [Right] The mesh used for the slump simulations.

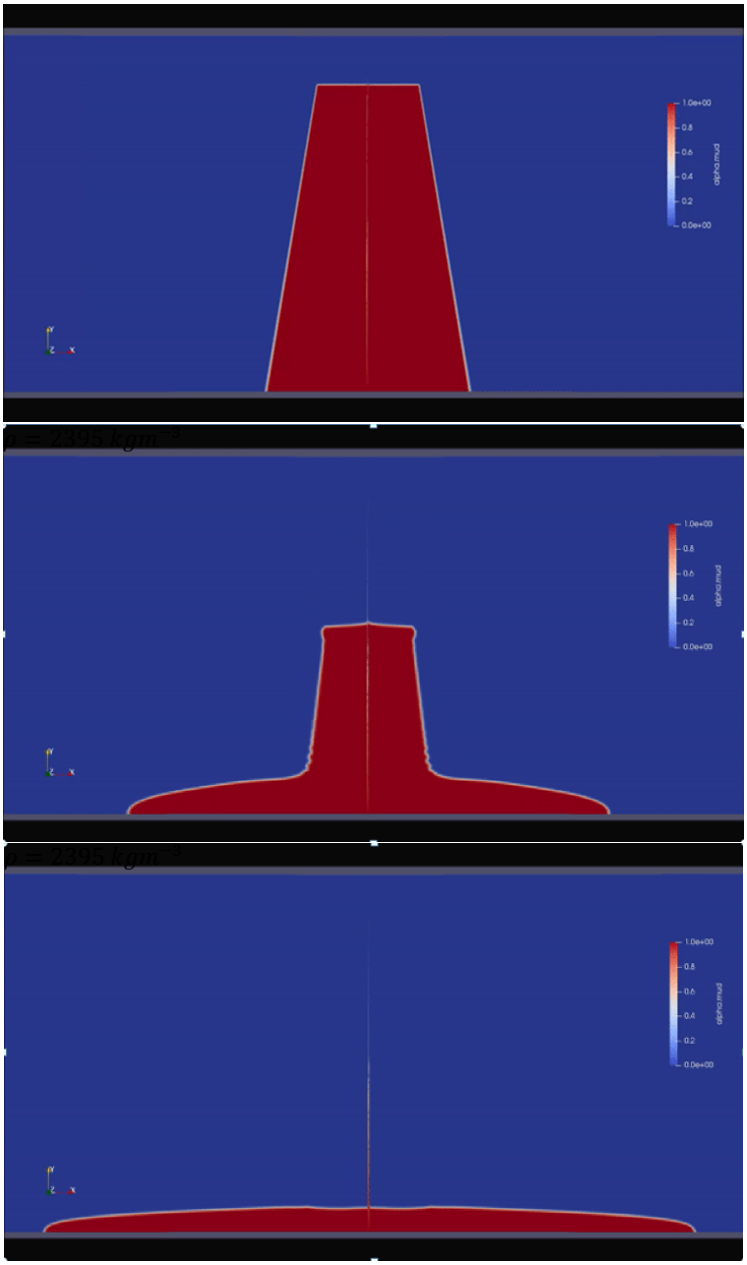

Figure 3.10: The evolution of the slump after t = 0 emulating the effect of rapidly removing and lifting the open frustum. The figure depicts the slump after 4s at the bottom and the slump at just before 2s in the middle.The snapshots from the simulation time-steps have been mirrored along the vertical plane to visualise the full slump diameter. The middle line is a by-product from Paraview of this mirroring. The spread stopped when the the shear stress in the paste became equal to or smaller than the yield stress of the paste.

The boundary conditions for this case are relatively simple with the bottom wall having a no-slip condition and the wall above being effectively open to the ambient surroundings and thus at atmospheric pressure. The mesh was made wide enough so that it can still retain the full expected diameter of the slump. The side walls were imposed to be no-slip walls as well.

Six different simulations were carried out with three meshes of increasing fineness for two different `maxAlphaCo` and `maxCo` of 0.03 and 0.07.

Figure 3.10 shows the evolution of the cement paste from t = 0 to the final time t = 4s when it was deemed that the spread of the cement paste has stopped since with new time-steps the increase in the spread diameter was minimal. The figure has been mirrored along the vertical axis to visualize a full slump. The middle line is a by-product of this mirroring.

As can be seen from Table 3.6, for the 0.07 Courant number the percentage difference between the reported final slump diameter and simulated final slump diameter decrease with increasing mesh cell count.

Table 3.6: Results from the CFD simulations carried out based on the experimental data from Jayasree and Gettu [44]. The final slump diameter was around 0.07m which is very close to the 0.071m reported by [44].

		Radius [m]		
No. of cells	Courant No.	CFD	Experiment	% difference
1341600	0.03	0.0689	0.0715	3.67
335400	0.03	0.0637	0.0715	10.94
83980	0.03	0.0655	0.0715	8.37
498958	0.07	0.0710	0.0715	0.76
334880	0.07	0.0766	0.0715	7.18
196768	0.07	0.0658	0.0715	7.92

For the 0.03 Courant number, the smallest percentage difference is for the case with the largest number of cells at 1341600 but then there is an increase in the percentage difference from the experimental slump diameter.

It must be stated that as with the case of the Marsh Funnel tests, the authors did not provide any indication of the experimental error involved in their works. Therefore we only have the convergence of the simulations to depend on to deem if the results are correct or otherwise.

In conclusion, it is for this reason that for subsequent simulations for the main campaign the Courant number of 0.07 was elected to be used throughout the rest of the study.

3.4. Concluding Remarks

This series of validation tests provided an insight into the capabilities of OpenFOAM's `interFoam` coupled with the Herschel-Bulkley rheological model.

The effect of the parameter `nu0` was understood and the Courant number of 0.07 (incorporated into the OpenFOAM settings through the `controlDict` file through `maxAlphaCo` and `maxCo`) was judged to be sufficient for this study.

The OpenFOAM files for the Marsh Funnel test and the Slump test are found in Appendices B and C respectively.

4

Simulation Setup

The simulation case required considerations into geometry, kinematics and the rheological properties of the selected fluid. This thesis is an investigation into the possibility that insufficient filling of the inner volume of the pipe with drilling mud is causing buoyancy issues that in turn cause friction with the borehole wall. The method of allowing in drilling mud through slots in the pulled pipe wall during pullback to counteract the effect of buoyancy is called 'passive ballasting' in this thesis.

As explained in the methodology, for the scope of this investigation, an initial benchmark case with all the parameters being representative of a typical case installation on the field is simulated. Then subsequent simulations will change one parameter at a time in order to see what the effect of that single parameter change is if all other parameters are remain the same.

4.1. Benchmark Case

The benchmark case that started the simulation campaign incorporates attributes taken from various sources. Geometrical attributes were taken from literature [49] , [60] and rheological attributes were taken from [68] and [60].

The benchmark case aimed to capture several phenomena at once. What is simulated, in effect, is the fluid behaviour of the drilling mud behind the pullhead and that above the slot and how both volumes enter the slot. This drilling mud is supplied from an outlet incorporated in the reamer in front of the swivel. As mentioned in the first chapter, the pipe is being pulled down into the borehole at an angle to the horizontal. This is the stage when drilling mud will start to flow through the slot. This is both because of the drilling mud being pumped from ahead of the swivel and also from the drilling mud from the pre-filling of the borehole. The hydrostatic pressure head is therefore another substantial source of flow of drilling mud into the slot. Following from this fact, we have the possibility to simulate and track the transient position of the free surface of drilling mud. Therefore this makes it a two-phase, transient fluid mechanics case problem.

These are the assumptions taken regarding this benchmark case and also the rest of the simulation cases:

1. The drilling mud enters the domain with zero swirl.
2. The drilling mud's flow regime is laminar when it enters the domain.
3. The flow regime for all the duration of the simulation is laminar and there is no transition to the turbulent regime at any point during the simulation time for any of the cases of the simulation campaign.
4. The flow rate of drilling fluid entering the domain is constant.
5. There are no changes in the properties of the air or the drilling mud due to temperature changes.
6. There are no surface tension effects - as explained in Section 2.3.4.
7. The drilling fluid is one homogenous suspension of constant properties throughout the fluid domain.
8. There are no appreciable changes in the rheological parameters of the drilling fluid for the duration of the simulation time - that is no thixotropy.
9. The pipe and the borehole are taken to be concentric.

4.2. Case Geometry

The geometry which will be the fluid domain consists of an annulus which is concentric with a cylinder. These represent the volume of space between the HDPE pipe and the ground wall of the borehole and the inner volume of the pipe respectively. These two volumes are connected via a bridge which represents the slot that allows in drilling mud into the inside of the pipe. The outer pipe diameter to borehole diameter ratio is 0.66 as recommended by [39] and [59]. The adopted borehole diameter of 1.2m is what is typically found in Maxi-HDD operations as explained earlier in Chapter 1.

It was expected that the contribution for the pressure required to drive the drilling mud inside the inner volume of the pipe would form a significant part of the hydrostatic pressure head of fluid above the slot if not the primary driver for this flow. The secondary driver would be the flow from the drilling fluid pump conveying mud from the reamer. Therefore it was decided to orient the slot in such a way that such contribution would expected to be the minimum possible. This means placing the slot's opening facing the 12 o'clock direction. In this way, we expect to fully test the capability of the slot to allow as much drilling mud through per unit time as possible and obtain a conservative view of how much drilling mud is capable of entering the inner pipe volume.

The length of the slot is taken to be 38cm and the width is 9cm. This is based on the observed dimensions for a slot in and HDPE pipe of 0.8m diameter used by an HDD contractor in the Netherlands.

Another feature of the geometry of the simulation domain is the volume of empty space that makes part of the inner volume of the pipe. This would be associated with the empty volume of the pullhead and any part of the inner pipe volume which is between the slot and the swivel. This represents an additional volume which needs to filled before the free surface on the inside of the pipe can catch up with the free surface in the borehole annulus. A good representative scale of the magnitude of this 'dead' volume is difficult to determine. The same can be said for the topology and form of this volume. Therefore the volume for this dead space was incorporated into the benchmark case as a cylindrical volume extension of the inner pipe, with a length of approximately one inner pipe diameter. One of the simulation tests uses a smaller dead volume in order to see what the effect of the volume size on the delay on fluid level equalization.

The rate of penetration is taken to be 0.15m/s. This is based on the reported typical pulling rate for a Maxi-HDD operation for a pullback stage used by an HDD contractor. In the simulations this aspect of the condition of the pullback stage is incorporated as a wall velocity boundary condition at the borehole wall.

The creation of the case geometry is carried out using Gmsh. The only plane of symmetry available for this case geometry is the vertical plane. This allows only half of the slot, annulus and inner volume of the pipe to be modelled.

Figure 4.1 shows the geometry created in Gmsh. The different coloured patches indicated the quadrilaterals over which a mapped structured mesh will be generated. There are thin quadrilaterals all along the axial length so that there could be better control of meshing along the boundary of the domain. The central cylinder which represents the inner volume of the pipe is meshed in such a way to achieve quadrilateral mesh elements inside the pipe which have sides of roughly the same length. This can be seen later on in Figure 4.4.

Table 4.1 lists all the relevant parameters adopted in the benchmark case. Figures 4.2 and 4.3 show the dimensions of the benchmark case in metres. The geometry shown is that exported to OpenFOAM from Gmsh.

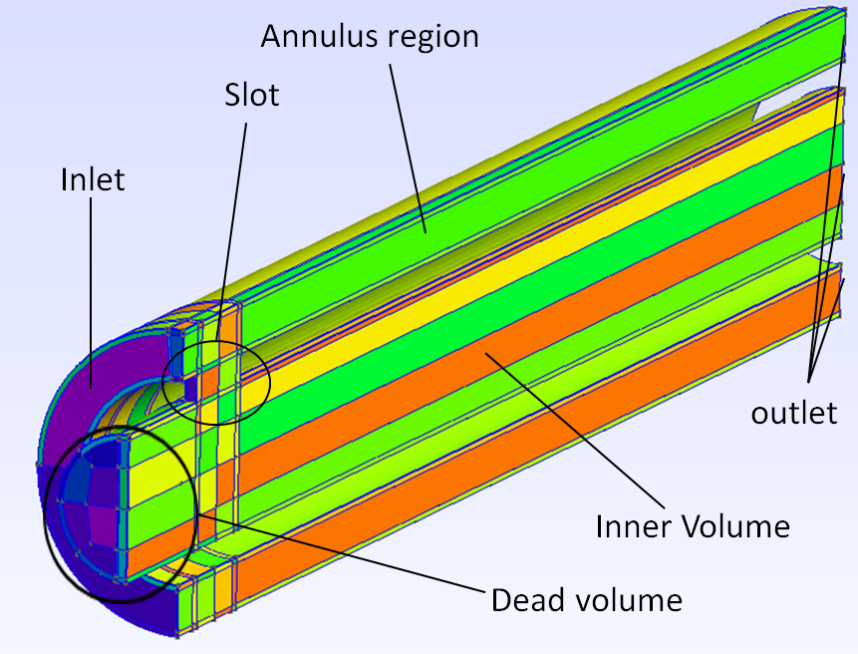

Figure 4.1: The geometry of the case created with Gmsh. Note the inlet, outlet, annulus region, inner volume of the pipe, the dead volume and the slot.

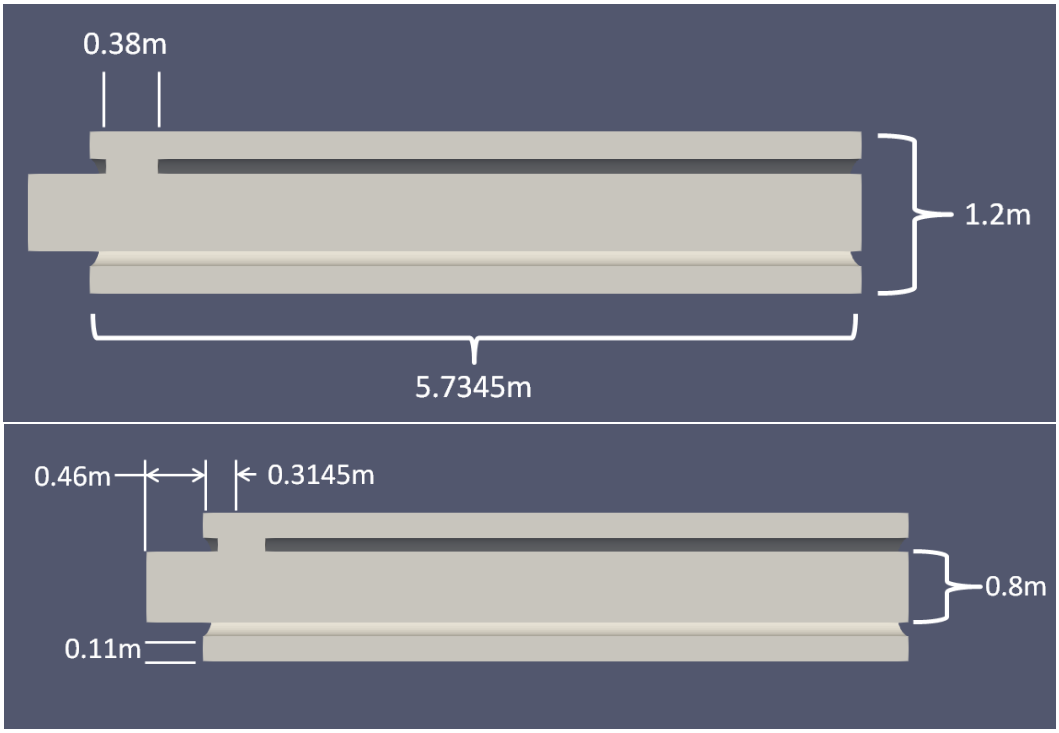

Figure 4.2: The dimensions of the geometry of the benchmark case exported from Gmsh to OpenFOAM.

Table 4.1: Description of all the relevant geometrical parameters for the main simulation case.

Geometric Feature	Dimensions
Angle of inclination	14°
Rate of penetration	0.15m/s
Borehole diameter	1.20m
HDPE pipe outer diameter	0.80m
HDPE pipe inner diameter	0.58m
HDPE pipe wall thickness	0.11m
Slot length	0.38m
Slot width	0.09m
Length of annulus region ahead of the slot – connected to the inlet	0.1245m
Length of the annulus and inner pipe volume behind the slot	5.23m
Length of the 'dead' volume	0.58m

Figure 4.3: Side view of the geometry. Note the dimensions of half-slot width. Use of symmetry is made for this case to save up on computational time.

4.3. Case Rheology

As seen from the studies which report the four-parameter Herschel-Bulkley characterizations of drilling mud [60], [68] there is a great degree of variation in drilling mud rheology. These parameters are affected by the weight concentration of bentonite, acidity and electrolyte concentration [45].

Talmon and Huisman [68] presents the rheology characteristics of clean freshly mixed bentonite-water suspensions at different bentonite weight concentrations. Rabiei et al. [60] presents the rheological parameters for drilling mud that has been mixed with cuttings from the reamer during pullback and is described to be a slurry. The bentonite concentration for these slurries was 8%.

Both the drilling mud samples from [68] and [60] indicate that the consistency index median was 0.15Pa s^n. The median flow behaviour index was 0.7. This indicates that these two parameters do not change appreciably when the drilling mud includes the cuttings from the reamer during pullback. It is assumed that it is implied that the fluid becomes uniform slurry with no dispersed pebbles or lumps of soil cuttings.

Finally the yield stress for Rabiei et al. [60] samples are on the order of 10Pa and those for the samples of Talmon and Huisman [68] have a median yield stress on the order of 0.2Pa.

Therefore it was decided that the liquid phase for the benchmark case will have properties closer to those reported by Rabiei et al. [60]. The density adopted for the fluid used in the benchmark case was also taken from details from Rabiei et al. [60] and this is equivalent to 1100kg/m^3.

The flow rate of 45 litres per second through the inlet section is assumed to be evenly distributed over the surface of the inlet. This value for a flow rate was based on taking this quantity to be proportional to the borehole diameter as reported in the works of Faghih et al. [30] and Rabiei et al. [58] and Shu et al. [66]. This in effect means that there is a constant fluid velocity of 7.17cm/s across the inlet at all times during the simulation.

The rheological parameters used for the benchmark case are listed in Table 4.2. What is actually input

Table 4.2: Parameters used for the drilling fluid rheology of the benchmark case

Parameter	Symbol	Value	Units
Density	ρ	1100	kgm^{-3}
Yield Stress	τ_0	10	Pa
Consistency Index	K	0.15	Pa s^n
Flow Behaviour Index	n	0.7	-
Flow rate	Q	45	ls^{-1}

into OpenFOAM to set the rheological parameters for the benchmark simultion case will be explained later on in Section 4.6.

4.4. Meshing

The mesh for the case was created by first creating the 2D plane geometry in the x-y plane. The geometry is created by defining points, then joining these points with either straight lines or circular arcs. The aim is to form a patch of sub-quadrilaterals within this 2D plane geometry so that applying a mapped structured grid made solely from quadrilaterals is possible. This is called a "Transfinite Surface" in Gmsh. Then the next step was to extrude these quadrilateral surfaces where necessary to create the 3D mesh body. The extrusion incorporates the creation of layers of these mapped quadrilateral surfaces, with each layer being of a finite thickness. Figure 4.4 shows the side-view of the mesh generated as well as the exported mesh to OpenFOAM from the side. This was done using the `gmshToFoam` utility.

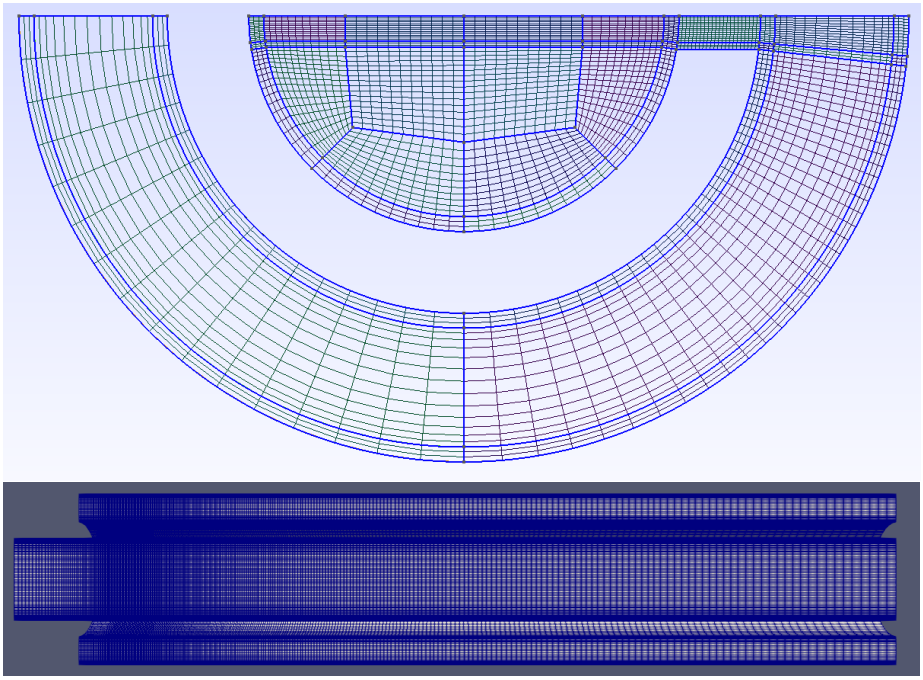

Figure 4.4: [Top] Side view of the mesh geometry created with Gmsh. Note the structured meshing made easier through dividing the section into smaller quadrangles. [Bottom] The same mesh exported into OpenFOAM and viewed from the side.

The first coarse mesh had 734632 hexahedral cells. All the cells were hexahedra. The first mesh refinement produced 1136840 cells. The second mesh refinement produced 1478200 cells.

4.5. Boundary and Initial Conditions

The boundary and initial conditions are specified within the OpenFOAM folder structure in the `0` folder. The three files contained within the `0` folder are `U`, `p_rgh` and `alpha.mud`.

The inlet of the domain stands at the annulus face at the front of the mesh. The outlet to atmosphere stands at the other end and comprises both the annulus face and the inner pipe cross-section at the other end away from the inlet.

The `U` file contains the boundary conditions relating to the velocity. This is specified as being zero or no-

Table 4.3: Parameters used in the benchmark simulation. Note that for `tau0` and `k`, these values are not direct yield stress and the consistency index but are divided by the fluid density, ρ.

`transportProperties` parameter	Value	Base Units
`nu0`	0.009091	L^2T^{-1}
`tau0`	0.009091	L^2T^{-2}
`k`	1.36E-04	L^2T^{-1}
`n`	0.7	-
`rho`	1100	ML^{-3}

slip at all wall surfaces except for those of the borehole wall which possesses a constant velocity of 0.15m/s in the positive z-axial direction which corresponds to the rate of penetration. The other non-zero velocity wall is the inlet which possesses a constant velocity directed inwards into the domain of 7.17cm/s.

The `p_rgh` file contains specifications for the pressure in the domain. The pressure is specified to have zero pressure gradient across all solid walls. This is given by the `fixedFluxPressure` setting and assigning the value to be `internalField` so that it could be initialized accordingly. This `fixedFluxPressure` setting is similar to specifying `zeroGradient` within OpenFOAM but with the added feature of taking care of gravity or surface tension effects automatically and if necessary. The inlet is also assigned to have a `fixedFluxPressure`. The outlet on the other hand is set to zero total pressure which is equivalent to being open to the atmosphere.

The third file is the `alpha.mud` file. This is the file which takes care of how the walls of the domain should contain the fluid inside and which apertures (known as 'patches' in OpenFOAM) should allow them in or out. This file would normally take a name indicative of the phase present. Usually for water for example it is named `alpha.water`. Recalling that '1' represents the liquid phase and '0' is the gaseous phase, the domain is declared to be all '0' upon the initialization of this file. All solid walls are assigned to be `zeroGradient`, therefore they are impermeable to any of the fluids inside. The inlet is assigned as having a fixed value of 1 since it supplies the drilling fluid. The outlet is assigned as an `inletOutlet`, meaning that it allows both fluids through as well as any recirculation or re-entry. The setup with the air and drilling mud phase set up at time t = 0, incorporating the angle to the horizontal is shown in Figure 4.5. The volume shown in blue is the air phase and the drilling mud is depicted as the volume in red. The interface is indicated in white. What can also be seen in this figure is the drilling mud right outside the pipe in the annulus region.

A schematic showing the boundary conditions for the benchmark case is shown in Figure 4.6. In this figure, red denotes the drilling mud phase and blue denotes the air phase. The snapshot is shown at the initial condition at t = 0s.

4.6. Other Settings

For assigning the initial distribution of liquid at zero time what is used in OpenFOAM for `interFoam`, the `setFieldsDict` file is used. This permits the alignment of the initial free surface horizontal position at 14° (angle of pipe ground entry) to be perpendicular to the direction of gravity vector. This is done using the `rotatedBoxToCell` field which allows the inclination of the free surface of drilling mud with respect to the orthogonal directions of the domain mesh. Lastly, the `cylinderToCell` field is used to reassign the inner pipe volume and the slot volume to being occupied by air.

The `constant` folder also contains three files. These are the `g` file, the `transportProperties` file and the `turbulenceProperties` file.

The `g` file assigns the direction of the gravity vector. In this case for a 14° angle of ground entry, the magnitude of acceleration due to gravity of 9.81m $\cdot s^{-2}$ is resolved into 9.517m $\cdot s^{-2}$ in the negative x-direction and 2.379 m $\cdot s^{-2}$ in the negative z-direction.

The `transportProperties` file declares the fluid rheology model of Herschel-Bulkley to be adopted. The declaration of `nu0`, `tau0`, `k`, `n` and `rho` give the values of the parameters as explained in Section 4.3 accordingly. The corresponding values put in the `transportProperties` file are shown in Table 4.3. Note that the values of `tau0` and `k` are divided by the density of the fluid, hence that is why the base units for these two parameters contain no units of mass.

The `transportProperties` file also specifies the properties for the air phase. In this case for the benchmark simulation run, the kinematic viscosity is taken to be 1.511e-05 m^2/s and the density is taken to be 1.2047 kg/m^3. These are the standard properties of air at sea level and 20°C.

Finally, the `sigma` parameter which denotes the surface tension between the two phases is set to zero.

The `turbulenceProperties` file caters for the inclusion of turbulence models into the simulation. In this case, the turbulence is switched off by setting the `simulationType` to `laminar`.

This follows from the procedure outlined in Chapter 2 section 2.2.2. Assuming an equivalence of the Hershel-Bulkley numbers given by 2.4 and 2.16 we can say that:

$$Hb = \frac{\tau_0}{\tau_w} = \frac{\tau_0}{K}\frac{(R_2 - R_1)^n}{U_0^n} \tag{4.1}$$

This gives:

$$Hb = \frac{\tau_0}{K}\frac{(R_2 - R_1)^n}{U_0^n} = \frac{10}{0.16}\frac{(0.6-0.4)^0.7}{0.0717^0.7} = 130.3 \tag{4.2}$$

The above result also gives:

$$\tau_w = \frac{\tau_0}{Hb} = \frac{10}{130.3} = 0.077Pa \tag{4.3}$$

The Reynolds number is given by:

$$Re = \frac{12\rho V^2}{\tau_w} = \frac{12 \cdot 1100 \cdot 0.0717^2}{0.077} = 843. \tag{4.4}$$

The wall shear stress is expected to be in the 0.077Pa range. We are now assuming that although there is relative motion between the two walls of the annulus (since there is a penetration velocity at 0.15m/s) this will have a minimal effect on changing the flow regime and the above computations are valid for a zero-relative wall velocity. This is because the relative shearing motion of the borehole walls relative to the pipe will have a lower relative velocity with respect to the incoming flow form the inlet compared to the relative motion of the incoming flow with the HDPE pipe walls.

Recalling from Figure 2.6, that the transition to turbulence occurs at around 2500 to 3000 for a diameter ratio between 0.5 and 0.7 this means that the flow conditions are well within the laminar region for an anticipated Reynolds number of 843. It is also assumed that the jet of drilling fluid that will ensue when it falls through the slot will also be laminar.

Later on in the simulation campaign, another case will be simulated where the yield stress of the drilling mud tested will be 0.2Pa. In that case the Herschel-Bulkley number will be given by:

$$Hb = \frac{\tau_0}{K}\frac{(R_2 - R_1)^n}{U_0^n} = \frac{0.2}{0.16}\frac{(0.6-0.4)^{0.7}}{0.0717^{0.7}} = 2.61 \tag{4.5}$$

The expected wall shear stress is still the same at:

$$\tau_w = \frac{\tau_0}{Hb} = \frac{0.2}{2.61} = 0.077Pa \tag{4.6}$$

The Reynolds number thus stays the same. Both cases are in the laminar regime.

The last folder, `system`, contains files which specify settings related to numerical schemes and solver settings. This is where the aforementioned `setFieldsDict` would be stored. The relevant files are `controlDict`, `fvSolution` and `fvSchemes`.

For all the simulation runs including the benchmark case, the `maxAlphaCo` and the `maxCo` for the Courant number settings were set at 0.07 as was done with the validation tests. These are declared in the `controlDict` file.

The `fvSolution` file contains the solver settings for `interFoam` and the PIMPLE algorithm within it. With regards to the MULES solver, the `MULESCorr` corrector is turned on. `cAlpha` is turned on which means that a conservative compression is made. There is no subcycling as `nAlphaSubCycle` is set to 1. The number of MULES iterations, `nLimiterIter` is set to 3.

PIMPLE settings are set to have no momentum prediction, and no correction for non-orthogonality as the mesh was deemed to be of good quality.

The `fvSchemes` has an Euler backward scheme which is turned on under `ddtSchemes`. Gradients were computed linearly in our case and Laplacians were set to `Gauss linear corrected` as this is sufficient for our case. For divergence schemes for velocity, `Gauss linearUpwind grad(U)` is used and for the `alpha` phase (drilling mud) within `interFoam`, `Gauss vanLeer` scheme is used to maintain a bounded solution.

The setup for the benchmark case at time t = 0 is shown in Figure 4.5. The OpenFOAM files used for the benchmark simulation are found in Appendix A.

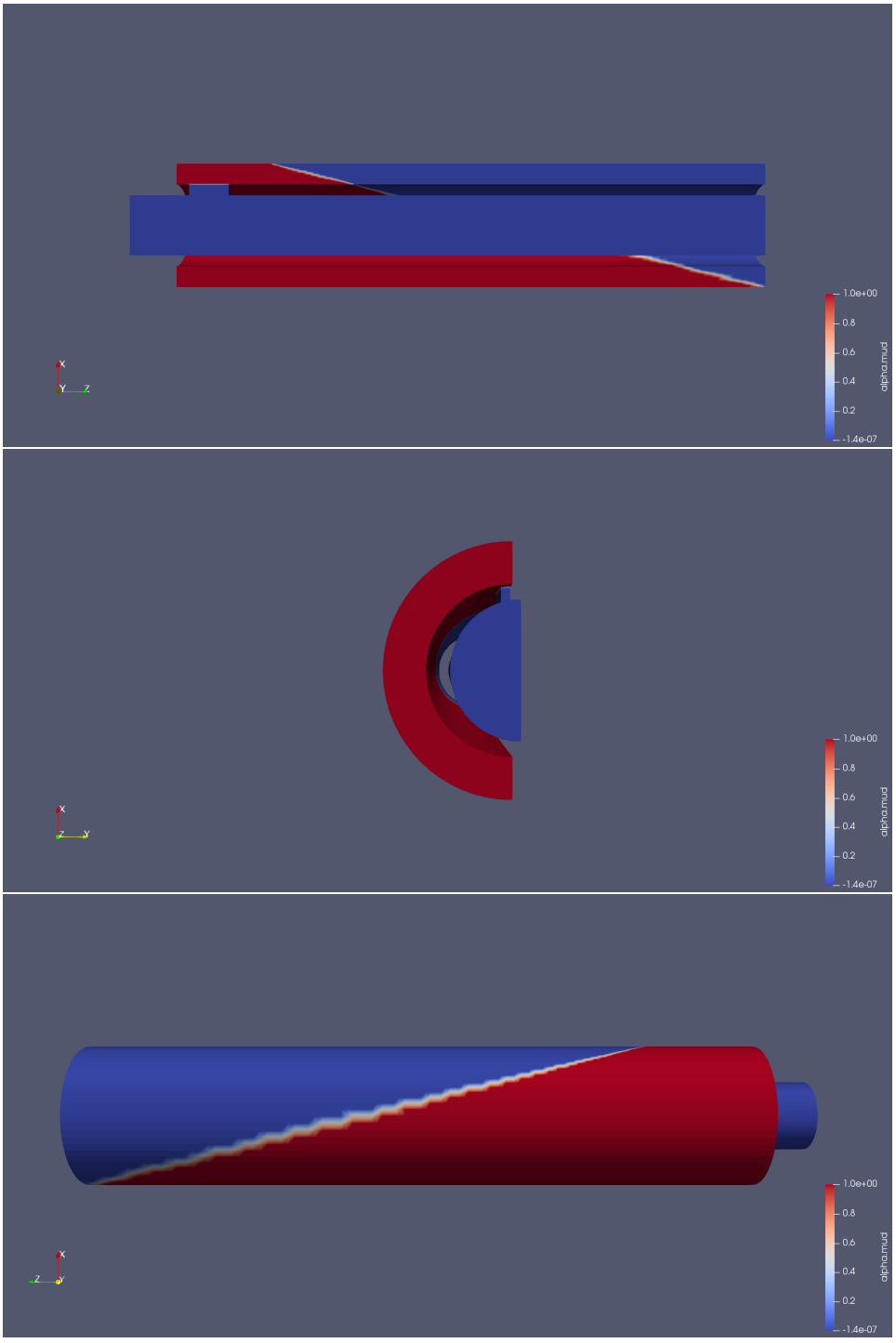

Figure 4.5: [Top] Side view of the benchmark case with the phases of the drilling mud and air added. [Middle] Inlet view of the same [Bottom] View of the other side showing the annulus region. The blue region is the air phase and the red volume is the drilling mud phase.

Table 4.4: The complete simulation set with every parameter changed from the benchmark case.

Case	Changed Parameter	Remark	Parameter in new case	Parameter in Benchmark
1	Yield Stress	The yield stress of the drilling mud is decreased.	0.2 Pa	10 Pa
2	Fluid Density	The density was reduced by 10%.	1000 kgm^{-3}	1100 kgm^{-3}
3	Pipe Slot Length	The slot length was increased by 30%	49.4cm	38cm
4	Flow Rate	The flow rate of the drilling mud coming through the inlet is increased by 30%	58.5 l/s	45 l/s
5	Entry Angle	The angle of entry entry is increased	18°	14°
6	Elliptical Slot	The slot area is changed from a rectangle to an ellipse of the same area	Elliptical shape semi-major axis: 19cm semi-minor axis: 5.73cm Area: 342cm^2	Rectangular shape Length: 38cm Width: 9cm Area: 342cm^2
7	Dead Volume	The dead volume inside the pipe is reduced by 75%	Cylindrical volume length: 14.5cm	Cylindrical volume length: 58cm
8	Newtonian Fluid	Substitute the drilling fluid with a fictitious Newtonian fluid	μ = 1.1e-3 kg/ms ρ = 1100 kgm^{-3}	Parameters of Table 4.3

4.7. The Simulation Cases

After the benchmark simulation was run, the rest of the simulations had one aspect which was changed in order to be compared with the initial benchmark case. The list of simulation runs is given in Table 4.4.

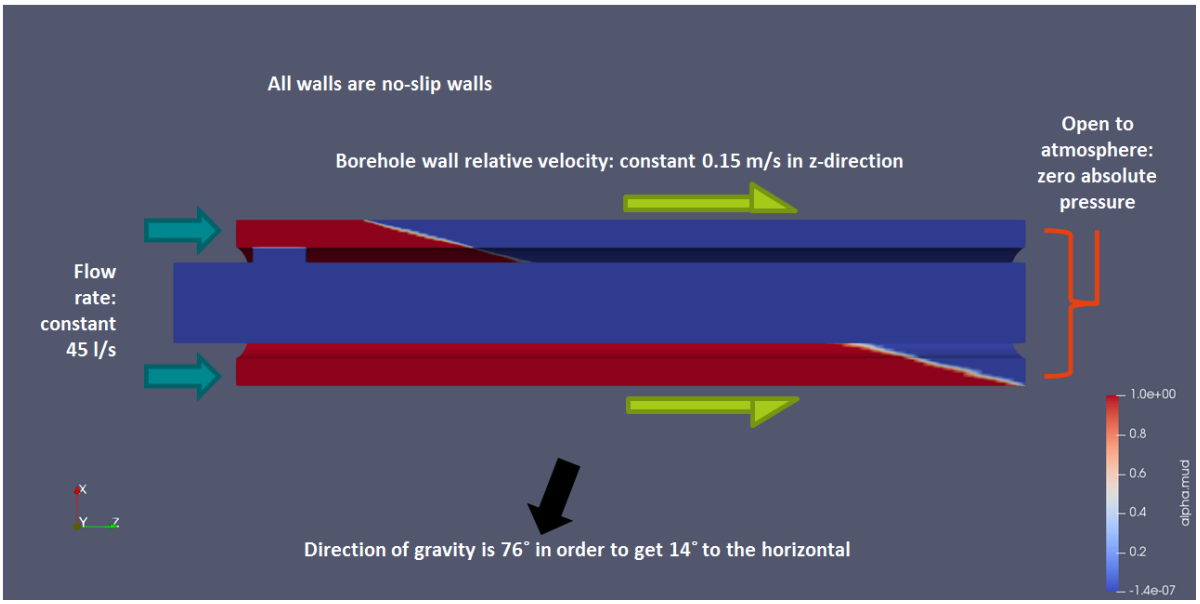

Figure 4.6: Boundary conditions for the benchmark case. All wall are no slip and the outermost walls of the borehole have a constant velocity of 0.15m/s in the z-direction. There is a constant uniform flow of 45l/s through the inlet. The direction of the vector for gravity is at 14° to the horizontal and the annulus region and the inner volume at the far end from the inlet are open to atmospheric pressure.

- The case for a reduction in yield stress of the drilling mud stems from the explanation given in section

4.3 due to the observed median yield stress for freshly mixed drilling fluids from the work of Talmon and Huisman [68].

- For the case of a reduction in fluid density, this was done merely to see if there are any effects on the performance from changing the density of the mud.
- The intuitive solution of trying to make the drilling mud flow faster from the annulus region into the inner pipe region by increasing the aperture area is investigated in case 3.
- For the sake of comparing to a case where there is 30% more flow from the mud return pump, case 4 investigates whether any lag in time for filling the inner pipe is due to there being insufficient flow from the pump itself.
- For case 5, the reason behind running this simulation is due to the possibility that during the initial few moments of the pullback process the hydrostatic head is the main driver of the flow in through the slot. With a steeper angle of entry at 18° as opposed to 14°, the hydrostatic pressure is increased.
- Case 6 tests the effect of the slot shape on the flow into the inner volume of the pipe. Since an ellipse possesses both roundedness and a degree of elongation that would be expected to be needed for structural strength for the aperture it was chosen as an alternative shape. Both the ellipse shape and the rectangular shape dimensions adopted have a length of 38cm. This means that they do not have the same equivalent hydraulic diameter if these two slots were to be treated as a duct. In fact it can be shown that the hydraulic diameter for the ellipse is 11% larger than that of the rectangular slot. The reason why both shapes were chosen to have the same length is so that the edges of the slot closest to the initial free surface and to the inlet could be both the same length in both cases. This is so that they are both exposed to the same hydrostatic pressure.

  The hydraulic diameter is given by:

$$\frac{4A}{P} \tag{4.7}$$

  For the rectangular slot of sides 38cm and 9cm, the hydraulic diameter is 14.6cm. The ellipse of semi-major axis length of 19cm and semi-minor axis length is 5.73cm has a perimeter of 83.4cm and thus hydraulic diameter of 16.4cm. This is 11% larger than that of the rectangular slot. However, their face area is the same.
- The influence of the dead volume's size is investigated with case 7.
- The last case for this simulation campaign is a case where the drilling mud is substituted with a fictitious fluid which is Newtonian. This has the same density of the drilling mud as the benchmark case at 1100kg/m^3. The constant dynamic viscosity is 1.1e-3kg/ms and the density is 1100 kg/m^3. The kinematic viscosity would be similar to that of water at 20° at 1E-6m^2/s. The same flow rate as the benchmark case is active. For an annulus flow, the turbulent regime starts as with normal cylindrical pipe flows at 2100 [27]. The Reynolds number for annulus flow is given by:

$$Re = \frac{2\rho U(R_2 - R_1)}{\mu} \tag{4.8}$$

  For this case, U is 0.0717m/s which gives a Reynolds number of 37400 which is in the turbulent regime. It is therefore assumed that the flow comes in from the inlet turbulent and this state persists throughout the whole simulation.

  The turbulence model used in this case was the k-epsilon model, which is a Reynolds-averaged stress model. This is implemented in OpenFOAM via the `turbulenceProperties` file in the 'constant folder. Additional files are needed in the `0` folder are those for `epsilon`, `k` and `nut`.

  In the `nut` file, the turbulent viscosity is specified as being zero at the solid walls.

  In the `k` file, the turbulent kinetic energy conditions are specified. For the inlet, the turbulent intensity is specified and is taken to have a value of 0.05.

In the `epsilon` file, the turbulent kinetic energy dissipation rate is specified. All solid walls are given an `epsilonWallFunction` and a uniform value of 200. Also the inlet is given turbulent mixing length of 0.005.

5

Results and Discussion

The results aimed to elicit the following details from the simulations:

1. How the fluid behaves as it acts under the influence of gravity and as it enters the inlet from below.
2. How fast the inside volume of the pipe accumulates drilling mud.
3. How fast the two free surfaces reach an equal or comparable level above a datum point common to both levels.

5.1. Post-Processing

All post-processing of the data from the OpenFOAM simulations are done with ParaView, which is an open-source visualisation application provided as a bundle along with OpenFOAM upon installation on one's workstation.

5.2. Benchmark Case Two-Phase Simulation

The simulation of the two-phase simulation of the benchmark case gives an insight into how the drilling mud is typically behaving during the first few seconds of the pullback. Snapshots are shown in Figures 5.1 and 5.2 at the initial condition at t = 0 and then at 5s and every 5 seconds until the final time step at 25s.

A Threshold filter is applied to the domain with the limiting parameter being the volume phase fraction `alpha.mud` set at 0.5. This would mean that the region of the domain bearing the air-drilling mud interface would be clearly seen in the animation of the simulation. The domain is then also given a colour scale map for velocity magnitude. Red indicates high velocities and blue indicates regions nearly at rest.

At the initial condition, the free surface is planar and there is yet no drilling mud in the inner volume. After that drilling mud starts to come in with sufficient pressure as to come through perpendicular to the slot. The jet strikes the surface of the inner pipe opposite to the slot and runs up the slopes of the circumference of the inner pipe. After 5 seconds the dead volume in the inner pipe is already almost completely filled. By 10 seconds there is a new free surface inside the inner volume which spans the entire sloped cross-section.

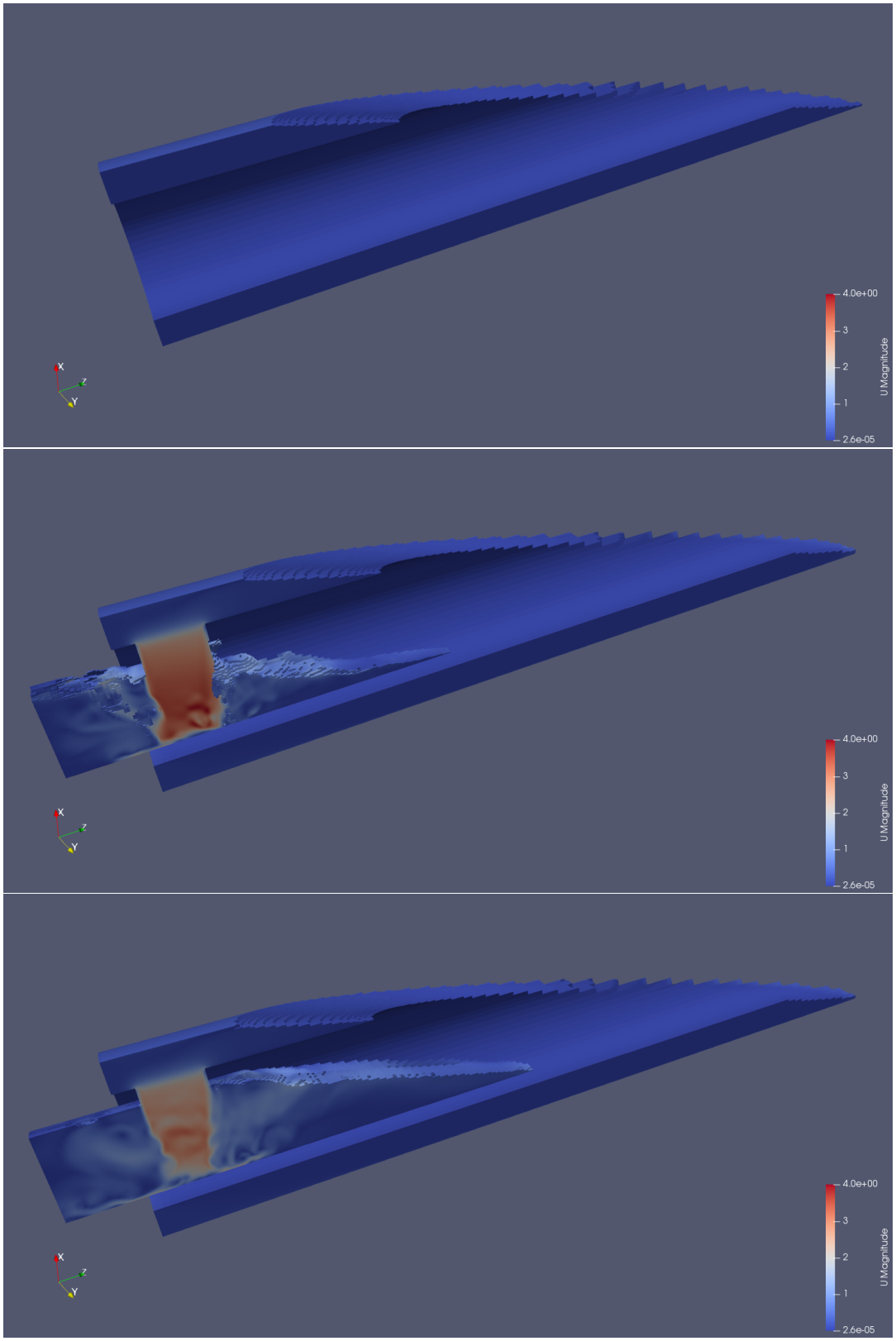

Figure 5.1: The flow of the drilling mud from the annulus region into the inner volume. What is shown is only the drilling mud phase. Redder regions indicate higher velocity. [Top] At time t = 0. The drilling mud is still in the annulus region and the inner pipe volume is empty. [Middle] At time t = 5s, already an appreciable amount of drilling mud has collected in the inner pipe volume and almost completely filled the dead volume [Bottom] At time t = 10s there is a continuous air-mud interface which is to the right of the slot and spans the entire cross-section of the inner pipe volume. Note the velocity scales at the bottom-right corner of every snapshot.

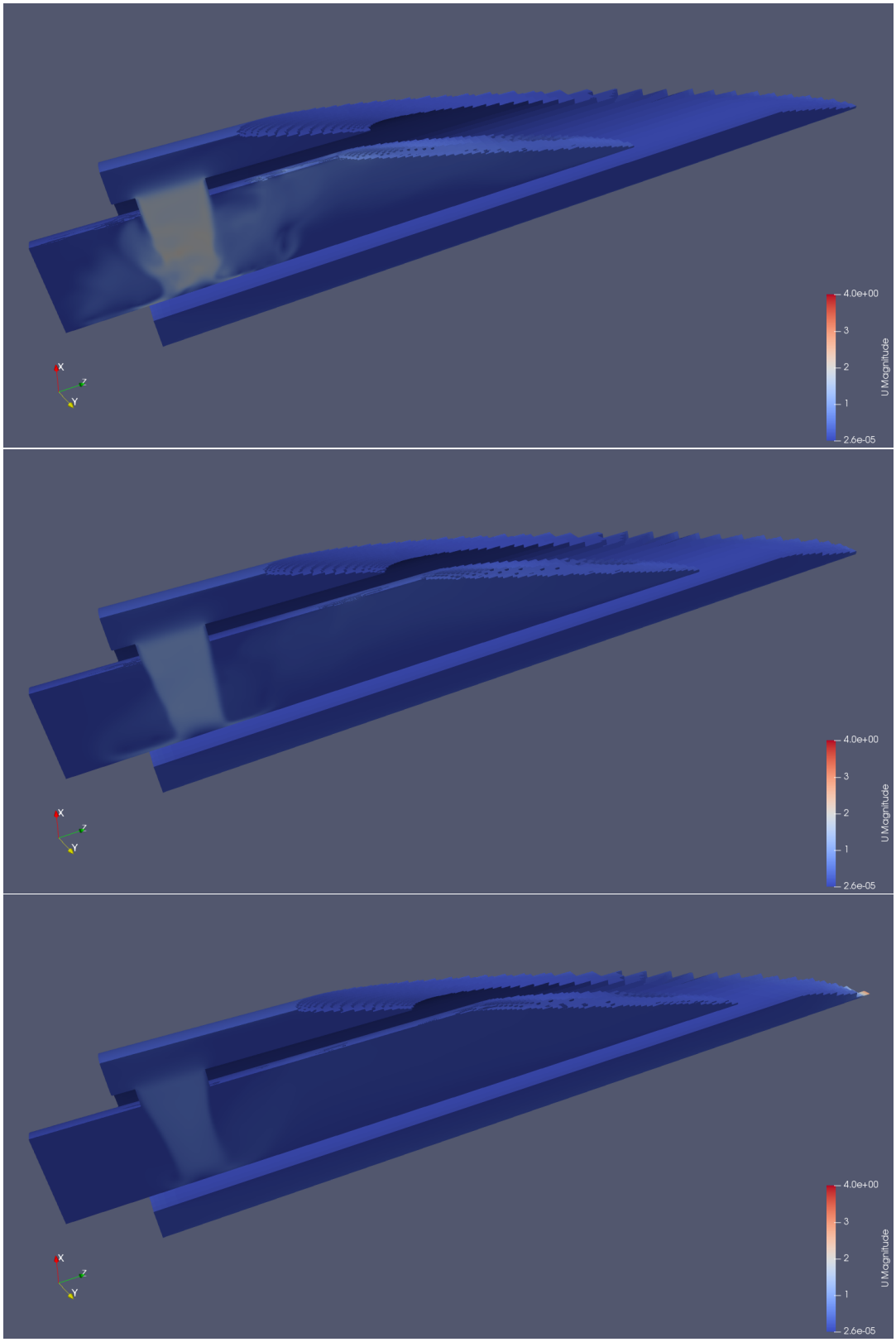

Figure 5.2: The flow of the drilling mud from the annulus region into the inner volume. What is shown is only the drilling mud phase. Note the velocity scales at the bottom-right corner of the snapshots. Redder regions indicate higher velocity. [Top] At time t = 15s. [Middle] At time t = 20s, the mud levels in the annulus region and the inner volume region are comparable. [Bottom] At time t = 25s the mud levels inside and outside the pipe appear to rise together with the same pace.

By 20 seconds the interface inside the pipe seems to be caught up with the interface in the annulus region.

At 25 seconds, the submerged jet of drilling mud coming into the inner volume is seen to be skewed upwards which suggests that there is stagnant drilling mud in that volume which is recirculating in the dead volume.

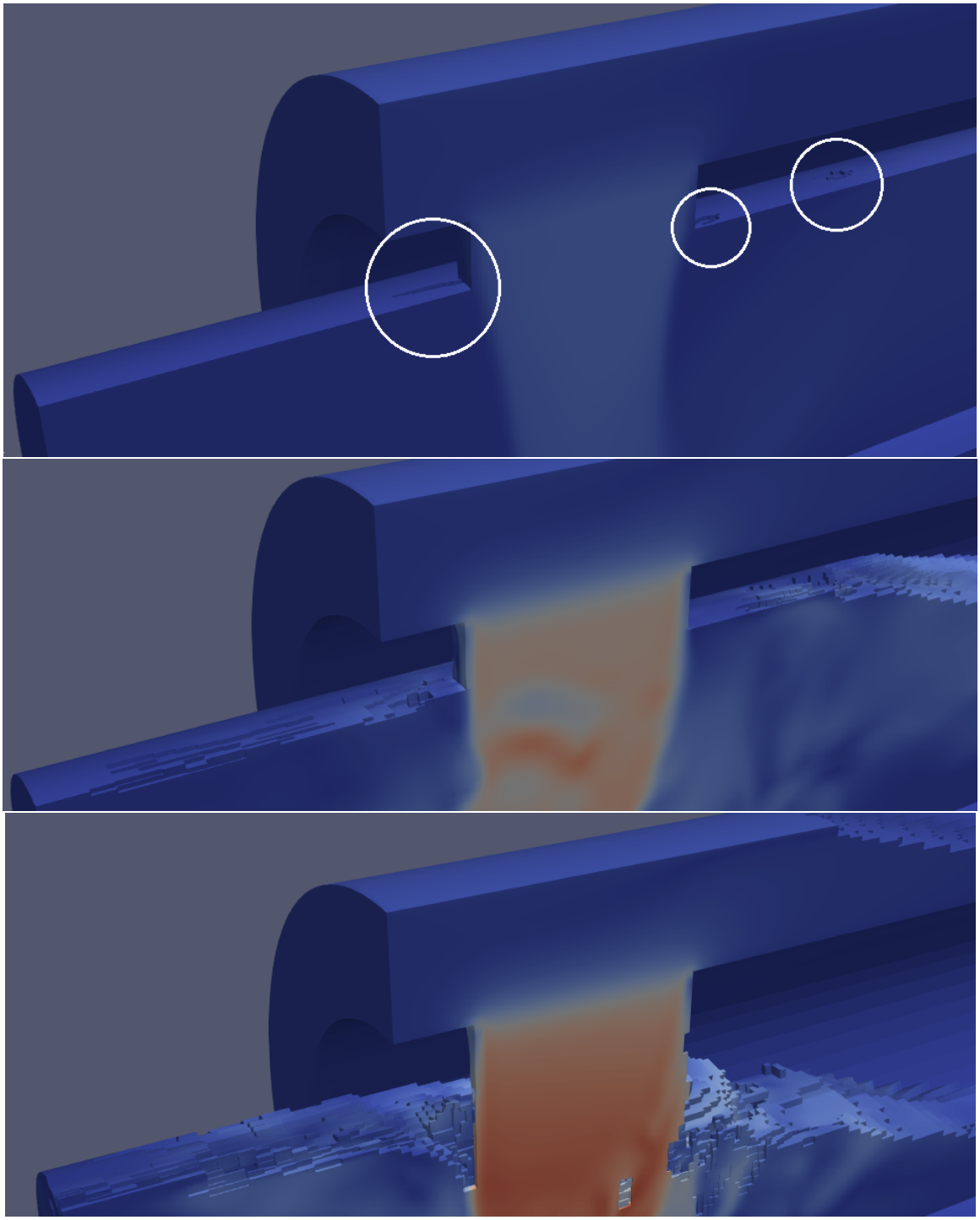

Figure 5.3: [Top] At time t = 25s the jet is fully developed and in a quasi-transient state. There are some air inclusions right at the entry into the inner volume. They are circled in white. [Middle and Bottom] Earlier time steps show the origin of these air inclusions.

At the upper end of the inner volume, individual regions of air are seen at 25s as in Figure 5.3. Their origin could be traced back to 6s from the initial condition when the dead volume reaches the state of being almost completely full. The jet also contributes to the spread and sustaining of these air pockets. It is observed that the diminishment of these air pockets is in pace with the movement of the free surface in the inner volume.

It is assumed that these air inclusions have a minor effect on the buoyancy of the pipe in the borehole. This is because a line plot of the volume fraction phase along several lines parallel to the pipe axes in ParaView

Table 5.1: Three levels of mesh refinement used for the benchmark case. The number of cells for each level are shown.

Mesh	Number of cells
1 - Coarse	734632
2 - Medium	1136840
3 - Fine	1478200

produced values on the order of 0.98. This indicates that these air inclusions are minimal and there are no sizeable bubbles in the inner volume.

5.3. Convergence Study

The initial mesh of the benchmark case was refined twice in order to check for convergence. The number of cells for the three mesh levels are shown in Table 5.1. The mass flow rates of drilling fluid into the slot show that for the first 2 seconds of the simulation, convergence is reached since there is good agreement between the mass flow rates as shown in Figure 5.4. The results that came after around 4 hours of simulation time for each of the three mesh levels is shown. This is why the coarsest mesh level 1 has time steps up to 3 seconds and mesh level 3, the finest, has up to 1 second. The other cases were not checked for mesh convergence due to either the changed geometry not changing the physics of the case appreciably (as with the longer slot case) or due to a minimal change in the inlet conditions (as with the decreased yield stress and the increased inlet flow rate). The decrease in yield stress case still retains the flow in the regime of a high Herschel-Bulkley number as can be seen from Figure 2.13. The plug ratio would still remain high. Thus any refinement in the radial direction of the mesh geometry is not required.

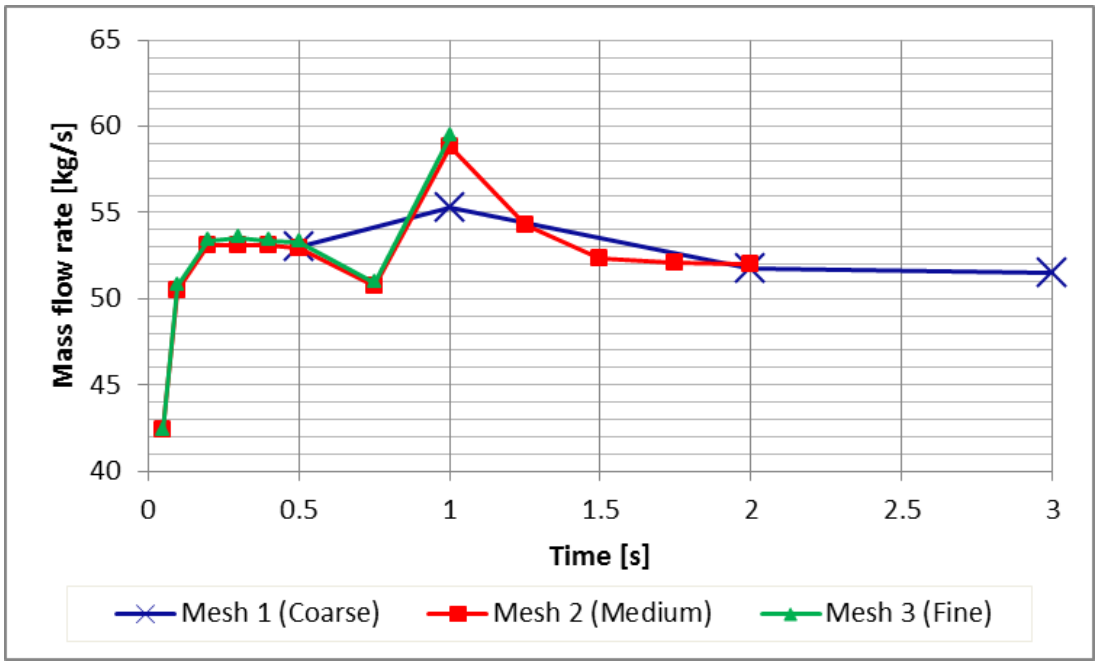

Figure 5.4: Mass flow rate of drilling mud through the slot plotted against time for the first 2 seconds of simulation time for three levels of mesh refinement. This was done on the benchmark case. The results that came after around 4 hours of simulation time for each of the three mesh levels is shown. This is why the coarsest mesh level 1 has time steps up to 3 seconds and mesh level 3, the finest, has up to 1 second.

5.4. Volumetric Flow rate vs. Time

The average volumetric flow rate at all the time steps of the simulation were extracted by applying a Slice filter plane tangential to the inner diameter of the pipe on ParaView. The flow rate is thus measured right at the point of entry into the inner volume of the pipe. The values for the velocities at each of the cell faces at the slot cross-section are extracted and then averaged based on the number of cell faces.

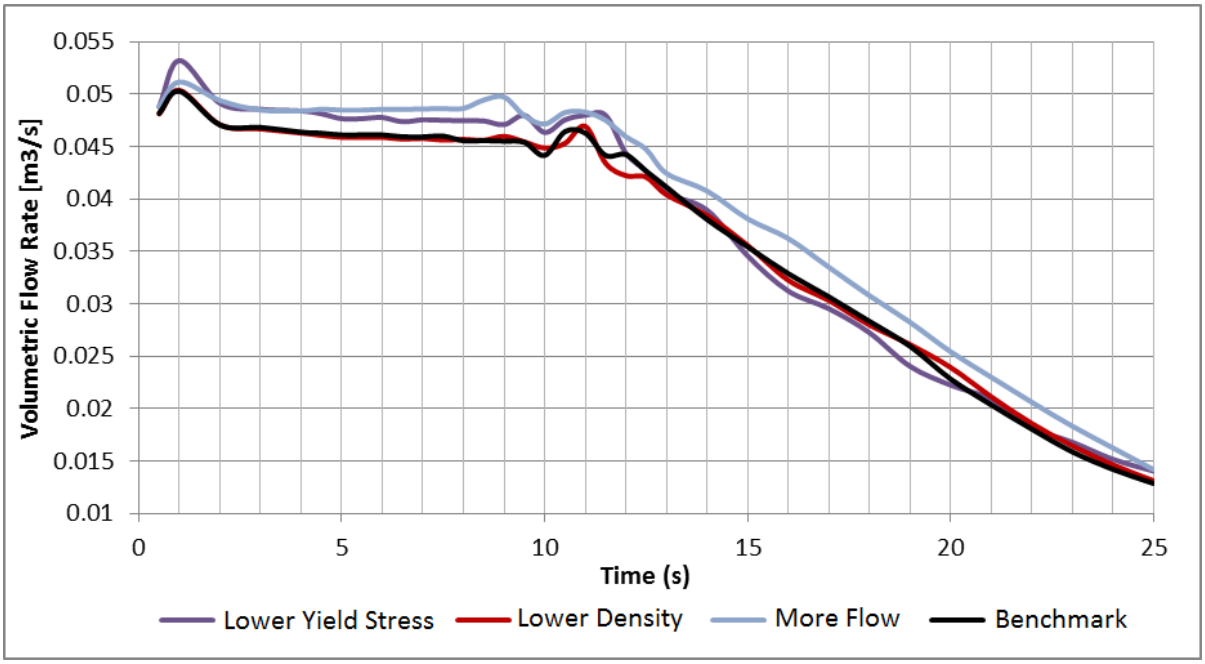

Figure 5.5: Volumetric flow rate through the slot for the benchmark case and an additional three other cases of lower density of drilling mud, lower yield stress of drilling mud and a higher mud pump flow rate. Note the initial phase of flow through the slot where the decrease in flow rate with time is much slower than the decrease we see after around 10s. This is the initial phase where the volume of drilling mud above the slot is drained through the slot and enters the inner pipe volume. The flow rate plateaus for the benchmark case after around 25s.

From Figure 5.5 we can see the volumetric flow rate through the slot plotted against time. The first three test cases are compared with the benchmark case. One can notice that the first 10 seconds are characterized by a linear decrease in flow rate followed by a buffer time of around 3 seconds after which the flow rate decreases also linearly but at a much faster rate which is estimated to be 8 times higher than that before 10 seconds. Therefore there are two distinct trends for the flow into the slot before 10s and then after 10s. The flow after 25s is not considered since it was not simulated, but one can already see that it starts to reach a plateau at 25s if one notes the black graph for the benchmark case in Figure 5.5.

For the benchmark case, the average volumetric flow rate is $0.047 m^3/s$.

Upon using a Glyph vector filter coupled with a Threshold filter to see only the mud phase on ParaView, one can see the velocity vector directions of all the regions in the domain. Shown in Figures 5.6 and 5.7 are snapshots of the time steps t = 0.25s, 5s, 10s, 15s, 20s and 25s. The drilling mud phase is shown as the transparent, mostly blue-tinged block. The vertical plane parallel to the x-y plane and at around 20cm away from the edge of the slot in the upper direction holds all the arrow vectors. One can notice the half-ring of red arrows at the borehole diameter indicating the relative velocity of the borehole wall to the pipe as it enters the borehole. The drilling mud in the lower half of the annulus still moves upwards because it is seen flowing in the positive z-direction. The fluid sitting on the upper half of the annulus is flowing in the direction of the slot aperture. The last picture of Figure 5.7 indicates that at 25s, the majority of the fluid, both in the annulus region and the inner pipe volume is moving upwards in the positive z-direction. The fact that some of the arrows are still directed towards the slot indicates that the inner volume is still being filled with fluid from the upper side of the slot, but its origin is from the inlet, not the volume above the slot.

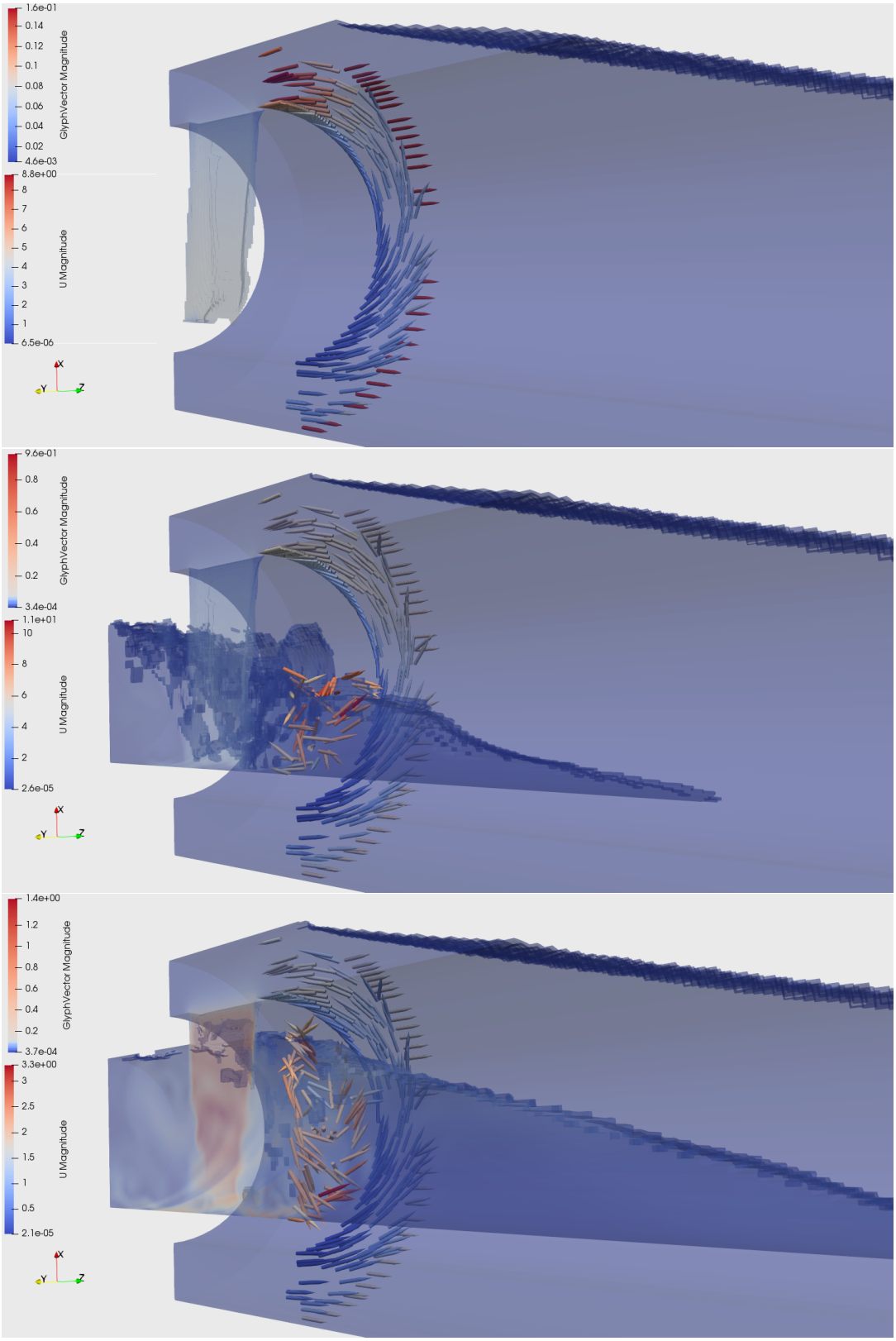

Figure 5.6: [Top] Arrow vectors at a plane 20cm away from the edge of the slot indicate that the absolute velocity of the fluid at the borehole wall is indeed 0.15m/s. The vectors at the upper half the annulus region indicate higher velocities from the rush of mud into the slot, while the fluid at the lower half of the annulus is moving much slower. The first full column of mud falling into the inner pipe is shown to form. [Middle] Same but now at 5s. The fluid inside the inner pipe does not exceed 1m/s in the plane shown.[Bottom] At 10s the inner pipe is experiencing what looks to be an anti-clockwise swirl of mud.

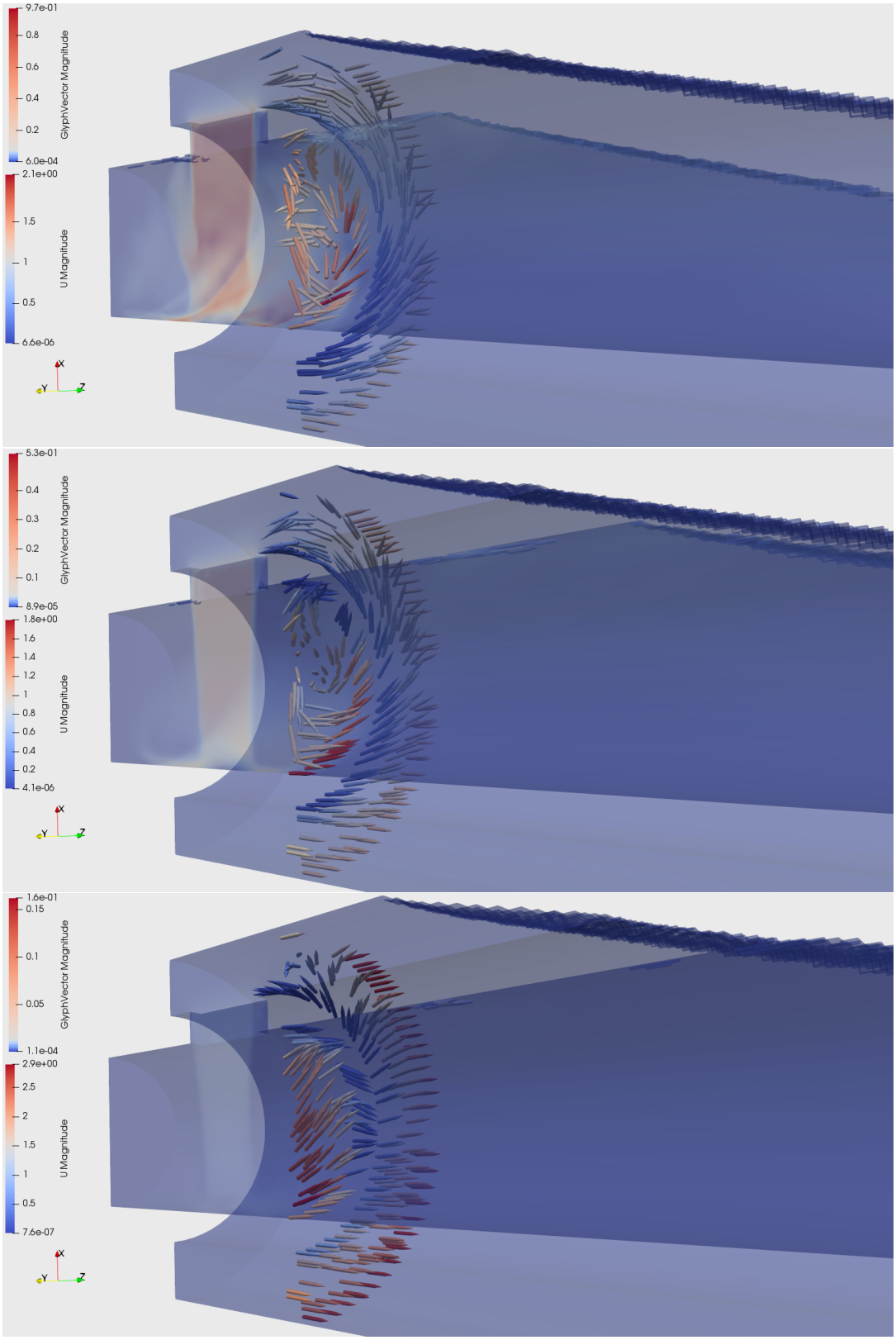

Figure 5.7: [Top] Drilling mud phase and velocity vectors at 15s. [Middle] Same at 20s. [Bottom] Same at 25s. As can be seen most of the mud both inside and outside the pipe is moving upwards towards the ground surface in the positive z-direction.

The volume of fluid that lies above the slot is finite. Therefore product of the average volumetric flow rate before the flow structure change and the time before this change is constant. This is also reflected in the graphs of Figures 5.5 and 5.8, where for example for the case of the steeper angle an average flow rate of

0.07m^3/s was sustained for around 7 seconds and for the case of the longer slot, 0.06m^3/s was sustained for 8 seconds indicating that there is around 47 to 50m^3 of drilling mud that passes through the slot before the flow rate starts to diminish with time.

5.5. Parametric Effects

The parameters listed earlier in Section 4.6 in Table 4.4 are discussed below. The cases of a decreased yield stress, lower drilling mud density, increased drilling mud flow rate are compared with the benchmark case in Figure 5.5. The rest of the cases - for a steeper pipe angle, elliptical pipe wall hole and a longer wall slot are compared with the benchmark case and with the behaviour of a fictitious Newtonian drilling mud in Figure 5.8. Each of the observations in this section will be rediscussed in the Discussion Section of 5.8.

5.5.1. Effect of Yield Stress

The yield stress test case is that where the yield stress of the drilling mud is reduced from 10Pa for the benchmark case to 0.2Pa.

As we can see from Figure 5.5, the only discernible effect for a drilling mud with a lower yield stress is during the time before the flow source redistribution at 10s there is an average of 4% higher volumetric flow rate. After 10s both the benchmark case and the modified yield stress case diminish in their volumetric flow rate at the same degree.

5.5.2. Effect of Less Density

The case where the density of the drilling mud is reduced from 1100kg/m^3 to 1000kg/m^3 whilst keeping all other parameters constant has minimal effect on improving the passing of drilling mud into the slot.

5.5.3. Effect of More Flow

Increasing the flow rate from the inlet by 30% from 45l/s to 58.5l/s has the effect of increasing the flow rate into the slot by 5.3% over the period before 10s compared to the benchmark case.

As we can see from Figure 5.5, after 10s the increase in slot flow rate compared to the benchmark case is at 8.7%. The increase in the mean flow rate affected the initial flow rate into the slot which indicates that during the first seconds, the flow into the slot is indeed not coming solely from the fluid above the slot but also the domain inlet as well.

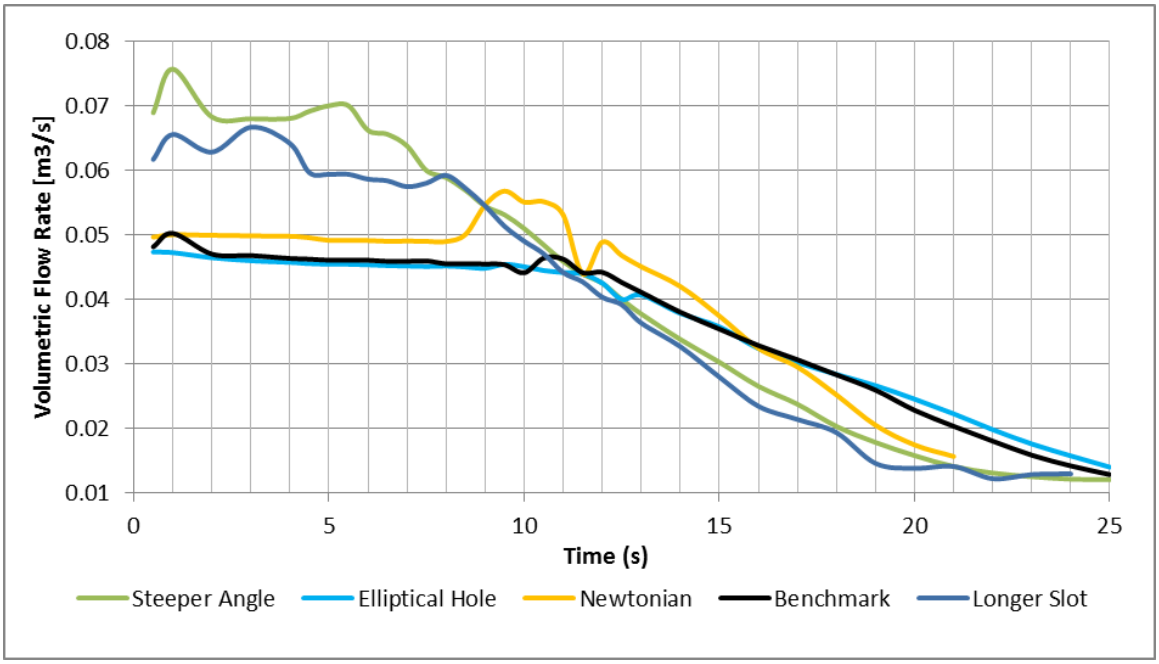

Figure 5.8: Volumetric flowrate through the slot for the benchmark case and an additional four other cases of a fictitious Newtonian fluid, an elliptical aperture, a steeper entry angle and a longer slot.

Table 5.2: The improvement in accumulation time inside the inner volume of the HDPE pipe after 20s for all tested cases. Note that for a given fixed pipe angle to the horizontal, the longer slot case where the slot was increased in length by 30% from the benchmark case provided the best increase in the accumulated volume inside the inner pipe volume.

Case	Accumulation Volume at 20s [m^3]	% Increase from Benchmark
Benchmark Case	0.626	0
Elliptical Hole	0.618	-1.35
Lower Density	0.624	-0.33
Lower Yield Stress	0.641	2.44
More Flow	0.663	5.89
Newtonian Fluid	0.67	7.00
Longer Slot	0.691	10.45
Steeper Angle	0.744	18.83

5.5.4. Effect of Steeper Angle

A steeper pipe entry angle of 18° has the effect of increasing the initial flow rate that comes above the slot. This is due to the higher hydrostatic pressure that results from a steeper angle.

Whereas the shift to a flow into the slot that is dominated by flow from the inlet occurs at 10s in the benchmark case, with a steeper angle, this shift happens around 4 to 6 seconds from the initial condition.

5.5.5. Effect of an Elliptical Hole

Using an elliptical hole also has no great effect on the characteristics of the flow patterns at any time during the simulation.

This means that for a given slot area, the flow through the slot is constant.

5.5.6. Effect of a Newtonian Fluid

The replacement by the drilling mud by a fictitious Newtonian fluid of the same density as the drilling mud and a kinematic viscosity similar to that of water, gives an increase by 5.7% of the flow rate into the slot in the initial stage. The second stage gives a faster decrease in the flow rate reduction.

Since the effective viscosity of this fictitious fluid is much lower than that of a typical drilling mud so the reduced viscous resistance contributed to a faster ingress of drilling mud into the slot during the first phase of the duration of the 25s simulation.

As secondary effect, the decrease in effective viscosity is the cause of the greater spike in flow rate during the change in flow structure at 10s.

5.5.7. Effect of a Longer Slot

An increase by 30% in the slot length from 38cm to 49.4cm yields an increase in the average flow rate at the beginning by 47% from 0.047 to 0.069m^3/s.

It is this modification to the benchmark case and the geometry of the pipeline that produces the highest increase in slot discharge rate for a given angle that the pipe makes with the horizontal.

5.6. Accumulation Time

In order to compare the rapidity by which each simulation case takes in drilling mud, the accumulated drilling mud after 20 seconds is compared.

Table 5.2 shows that for a given pipe geometry and borehole size, increasing the slot length by 30% will increase the accumulation speed by 10.45%. An increase of the angle of ground entry of 4° increased the accumulation speed by 18.83%.

These two improvements are both more effective than increasing the mud pump's flow by 30%.

5.7. The Air-Drilling Mud Interface

An additional simulation was carried out in order to see what is the effect of smaller dead volume. The dead volume is reduced by 75% in this case. The air-drilling mud interface position for both the inner volume and the annulus region is tracked for the smaller dead volume case, the longer slot case and the benchmark case.

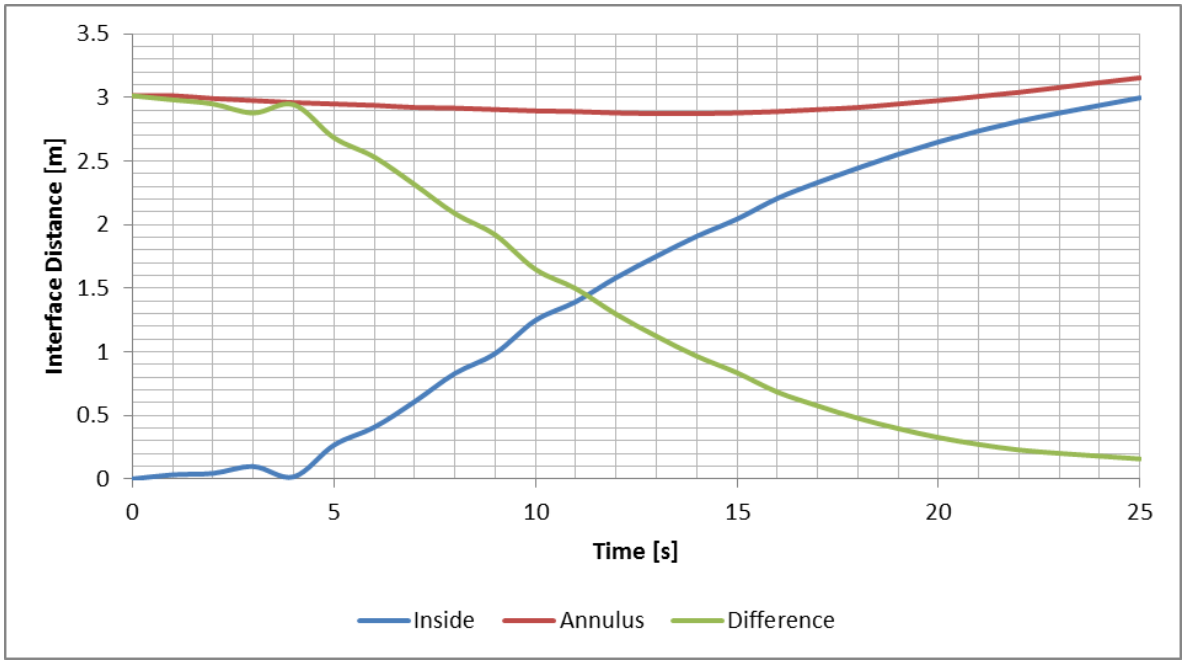

Figure 5.9: Distance of the air-mud interfaces inside the inner volume and outside in the annulus region from the datum point which is the midplane of the slot. This is for the benchmark case. For the annulus region, the level recedes and rises again after t = 13s. The inner pipe volume rises 5s after the initial condition.

Figure 5.9 shows the interface heights above the midplane of the slot for the benchmark case. The annulus level recedes as drilling mud discharges into the inner volume and at around 13s the level starts rising again back to the direction where it came from. The interface on the inside of the pipe becomes significant at around 4 seconds. The two interfaces keep a difference in level at 17cm.

This plot was extracted by using the 'Plot over Line' filter utility on ParaView. The volume phase fraction is plotted along the pipe axial distance away from the slot midplane. This is done for both the annulus region and for the inner volume and for all time-steps. The point where the volume phase fraction is 0.5 is taken to be the air-drilling fluid interface.

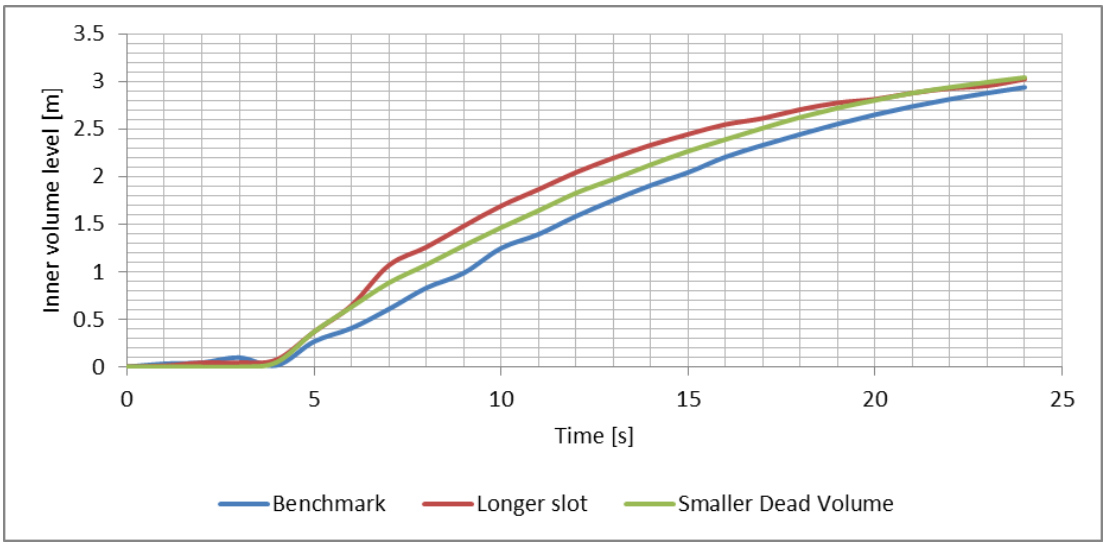

Figure 5.10: Inner volume liquid level evolution with time comparison between the benchmark case, the longer slot case and the smaller dead volume case. Note that longer slot case still is more responsive despite the head start of the smaller dead volume case in filling the inner pipe.

Comparison of the benchmark case with the longer slot case and smaller dead volume case shows that the longer slot case takes the lead already by 7 seconds. This is seen in Figure 5.10.

Table 5.3: The difference in fluid levels inside and outside the pipe after 20s for the benchmark, the longer slot and smaller dead volume case.

Case	Difference in Drilling Fluid level [m]
Benchmark	0.18
Longer slot	0.10
Smaller Dead Volume	0.17

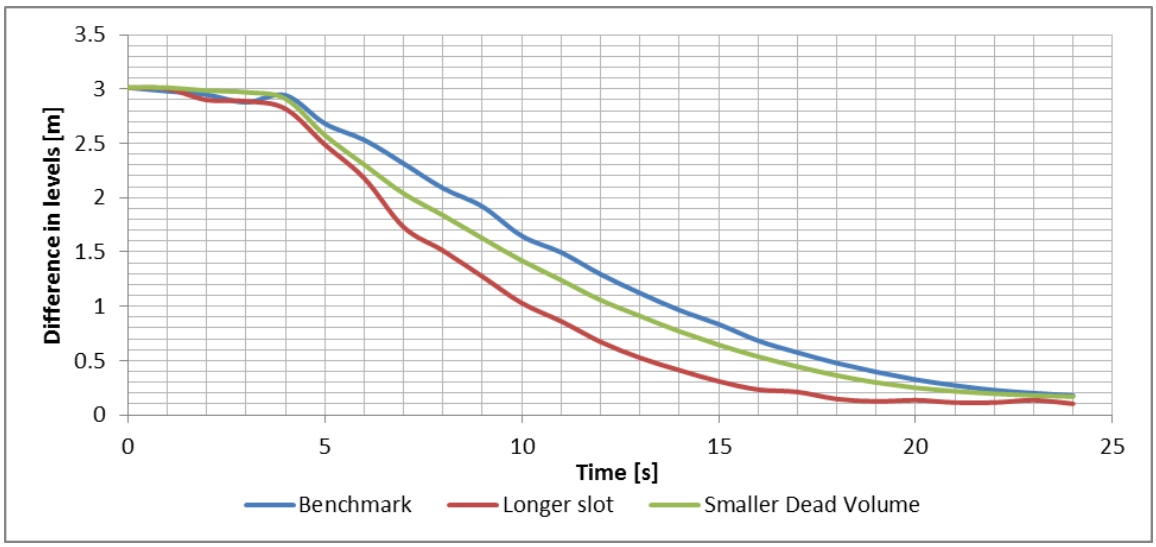

Figure 5.11: Change in the difference between drilling mud levels between the inside and the annulus region. The longer slot case retains the lowest difference compared to a smaller dead volume. The precise values for the annulus-inner volume level difference at 20s is given in Table 5.3.

The difference in the level between the annulus region and the inner volume is kept to be the least for the case of the longer slot at 10cm as can be seen from Table 5.3.

This analysis concludes that the effect of a smaller dead volume within the inner pipe does indeed help in preventing that there is a significant mismatch in the mud levels between the inside and the outside of the pipe and a longer slot also prevents this from happening and is also more effective even when the dead volume is still 4 times larger than the smaller dead volume simulation. This is seen in Figure 5.11 since the red curve representing the longer slot case maintains a lower difference between the annulus and inner pipe mud levels already at time t = 7s compared to the benchmark and smaller dead volume cases.

A faster response to maintaining a small difference between mud levels inside and outside pipe is important in preventing buoyancy issues further on during the pullback process.

A slot 30% longer compared to the current practice thus proves to be a good method of assuring buoyancy control by passive ballasting.

5.8. Discussion

These results show that the aperture can be treated as a slot since the aspect ratio of the slot with its very short depth (the thickness of the pipe wall) cannot be treated as a duct. Therefore any further investigation into the matter using hydraulic diameters is unnecessary since the slot is in effect a simple opening and not a duct as would be the case for two tanks filled with unequal amounts of liquid and connected via a pipe for example.

The reduction of the yield stress from 10Pa which is based on the drilling mud characterization in Rabiei et al. [60] to 0.2Pa which is taken from Talmon and Huisman [68] is a means to compare the effect of including reaming in the process of pullback. This is because 10Pa is representative of a typical drilling mud that has been mixed with cuttings from the reaming process incorporated within pullback. 0.2Pa represents a drilling mud that is freshly produced from an on-field mixer.

Recall that the case with the reduced yield stress achieved 2.44% more filling of the inner volume within 20s compared to the benchmark case. This is only a slight increase.

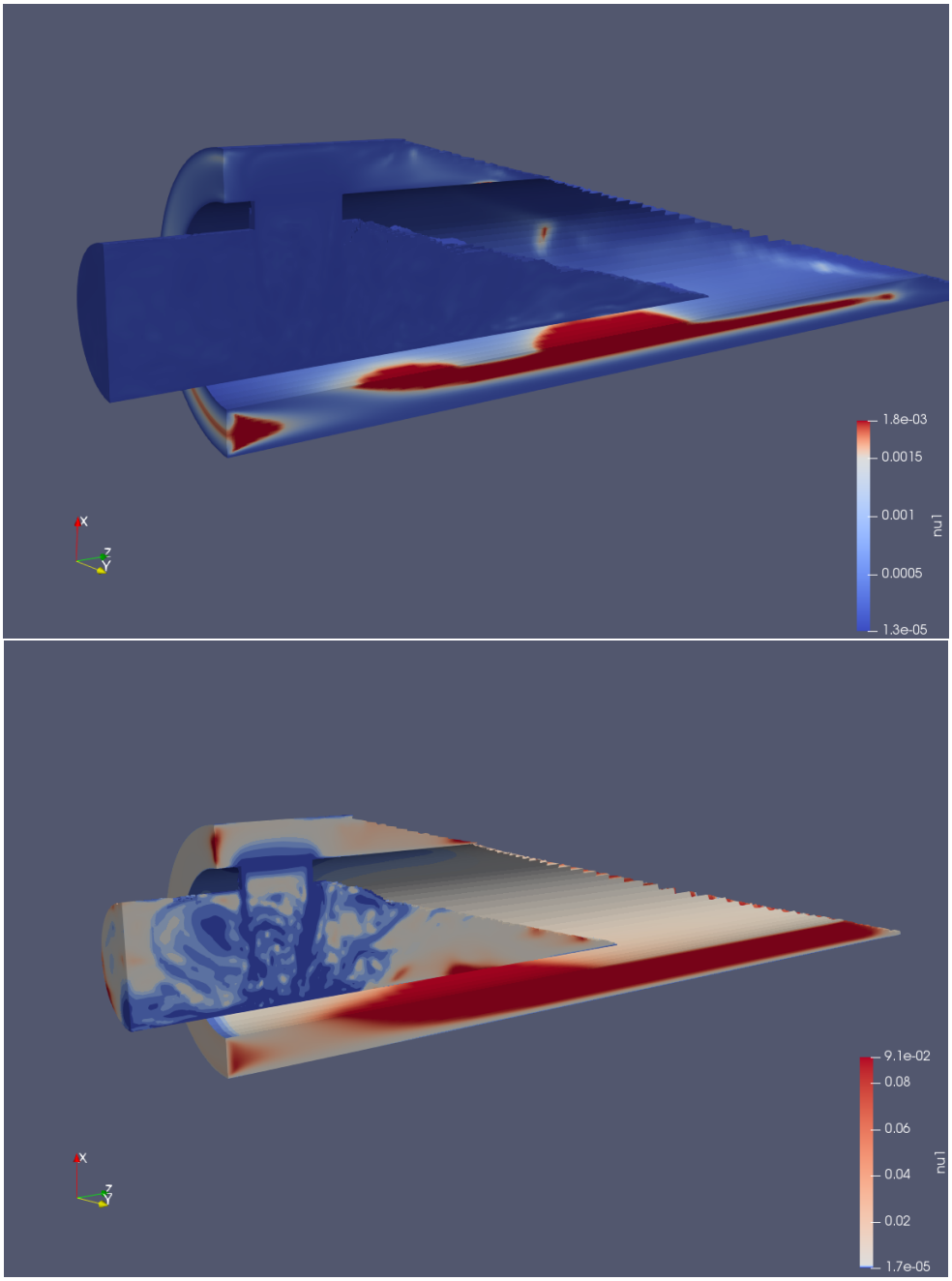

Figure 5.12: Comparison of effective viscosity in the computational domain between the benchmark case (Top) and the reduced yield stress case (Bottom). Scale bars show the effective viscosity, which in OpenFOAM is written as `nu1`.

From the two diagrams of the domain for the reduced yield stress case and the benchmark case in Figure 5.12 one can see that the benchmark case has most of its domain above 1.65Pa·s of effective dynamic viscosity. This contrasts with the reduced yield stress case where this limit is reached only at the bottom end of the annulus region marked in red. This means that there effects attributed to unyielded regions are more pronounced in the benchmark case but still these effects are not the main contributors to the difference in filling time since when compared to the Newtonian fluid case, the flow into the slot is faster than the benchmark by 7%.

The Newtonian fluid case had a fixed viscosity of 0.001Pa·s. Therefore an increase in the flow through the slot is mainly attributable to the decreased viscosity and not due to the diminished yield pseudoplastic effects. The reduced effective viscosity, which in OpenFOAM appears as `nu1`, as can also be seen in Figure 5.12 shows that there are benefits to having a lower effective kinematic viscosity because of reasons attributable to Poiseuille's law:

$$Q = \frac{\Delta p \pi R^4}{8 \mu L} \tag{5.1}$$

where decreasing the effective viscosity μ, would increase the flow rate Q for a given pressure difference Δp, pipe length L and radius R.

The effect of increasing the flow rate from the inlet by 30% increased the efficiency of passing drilling mud through the slot by 5.89%. From a physical perspective this meant that there was an increase in the influence of momentum. Any improvement from this modification would be solely from the increased flow rate from the inlet and not from the volume of drilling mud above the slot. Therefore this improvement would only come about from an increase in the drilling mud pump.

The investigation of the reduction of the density from 1100kg/m^3 to 1000kg/m^3 was meant to find whether a lower bentonite content associated with a lowered density is another means by which more drilling mud can be passed through the slot. The effect was found to be minimal and in fact decreased the accumulation after 20s by 0.33% as compared to the benchmark case. If density would have any effect in this situation it would be because of the acceleration of the fluid, and that happens during the initial stage where the volume of fluid above the slot is falling through into the slot. This means that gravity as an individual force would affect the ingress of drilling mud into the slot but to a small degree. Further investigation into this matter is needed to fully describe and characterise this effect, but for the purpose of this study this test has settled the question whether the bentonite content has any effect on the accumulation.

The effect of the penetration rate velocity was not explicitly investigated since its magnitude of 0.15m/s was kept constant throughout all the simulations. From Figure 5.6 we can see that there is indeed an effect of shearing away the adjacent drilling mud from the motion of the wall as expected but there are no appreciable effects of this wall motion on the flow of the drilling mud inside to the slot at least for this wall velocity.

Finally some comments are in order about the effect of the angle of entry of the pipe into the borehole. The case where the angle of entry is at 18° is a deviation from the benchmark case of 14° of inclination. It was correctly assumed that the contribution to the flow into the slot at the initial period before the flow restructuring was being driven by gravity. This can be proven by taking the peak velocity of the incoming jet at 0.25s and compare the results from the benchmark case and the steeper angle case. From energy conservation, the square of the jet velocity is proportional to the height of the liquid column. Thus the ratio of the squares of the jet velocities and the ratio of the column heights for both cases should be comparable. Thus we have:

$$\frac{v_1^2}{v_2^2} = \frac{h_1}{h_2} \tag{5.2}$$

Now the column height of liquid is given by :

$$d \cdot sin(\theta) \tag{5.3}$$

Where d is the fluid level inside the annulus region measured along and coaxial with the pipe.
The comparison reduces to:

$$\frac{v_1^2}{v_2^2} = \frac{sin(\theta_1)}{sin(\theta_2)} \tag{5.4}$$

For a peak jet velocity of 4.7 m/s and 3.9 m/s and the angles of inclination of 18° and 14° gives:

$$1.45 \approx 1.27 \tag{5.5}$$

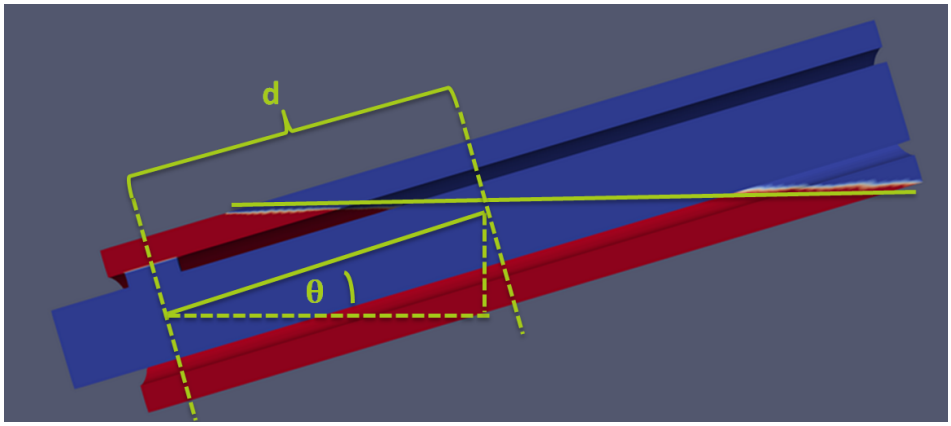

Figure 5.13: The measurement of the distance d. The hydrostatic pressure on the slot depends on this distance. This distance is measured from the midplane of slot up to the midpoint between the two points where the air-mud interface meets the outer borehole sloped circumference.

Therefore we can say that any improvement which increases the hydrostatic pressure will increase the rate of filling through the slot. However, this is difficult to achieve in practice since there may be other technical considerations for choosing a particular entry angle which have to do with the practice of horizontal directional drilling.

6

Conclusions and Recommendations

6.1. Conclusions

The final stage of horizontal directional drilling of pipe pullback presents several challenges, one of which being buoyancy caused by the drilling mud inside the borehole. This causes the pipe being pulled inside the borehole to brush against the upper side of the wall. Methods to minimize this occurrence include creating slots in the walls of the HDPE pipe at the front end just behind the pull-head. These slots aim to allow inside the pipe the drilling mud so that apart from serving as a lubricant it serves to ballast the pipe and bring it down away from the borehole wall. This study aims to investigate whether the current method of using these slots for 'passive ballasting' is working as well as it is intended to be.

The methodology used to examine how the drilling mud behaves during pullback involved using OpenFOAM, from which in turn we used the `interFoam` solver. This solver allows the study of multiphase flows, which in this case are the drilling mud and air using the Volume of Fluid Method. CFD simulations were carried out to observe how a given ideal drilling mud of typical rheological characteristics (drilling mud is modelled as a Herschel-Bulkley fluid) enters through the slot in the pipe wall. The first benchmark simulation incorporated all the attributes and parameters found in normal conditions. Subsequent simulations ran with one selected parameter changed from the normal case. This provided an opportunity to assess the effect of each individual parameter on maximising the throughput of drilling mud through the slot.

Among the parameters tested were the yield stress of the drilling fluid modelled as a Herschel-Bulkley; the density of the drilling mud; the angle of inclination of the borehole with respect to the horizontal; the slot length; using an elliptical aperture and the flow rate of drilling fluid from the pump. Other tests included substituting the drilling mud for a fictitious Newtonian fluid and also a case where the empty volume that is on the inside of the pipe is reduced.

The results show that increasing the slot length by 30% from the current embodiment of the pipe pullback process increases the flow rate through the slot by 10.45% based on the accumulated volume of drilling mud after 20s have elapsed. This improvement is better than increasing the flow rate of the mud pump by 30% which improves the flow rate by 5.89%.

As expected, a longer slot also displayed the characteristic of achieving a faster response rate of the drilling mud – air interface on the inside of the pipe catching up with the interface in the annulus region. This is indicative of better buoyancy diminishing characteristics.

The following insights can be taken regarding practical issues for ensuring the appropriate execution of passive ballasting:

1. With the current method of using four 38cm long slots for an 80cm diameter HDPE pipe arranged at 90° from each other along the length of the initial portion of the pipe is sufficient as a measure to ensure that there is not a mismatch in mud levels between the inside and the outside of the pipe.

2. While the use of higher density drilling mud does aid in reducing the filling time, it may present further buoyancy issues with the HDPE pipe.

3. The use of a longer slot can be adopted as a precautionary measure to ensure that indeed as much mud flow into the pipe as possible but there may be integrity issues with regards to the tensile strength of the pipe.

4. The indication is that drilling fluid with a lower yield stress does flow easier through the slot. For this lower yield stress to be achieved no reaming action during pullback is permitted so that the drilling mud is not mixed with the ground cuttings and the yield stress has to be less than at least 10Pa.

6.2. Recommendations for Future Work

Here are some further recommendations for more aspects which can be investigated based on the current results.

- Since a Newtonian fluid with less dynamic viscosity passed through the slot quicker the equivalent effect of lower consistency index in a drilling mud should be investigated. Further research into the lowest attainable consistency index in a drilling mud should be conducted.
- The effect of a higher column height should be investigated further.
- The influence of the slot's angular position around the axis of the pulled-in pipe.
- An investigation into what happens during the stage when the pulled-in pipe reaches the horizontal part of the borehole.
- An assessment of the influence of thixotropy and the aging of drilling fluid.
- The possibility of an effect of the inclination of the slot aperture as opposed to being perpendicular to the pipe axis.
- The effect of the pipe-to-borehole diameter ratio.

Appendix A - Benchmark Case Files

These are the files used to set up the simulation for the benchmark case from the main simulation campaign. Shown below is a schematic of the folder structure used. This is typical for all OpenFOAM simulations.

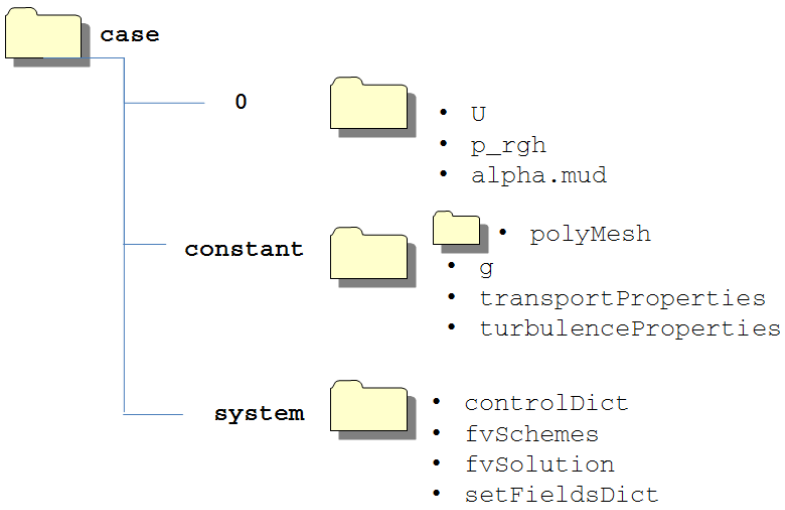

Figure A.1: The folder structure for the simulation cases in OpenFOAM. The polyMesh folder contains the mesh converted from Gmsh.

A.1. 0 folder

A.1.1. U file

```
/*---------------------------------*- C++ -*----------------------------------*\
| =========                 |                                                 |
| \\      /  F ield         | OpenFOAM: The Open Source CFD Toolbox           |
|  \\    /   O peration     | Version:  dev                                   |
|   \\  /    A nd           | Web:      www.OpenFOAM.org                      |
|    \\/     M anipulation  |                                                 |
\*---------------------------------------------------------------------------*/
FoamFile
{
    version     2.0;
    format      ascii;
    class       volVectorField;
    location    "0";
    object      U;
```

```
}
// * * * * * * * * * * * * * * * * * * * * * * * * * * * * * * * * * * * * * //

dimensions      [0 1 -1 0 0 0 0];

internalField   uniform (0 0 0);

boundaryField
{

    boreholeWall
    {
        type            movingWallVelocity;// moving borehole wall
        value           uniform (0 0 0.15);
    }

    outsidePipeWall
    {
        type            noSlip;
    }

    slotWall
    {
        type            noSlip;
    }

    insidePipeWall
    {
        type            noSlip;
    }

   bucketWall
    {
        type            noSlip;
    }

    inlet
    {
        type            fixedValue;
        value           uniform (0 0 0.071656051); // this is 45 litres per second
    }

    outlet
    {
        type            pressureInletOutletVelocity;
        value           uniform (0 0 0);
    }

    symmetry
    {
       type             symmetryPlane;
    }
}

// ************************************************************************* //
```

A.1.2. p_rgh file

```
/*--------------------------------*- C++ -*----------------------------------*\
| =========                 |                                                 |
| \\      /  F ield         | OpenFOAM: The Open Source CFD Toolbox           |
|  \\    /   O peration     | Version:  dev                                   |
|   \\  /    A nd           | Web:      www.OpenFOAM.org                      |
|    \\/     M anipulation  |                                                 |
\*---------------------------------------------------------------------------*/
FoamFile
{
    version     2.0;
    format      ascii;
    class       volScalarField;
    object      p_rgh;
}
// * * * * * * * * * * * * * * * * * * * * * * * * * * * * * * * * * * * * * //

dimensions      [1 -1 -2 0 0 0 0];

internalField   uniform 0;

boundaryField
{
    insidePipeWall
    {
        type            fixedFluxPressure;
        value           $internalField;
    }
     outsidePipeWall
    {
        type            fixedFluxPressure;
        value           $internalField;
    }
     slotWall
    {
        type            fixedFluxPressure;
        value           $internalField;
    }
     boreholeWall
    {
        type            fixedFluxPressure;
        value           $internalField;
    }
    bucketWall
    {
        type            fixedFluxPressure;
        value           $internalField;
    }
     outlet
     {
        type            totalPressure;
        p0              uniform 0;
    }
    inlet
```

```
    {
        type            fixedFluxPressure;
        value           $internalField;
    }
    symmetry
    {
        type      symmetryPlane;
    }

}

// ************************************************************************* //
```

A.1.3. alpha.mud file

```
/*--------------------------------*- C++ -*----------------------------------*\
| =========                 |                                                 |
| \\      /  F ield         | OpenFOAM: The Open Source CFD Toolbox           |
|  \\    /   O peration     | Version:  5.x                                   |
|   \\  /    A nd           | Web:      www.OpenFOAM.org                      |
|    \\/     M anipulation  |                                                 |
\*---------------------------------------------------------------------------*/
/*   Windows 32 and 64 bit porting by blueCAPE: http://www.bluecape.com.pt    *\
|  Based on Windows porting (2.0.x v4) by Symscape: http://www.symscape.com    |
\*---------------------------------------------------------------------------*/
FoamFile
{
    version     2.0;
    format      binary;
    class       volScalarField;
    location    "0";
    object      alpha.mud;
}
// * * * * * * * * * * * * * * * * * * * * * * * * * * * * * * * * * * * * * //

dimensions      [0 0 0 0 0 0 0];

internalField   uniform 0;

boundaryField
{
    outlet
    {
        type            inletOutlet;
        inletValue      uniform 0;
        value           uniform 0;
    }
    symmetry
    {
        type            symmetryPlane;
    }
    outsidePipeWall
    {
        type            zeroGradient;
    }
    insidePipeWall
    {
```

```
        type            zeroGradient;
    }
    slotWall
    {
        type            zeroGradient;
    }
    bucketWall
    {
        type            zeroGradient;
    }
    boreholeWall
    {
        type            zeroGradient;
    }
    inlet
    {
        type            fixedValue;
        value           uniform 1;
    }
}

// ************************************************************************* //
```

A.2. constant folder

A.2.1. g file

```
/*--------------------------------*- C++ -*----------------------------------*\
| =========                 |                                                 |
| \\      /  F ield         | OpenFOAM: The Open Source CFD Toolbox           |
|  \\    /   O peration     | Version:  4.1                                   |
|   \\  /    A nd           | Web:      www.OpenFOAM.org                      |
|    \\/     M anipulation  |                                                 |
\*---------------------------------------------------------------------------*/
FoamFile
{
    version     2.0;
    format      ascii;
    class       uniformDimensionedVectorField;
    location    "constant";
    object      g;
}
// * * * * * * * * * * * * * * * * * * * * * * * * * * * * * * * * * * * * * * * * //

dimensions      [0 1 -2 0 0 0 0];
value           (-9.517 0 -2.379);

// ************************************************************************* //
```

A.2.2. transportProperties file

```
/*--------------------------------*- C++ -*----------------------------------*\
| =========                 |                                                 |
| \\      /  F ield         | OpenFOAM: The Open Source CFD Toolbox           |
|  \\    /   O peration     | Version:  4.1                                   |
|   \\  /    A nd           | Web:      www.OpenFOAM.org                      |
|    \\/     M anipulation  |                                                 |
\*---------------------------------------------------------------------------*/
```

```
FoamFile
{
    version     2.0;
    format      ascii;
    class       dictionary;
    location    "constant";
    object      transportProperties;
}
// * * * * * * * * * * * * * * * * * * * * * * * * * * * * * * * * * * * * * * * * * * * * * * * * * * * * * * * * //

phases (mud air);
//Yield Stress  10
//K viscosity   0.15
//exponent      0.7
//Density       1100
// nu0 = 10 x tau0

mud
{
    transportModel  HerschelBulkley;
    rho             [1 -3 0 0 0 0 0] 1100;
    HerschelBulkleyCoeffs
    {
    nu0       [ 0 2 -1 0 0 0 0 ] 0.00909090909;
    tau0      [ 0 2 -2 0 0 0 0 ]  0.00909090909;
    k         [ 0 2  -1 0 0 0 0 ]  1.36363636e-4;
    n         [ 0 0 0 0 0 0 0 ] 0.7;
}

}

air
{
    transportModel  Newtonian;
    nu              [0 2 -1 0 0 0 0] 1.511e-05;
    rho             [1 -3 0 0 0 0 0] 1.2047;
}

sigma           [1 0 -2 0 0 0 0] 0;

// ************************************************************************* //
```

A.2.3. turbulenceProperties file

```
/*--------------------------------*- C++ -*----------------------------------*\
| =========                 |                                                 |
| \\      /  F ield         | OpenFOAM: The Open Source CFD Toolbox           |
|  \\    /   O peration     | Version:  4.1                                   |
|   \\  /    A nd           | Web:      www.OpenFOAM.org                      |
|    \\/     M anipulation  |                                                 |
\*---------------------------------------------------------------------------*/
FoamFile
{
    version     2.0;
    format      ascii;
    class       dictionary;
    location    "constant";
```

```
    object      turbulenceProperties;
}
// * * * * * * * * * * * * * * * * * * * * * * * * * * * * * * * * * * * * * * * * * * * * //

simulationType  laminar;

// ************************************************************************* //
```

A.3. system folder

A.3.1. controlDict file

```
/*--------------------------------*- C++ -*----------------------------------*\
| =========                 |                                                 |
| \\      /  F ield         | OpenFOAM: The Open Source CFD Toolbox           |
|  \\    /   O peration     | Version:  4.1                                   |
|   \\  /    A nd           | Web:      www.OpenFOAM.org                      |
|    \\/     M anipulation  |                                                 |
\*---------------------------------------------------------------------------*/
FoamFile
{
    version     2.0;
    format      ascii;
    class       dictionary;
    location    "system";
    object      controlDict;
}
// * * * * * * * * * * * * * * * * * * * * * * * * * * * * * * * * * * * * * * * * * * * * //

application     interFoam;

startFrom       startTime;

startTime       0;

stopAt          endTime;

endTime         0.1;

deltaT          0.0001;

writeControl    adjustableRunTime;

writeInterval   0.05;

purgeWrite      0;

writeFormat     binary;

writePrecision  6;

writeCompression uncompressed;

timeFormat      general;

timePrecision   6;
```

```
runTimeModifiable yes;

adjustTimeStep  on;

maxCo           0.07;
maxAlphaCo      0.07;

maxDeltaT       1;

// ************************************************************************* //
```

A.3.2. fvSchemes file

```
/*--------------------------------*- C++ -*----------------------------------*\
| =========                 |                                                 |
| \\      /  F ield         | OpenFOAM: The Open Source CFD Toolbox           |
|  \\    /   O peration     | Version:  4.1                                   |
|   \\  /    A nd           | Web:      www.OpenFOAM.org                      |
|    \\/     M anipulation  |                                                 |
\*---------------------------------------------------------------------------*/
FoamFile
{
    version     2.0;
    format      ascii;
    class       dictionary;
    location    "system";
    object      fvSchemes;
}
// * * * * * * * * * * * * * * * * * * * * * * * * * * * * * * * * * * * * * //

ddtSchemes
{
    default         Euler;
}

gradSchemes
{
    default         Gauss linear;
}

divSchemes
{
    div(rhoPhi,U)   Gauss linearUpwind grad(U);
    div(phi,alpha)  Gauss vanLeer;
    div(phirb,alpha) Gauss linear;
    div(phi,k)      Gauss upwind;
    div(phi,epsilon) Gauss upwind;
    div(((rho*nuEff)*dev2(T(grad(U))))) Gauss linear;
}

laplacianSchemes
{
    default         Gauss linear corrected;
}

interpolationSchemes
{
```

```
    default         linear;
}

snGradSchemes
{
    default         corrected;
}

// ************************************************************************* //
```

A.3.3. fvSolution file

```
/*---------------------------------*- C++ -*----------------------------------*\
| =========                 |                                                 |
| \\      /  F ield         | OpenFOAM: The Open Source CFD Toolbox           |
|  \\    /   O peration     | Version:  4.1                                   |
|   \\  /    A nd           | Web:      www.OpenFOAM.org                      |
|    \\/     M anipulation  |                                                 |
\*---------------------------------------------------------------------------*/
FoamFile
{
    version     2.0;
    format      ascii;
    class       dictionary;
    location    "system";
    object      fvSolution;
}
// * * * * * * * * * * * * * * * * * * * * * * * * * * * * * * * * * * * * * //

solvers
{
    "alpha.mud.*"
    {
        nAlphaCorr      2;
        nAlphaSubCycles 1;
        cAlpha          1;

        MULESCorr       yes;
        nLimiterIter    3;

        solver          smoothSolver;
        smoother        symGaussSeidel;
        tolerance       1e-8;
        relTol          0;
    }

    pcorr
    {
        solver          PCG;
        preconditioner  DIC;
        tolerance       1e-5;
        relTol          0;
    }
    pcorrFinal
    {
        $pcorr;
        tolerance       0.1;
```

```
        relTol          0;
    }
    p_rgh
    {
        solver          PCG;
        preconditioner  DIC;
        tolerance       1e-07;
        relTol          0.05;
    }

    p_rghFinal
    {
        $p_rgh;
        relTol          0;
    }

    "(U|k|epsilon).*"
    {
        solver          smoothSolver;
        smoother        symGaussSeidel;
        tolerance       1e-06;
        relTol          0;
        minIter         1;
    }
}

PIMPLE
{
    momentumPredictor    no;
    nOuterCcorrectors    1;
    nCorrectors          3;
    nNonOrthogonalCorrectors 0;
    pRefCell 0;
    pRefValue 0;
}

relaxationFactors
{
    equations
    {
        ".*"                1;
    }
}

// ************************************************************************* //
```

A.3.4. setFieldsDict file

```
/*--------------------------------*- C++ -*----------------------------------*\
| =========                 |                                                 |
| \\      /  F ield         | OpenFOAM: The Open Source CFD Toolbox           |
|  \\    /   O peration     | Version:  4.1                                   |
|   \\  /    A nd           | Web:      www.OpenFOAM.org                      |
|    \\/     M anipulation  |                                                 |
\*---------------------------------------------------------------------------*/
FoamFile
{
```

```
    version     2.0;
    format      ascii;
    class       dictionary;
    location    "system";
    object      setFieldsDict;
}
// * * * * * * * * * * * * * * * * * * * * * * * * * * * * * * * * * * * * * * * * * * * * * * * * * * * * * * * * //

defaultFieldValues
(
    volScalarFieldValue alpha.mud 0
);

regions
(
        rotatedBoxToCell
    {
       origin   (-0.6 0 5.41);
       i        (2.5 0 -10);
       j        (0 -10 0);
       k        (0 0 -10);
       fieldValues
       (
           volScalarFieldValue alpha.mud 1
       );
    }

            cylinderToCell
    {
       p1       (0 0 -10); // start point on cylinder axis
       p2       (0 0 10);   // end point on cylinder axis
       radius   0.4;
       fieldValues
       (
           volScalarFieldValue alpha.mud 0
       );
    }
);

// ************************************************************************* //
```

B

Appendix B - Marsh Funnel Case Files

These are the files used to run a typical case from the Marsh Funnel simulations used for the validation process.

B.1. 0 folder

B.1.1. U file

```
/*--------------------------------*- C++ -*----------------------------------*\
| =========                 |                                                 |
| \\      /  F ield         | OpenFOAM: The Open Source CFD Toolbox           |
|  \\    /   O peration     | Version:  dev                                   |
|   \\  /    A nd           | Web:      www.OpenFOAM.org                      |
|    \\/     M anipulation  |                                                 |
\*---------------------------------------------------------------------------*/
FoamFile
{
    version     2.0;
    format      ascii;
    class       volVectorField;
    location    "0";
    object      U;
}
// * * * * * * * * * * * * * * * * * * * * * * * * * * * * * * * * * * * * * //

dimensions      [0 1 -1 0 0 0 0];

internalField   uniform (0 0 0);

boundaryField
{
    walls
    {
        type            noSlip;
    }
    atmos
    {
        type            pressureInletOutletVelocity;
        value           uniform (0 0 0);
    }
    wedge0
```

```
    {
        type            wedge;
    }
    outlet
    {
        type            pressureInletOutletVelocity;
        value           uniform (0 0 0);
    }
    wedge1
    {
       type             wedge;

     }
}

// ************************************************************************* //
```

B.1.2. p_rgh file

```
/*--------------------------------*- C++ -*----------------------------------*\
| =========                 |                                                 |
| \\      /  F ield         | OpenFOAM: The Open Source CFD Toolbox           |
|  \\    /   O peration     | Version:  dev                                   |
|   \\  /    A nd           | Web:      www.OpenFOAM.org                      |
|    \\/     M anipulation  |                                                 |
\*---------------------------------------------------------------------------*/
FoamFile
{
    version     2.0;
    format      ascii;
    class       volScalarField;
    object      p_rgh;
}
// * * * * * * * * * * * * * * * * * * * * * * * * * * * * * * * * * * * * * //

dimensions      [1 -1 -2 0 0 0 0];

internalField   uniform 0;

boundaryField
{
    walls
    {
        type            fixedFluxPressure;
        value           uniform 0;
    }
   outlet
      {
        type            totalPressure;
        p0              uniform 0;
    }
    atmos
    {
        type            totalPressure;
        p0              uniform 0;
    }
    wedge1
```

```
    {
        type            wedge;
    }
    wedge0
    {
        type            wedge;
    }

}

// ************************************************************************* //
```

B.1.3. alpha.mud file

```
/*--------------------------------*- C++ -*----------------------------------*\
| =========                 |                                                 |
| \\      /  F ield         | OpenFOAM: The Open Source CFD Toolbox           |
|  \\    /   O peration     | Version:  dev                                   |
|   \\  /    A nd           | Web:      www.OpenFOAM.org                      |
|    \\/     M anipulation  |                                                 |
\*---------------------------------------------------------------------------*/
FoamFile
{
    version     2.0;
    format      ascii;
    class       volScalarField;
    object      alpha.mud;
}
// * * * * * * * * * * * * * * * * * * * * * * * * * * * * * * * * * * * * * //

dimensions      [0 0 0 0 0 0 0];

internalField   uniform 0;

boundaryField
{
    walls
    {
        type            zeroGradient;
    }
    atmos
    {
        type            inletOutlet;
        inletValue      uniform 0;
        value           uniform 0;
    }
    wedge1
    {
        type            wedge;
    }
    outlet
     {
        type            zeroGradient;

    }
    wedge0
    {
```

```
        type            wedge;
    }

}

// ************************************************************************* //
```

B.2. constant folder

B.2.1. g file

```
/*--------------------------------*- C++ -*----------------------------------*\
| =========                 |                                                 |
| \\      /  F ield         | OpenFOAM: The Open Source CFD Toolbox           |
|  \\    /   O peration     | Version:  4.1                                   |
|   \\  /    A nd           | Web:      www.OpenFOAM.org                      |
|    \\/     M anipulation  |                                                 |
\*---------------------------------------------------------------------------*/
FoamFile
{
    version     2.0;
    format      ascii;
    class       uniformDimensionedVectorField;
    location    "constant";
    object      g;
}
// * * * * * * * * * * * * * * * * * * * * * * * * * * * * * * * * * * * * * //

dimensions      [0 1 -2 0 0 0 0];
value           (0 -9.81 0);


// ************************************************************************* //
```

B.2.2. transportProperties file

```
/*--------------------------------*- C++ -*----------------------------------*\
| =========                 |                                                 |
| \\      /  F ield         | OpenFOAM: The Open Source CFD Toolbox           |
|  \\    /   O peration     | Version:  4.1                                   |
|   \\  /    A nd           | Web:      www.OpenFOAM.org                      |
|    \\/     M anipulation  |                                                 |
\*---------------------------------------------------------------------------*/
FoamFile
{
    version     2.0;
    format      ascii;
    class       dictionary;
    location    "constant";
    object      transportProperties;
}
// * * * * * * * * * * * * * * * * * * * * * * * * * * * * * * * * * * * * * //

phases (mud air);

mud
{
    transportModel  HerschelBulkley;
```

```
    rho             [1 -3 0 0 0 0 0] 1873;
    HerschelBulkleyCoeffs
    {
    nu0       [ 0 2 -1 0 0 0 0 ] 5.766150561e-3 ;   // 1 x tau0
    tau0      [ 0 2 -2 0 0 0 0 ] 5.766150561e-3;    // 10.8/1873 = 5.766150561e-3
    k         [ 0 2  -1 0 0 0 0 ] 2.61623865e-3 ; //4.9/1873 = 2.61623865e-3
    n         [ 0 0 0 0 0 0 0 ] 0.455;

}

}

air
{
    transportModel  Newtonian;
    nu              [0 2 -1 0 0 0 0] 1.48e-05;
    rho             [1 -3 0 0 0 0 0] 1;
}

sigma           [1 0 -2 0 0 0 0] 0;


// ************************************************************************* //
```

B.2.3. turbulenceProperties file

```
/*--------------------------------*- C++ -*----------------------------------*\
| =========                 |                                                 |
| \\      /  F ield         | OpenFOAM: The Open Source CFD Toolbox           |
|  \\    /   O peration     | Version:  4.1                                   |
|   \\  /    A nd           | Web:      www.OpenFOAM.org                      |
|    \\/     M anipulation  |                                                 |
\*---------------------------------------------------------------------------*/
FoamFile
{
    version     2.0;
    format      ascii;
    class       dictionary;
    location    "constant";
    object      turbulenceProperties;
}
// * * * * * * * * * * * * * * * * * * * * * * * * * * * * * * * * * * * * * //

simulationType  laminar;


// ************************************************************************* //
```

B.3. system folder

B.3.1. controlDict file

```
/*--------------------------------*- C++ -*----------------------------------*\
| =========                 |                                                 |
| \\      /  F ield         | OpenFOAM: The Open Source CFD Toolbox           |
|  \\    /   O peration     | Version:  4.1                                   |
|   \\  /    A nd           | Web:      www.OpenFOAM.org                      |
```

```
|    \\/     M anipulation  |                                                        |
\*---------------------------------------------------------------------------------*/
FoamFile
{
    version     2.0;
    format      ascii;
    class       dictionary;
    location    "system";
    object      controlDict;
}
// * * * * * * * * * * * * * * * * * * * * * * * * * * * * * * * * * * * * * * * * //

application     interFoam;

startFrom       startTime;

startTime       0;

stopAt          endTime;

endTime         30;

deltaT          0.001;

writeControl    adjustableRunTime;

writeInterval   0.05;

purgeWrite      0;

writeFormat     binary;

writePrecision  6;

writeCompression uncompressed;

timeFormat      general;

timePrecision   6;

runTimeModifiable yes;

adjustTimeStep  on;

maxCo           0.1;
maxAlphaCo      0.1;

maxDeltaT       1;

functions
{
   #includeFunc flowRatePatch
}


// ************************************************************************* //
```

B.3.2. fvSchemes file

```
/*--------------------------------*- C++ -*----------------------------------*\
| =========                 |                                                 |
| \\      /  F ield         | OpenFOAM: The Open Source CFD Toolbox           |
|  \\    /   O peration     | Version:  4.1                                   |
|   \\  /    A nd           | Web:      www.OpenFOAM.org                      |
|    \\/     M anipulation  |                                                 |
\*---------------------------------------------------------------------------*/
FoamFile
{
    version     2.0;
    format      ascii;
    class       dictionary;
    location    "system";
    object      fvSchemes;
}
// * * * * * * * * * * * * * * * * * * * * * * * * * * * * * * * * * * * * * //

ddtSchemes
{
    default         Euler;
}

gradSchemes
{

default cellMDLimited Gauss linear 0.5;
grad(U) cellMDLimited Gauss linear 0.5;

}

divSchemes
{
    div(rhoPhi,U)   Gauss linearUpwind grad(U);
    div(phi,alpha)  Gauss vanLeer;
    div(phirb,alpha) Gauss linear;
    div(phi,k)      Gauss upwind;
    div(phi,epsilon) Gauss upwind;
    div(((rho*nuEff)*dev2(T(grad(U))))) Gauss linear;
}

laplacianSchemes
{
    default         Gauss linear limited 1.0;
}

interpolationSchemes
{
    default         linear;
}

snGradSchemes
{
    default         limited 1.0;
}
```

```
// ************************************************************************* //
```

B.3.3. fvSolution file

```
/*---------------------------------*- C++ -*----------------------------------*\
| =========                 |                                                 |
| \\      /  F ield         | OpenFOAM: The Open Source CFD Toolbox           |
|  \\    /   O peration     | Version:  4.1                                   |
|   \\  /    A nd           | Web:      www.OpenFOAM.org                      |
|    \\/     M anipulation  |                                                 |
\*---------------------------------------------------------------------------*/
FoamFile
{
    version     2.0;
    format      ascii;
    class       dictionary;
    location    "system";
    object      fvSolution;
}
// * * * * * * * * * * * * * * * * * * * * * * * * * * * * * * * * * * * * * //

solvers
{
    "alpha.mud.*"
    {
        nAlphaCorr      2;
        nAlphaSubCycles 1;
        cAlpha          1;

        MULESCorr       yes;
        nLimiterIter    3;

        solver          smoothSolver;
        smoother        symGaussSeidel;
        tolerance       1e-8;
        relTol          0;
    }

    pcorr
    {
        solver          PCG;
        preconditioner  DIC;
        tolerance       1e-5;
        relTol          0;
    }
    pcorrFinal
    {
        $pcorr;
        tolerance       0.1;
        relTol          0;
    }
    p_rgh
    {
        solver          PCG;
        preconditioner  DIC;
        tolerance       1e-07;
```

```
        relTol          0.05;
    }

    p_rghFinal
    {
        $p_rgh;
        relTol          0;
    }

    "(U|k|epsilon).*"
    {
        solver          smoothSolver;
        smoother        symGaussSeidel;
        tolerance       1e-06;
        relTol          0;
        minIter         1;
    }
}

PIMPLE
{
    momentumPredictor    no;
    nOuterCorrectors     1;
    nCorrectors          3;
    nNonOrthogonalCorrectors 0;
    pRefCell 0;
    pRefValue 0;
}

relaxationFactors
{
    equations
    {
        ".*"                1;
    }
}

// ************************************************************************* //
```

B.3.4. setFieldsDict file

```
/*--------------------------------*- C++ -*----------------------------------*\
| =========                 |                                                 |
| \\      /  F ield         | OpenFOAM: The Open Source CFD Toolbox           |
|  \\    /   O peration     | Version:  4.1                                   |
|   \\  /    A nd           | Web:      www.OpenFOAM.org                      |
|    \\/     M anipulation  |                                                 |
\*---------------------------------------------------------------------------*/
FoamFile
{
    version     2.0;
    format      ascii;
    class       dictionary;
    location    "system";
    object      setFieldsDict;
}
// * * * * * * * * * * * * * * * * * * * * * * * * * * * * * * * * * * * * * //
```

```
defaultFieldValues
(
    volScalarFieldValue alpha.mud 0
);

regions
(
    regionToCell
    {
        set interior;
        insidePoint ((0.001 0.001 0));
        fieldValues
        (
            volScalarFieldValue alpha.mud 1
        );
    }
);


// ************************************************************************* //
```

C

Appendix C - Slump Test Case Files

This appendix shows the files used for running the simulations related to the slump test validation case.

C.1. 0 folder

C.1.1. U file

```
/*--------------------------------*- C++ -*----------------------------------*\
| =========                 |                                                 |
| \\      /  F ield         | OpenFOAM: The Open Source CFD Toolbox           |
|  \\    /   O peration     | Version:  dev                                   |
|   \\  /    A nd           | Web:      www.OpenFOAM.org                      |
|    \\/     M anipulation  |                                                 |
\*---------------------------------------------------------------------------*/
FoamFile
{
    version     2.0;
    format      ascii;
    class       volVectorField;
    location    "0";
    object      U;
}
// * * * * * * * * * * * * * * * * * * * * * * * * * * * * * * * * * * * * //

dimensions      [0 1 -1 0 0 0 0];

internalField   uniform (0 0 0);

boundaryField
{
    side
    {
        type            noSlip;
    }
    top
    {
        type            pressureInletOutletVelocity;
        value           uniform (0 0 0);
    }
    wedge0
    {
        type            wedge;
```

```
    }
    bottom
    {
        type            noSlip;
    }
    wedge1
    {
       type             wedge;
    }

}

// ************************************************************************* //
```

C.1.2. p_rgh

```
/*--------------------------------*- C++ -*----------------------------------*\
| =========                 |                                                 |
| \\      /  F ield         | OpenFOAM: The Open Source CFD Toolbox           |
|  \\    /   O peration     | Version:  dev                                   |
|   \\  /    A nd           | Web:      www.OpenFOAM.org                      |
|    \\/     M anipulation  |                                                 |
\*---------------------------------------------------------------------------*/
FoamFile
{
    version     2.0;
    format      ascii;
    class       volScalarField;
    object      p_rgh;
}
// * * * * * * * * * * * * * * * * * * * * * * * * * * * * * * * * * * * * * //

dimensions      [1 -1 -2 0 0 0 0];

internalField   uniform 0;

boundaryField
{
    bottom
    {
        type            fixedFluxPressure;
        value           uniform 0;
    }
   side
    {
        type            fixedFluxPressure;
        value           uniform 0;
    }
    top
    {
        type            totalPressure;
        p0              uniform 0;
    }
    wedge1
    {
        type            wedge;
    }
```

```
    wedge0
    {
        type            wedge;
    }

}

// ************************************************************************* //
```

C.1.3. alpha.mud

```
/*--------------------------------*- C++ -*----------------------------------*\
| =========                 |                                                 |
| \\      /  F ield         | OpenFOAM: The Open Source CFD Toolbox           |
|  \\    /   O peration     | Version:  dev                                   |
|   \\  /    A nd           | Web:      www.OpenFOAM.org                      |
|    \\/     M anipulation  |                                                 |
\*---------------------------------------------------------------------------*/
FoamFile
{
    version     2.0;
    format      ascii;
    class       volScalarField;
    object      alpha.mud;
}
// * * * * * * * * * * * * * * * * * * * * * * * * * * * * * * * * * * * * * //

dimensions      [0 0 0 0 0 0 0];

internalField   uniform 0;

boundaryField
{
    side
    {
        type            zeroGradient;
    }
    top
    {
        type            inletOutlet;
        inletValue      uniform 0;
        value           uniform 0;
    }
    wedge1
    {
        type            wedge;
    }
    bottom
    {
        type            zeroGradient;
    }
    wedge0
    {
       type          wedge;
    }

}
```

```
// ************************************************************************* //
```

C.2. constant folder

C.2.1. g file

```
/*--------------------------------*- C++ -*----------------------------------*\
| =========                 |                                                 |
| \\      /  F ield         | OpenFOAM: The Open Source CFD Toolbox           |
|  \\    /   O peration     | Version:  4.1                                   |
|   \\  /    A nd           | Web:      www.OpenFOAM.org                      |
|    \\/     M anipulation  |                                                 |
\*---------------------------------------------------------------------------*/
FoamFile
{
    version     2.0;
    format      ascii;
    class       uniformDimensionedVectorField;
    location    "constant";
    object      g;
}
// * * * * * * * * * * * * * * * * * * * * * * * * * * * * * * * * * * * * * //

dimensions      [0 1 -2 0 0 0 0];
value           (0 -9.81 0);


// ************************************************************************* //
```

C.2.2. transportProperties file

```
/*--------------------------------*- C++ -*----------------------------------*\
| =========                 |                                                 |
| \\      /  F ield         | OpenFOAM: The Open Source CFD Toolbox           |
|  \\    /   O peration     | Version:  4.1                                   |
|   \\  /    A nd           | Web:      www.OpenFOAM.org                      |
|    \\/     M anipulation  |                                                 |
\*---------------------------------------------------------------------------*/
FoamFile
{
    version     2.0;
    format      ascii;
    class       dictionary;
    location    "constant";
    object      transportProperties;
}
// * * * * * * * * * * * * * * * * * * * * * * * * * * * * * * * * * * * * * //

phases (mud air);
// JAYASREE SNF-S1:0.2
// expected final diameter is 143mm



mud
{
    transportModel  HerschelBulkley;
```

```
    rho             [1 -3 0 0 0 0 0] 2394.885;
    HerschelBulkleyCoeffs
    {
    nu0       [ 0 2 -1 0 0 0 0 ] 0.0051317704;    //
    tau0      [ 0 2 -2 0 0 0 0 ] 0.0051317704; //
    k         [ 0 2  -1 0 0 0 0 ]  0.000278928 ;
    n         [ 0 0 0 0 0 0 0 ] 0.723;
}

}

air
{
    transportModel  Newtonian;
    nu              [0 2 -1 0 0 0 0] 1.48e-05;
    rho             [1 -3 0 0 0 0 0] 1;
}

sigma           [1 0 -2 0 0 0 0] 0;


// ************************************************************************* //
```

C.2.3. turbulenceProperties file

```
/*--------------------------------*- C++ -*----------------------------------*\
| =========                 |                                                 |
| \\      /  F ield         | OpenFOAM: The Open Source CFD Toolbox           |
|  \\    /   O peration     | Version:  4.1                                   |
|   \\  /    A nd           | Web:      www.OpenFOAM.org                      |
|    \\/     M anipulation  |                                                 |
\*---------------------------------------------------------------------------*/
FoamFile
{
    version     2.0;
    format      ascii;
    class       dictionary;
    location    "constant";
    object      turbulenceProperties;
}
// * * * * * * * * * * * * * * * * * * * * * * * * * * * * * * * * * * * * * //

simulationType  laminar;

// ************************************************************************* //
```

C.3. system folder

C.3.1. controlDict file

```
/*--------------------------------*- C++ -*----------------------------------*\
| =========                 |                                                 |
| \\      /  F ield         | OpenFOAM: The Open Source CFD Toolbox           |
|  \\    /   O peration     | Version:  4.1                                   |
|   \\  /    A nd           | Web:      www.OpenFOAM.org                      |
|    \\/     M anipulation  |                                                 |
\*---------------------------------------------------------------------------*/
FoamFile
```

```
{
    version     2.0;
    format      ascii;
    class       dictionary;
    location    "system";
    object      controlDict;
}
// * * * * * * * * * * * * * * * * * * * * * * * * * * * * * * * * * * * * * * * * * * * * //

application     interFoam;

startFrom       startTime;

startTime       2.1;

stopAt          endTime;

endTime         4;

deltaT          0.001;

writeControl    adjustableRunTime;

writeInterval   0.1;

purgeWrite      0;

writeFormat     binary;

writePrecision  6;

writeCompression uncompressed;

timeFormat      general;

timePrecision   6;

runTimeModifiable yes;

adjustTimeStep  on;

maxCo           0.03;
maxAlphaCo      0.03;

maxDeltaT       1;

// ************************************************************************* //
```

C.3.2. fvSchemes file

```
/*--------------------------------*- C++ -*----------------------------------*\
| =========                 |                                                 |
| \\      /  F ield         | OpenFOAM: The Open Source CFD Toolbox           |
|  \\    /   O peration     | Version:  4.1                                   |
|   \\  /    A nd           | Web:      www.OpenFOAM.org                      |
|    \\/     M anipulation  |                                                 |
\*---------------------------------------------------------------------------*/
```

```
FoamFile
{
    version     2.0;
    format      ascii;
    class       dictionary;
    location    "system";
    object      fvSchemes;
}
// * * * * * * * * * * * * * * * * * * * * * * * * * * * * * * * * * * * * * * * * * * * * * * * * * * * * //

ddtSchemes
{
    default          Euler;
}

gradSchemes
{
    default          Gauss linear;
}

divSchemes
{
    div(rhoPhi,U)    Gauss linearUpwind grad(U);
    div(phi,alpha)   Gauss vanLeer;
    div(phirb,alpha) Gauss linear;
    div(phi,k)       Gauss upwind;
    div(phi,epsilon) Gauss upwind;
    div(((rho*nuEff)*dev2(T(grad(U))))) Gauss linear;
}

laplacianSchemes
{
    default          Gauss linear corrected;
}

interpolationSchemes
{
    default          linear;
}

snGradSchemes
{
    default          corrected;
}


// ************************************************************************* //
```

C.3.3. fvSolution file

```
/*---------------------------------*- C++ -*----------------------------------*\
| =========                 |                                                 |
| \\      /  F ield         | OpenFOAM: The Open Source CFD Toolbox           |
|  \\    /   O peration     | Version:  4.1                                   |
|   \\  /    A nd           | Web:      www.OpenFOAM.org                      |
|    \\/     M anipulation  |                                                 |
\*---------------------------------------------------------------------------*/
```

```
FoamFile
{
    version     2.0;
    format      ascii;
    class       dictionary;
    location    "system";
    object      fvSolution;
}
// * * * * * * * * * * * * * * * * * * * * * * * * * * * * * * * * * * * * * * * * * * * * * * * * * //

solvers
{
    "alpha.mud.*"
    {
        nAlphaCorr      2;
        nAlphaSubCycles 1;
        cAlpha          1;

        MULESCorr       yes;
        nLimiterIter    3;

        solver          smoothSolver;
        smoother        symGaussSeidel;
        tolerance       1e-8;
        relTol          0;
    }

    pcorr
    {
        solver          PCG;
        preconditioner  DIC;
        tolerance       1e-5;
        relTol          0;
    }
    pcorrFinal
    {
        $pcorr;
        tolerance       0.1;
        relTol          0;
    }
    p_rgh
    {
        solver          PCG;
        preconditioner  DIC;
        tolerance       1e-07;
        relTol          0.05;
    }

    p_rghFinal
    {
        $p_rgh;
        relTol          0;
    }

    "(U|k|epsilon).*"
    {
```

```
        solver          smoothSolver;
        smoother        symGaussSeidel;
        tolerance       1e-06;
        relTol          0;
        minIter         1;
    }
}

PIMPLE
{
    momentumPredictor    no;
    nOuterCorrectors     1;
    nCorrectors          3;
    nNonOrthogonalCorrectors 0;
    pRefCell 0;
    pRefValue 0;
}

relaxationFactors
{
    equations
    {
        ".*"                1;
    }
}

// ************************************************************************* //
```

C.3.4. setFieldsDict file

```
/*--------------------------------*- C++ -*----------------------------------*\
| =========                 |                                                 |
| \\      /  F ield         | OpenFOAM: The Open Source CFD Toolbox           |
|  \\    /   O peration     | Version:  4.1                                   |
|   \\  /    A nd           | Web:      www.OpenFOAM.org                      |
|    \\/     M anipulation  |                                                 |
\*---------------------------------------------------------------------------*/
FoamFile
{
    version     2.0;
    format      ascii;
    class       dictionary;
    location    "system";
    object      setFieldsDict;
}
// * * * * * * * * * * * * * * * * * * * * * * * * * * * * * * * * * * * * * //

defaultFieldValues
(
    volScalarFieldValue alpha.mud 0
);

regions
(
    regionToCell
    {
        set interior;
```

```
        insidePoint ((0.01 0.01 0));
        fieldValues
        (
            volScalarFieldValue alpha.mud 1
        );
    }
);


// ************************************************************************* //
```

Bibliography

[1] Theoretical investigation of the primary breakup of high-viscosity liquids in twin-fluid nozzles. URL http://vbt.ebi.kit.edu/index.pl/en/Haupt_Menu_Institute_M03/themen/Theoretische_Untersuchung_Primaerzerfalls_hochviskoser_Fluide_Zweistoffduesen/index.html.

[2] Gmsh. URL http://gmsh.info/.

[3] *EN 445 Grout for prestressing tendons - Test methods*. European Committee for Standardization (CEN), 1996.

[4] *NEN 3650 (en): Requirements for Pipeline systems*. Netherlands Standardization Institute, 2007.

[5] *API 13 B Recommended Practice for Field Testing Water-based Drilling Fluids*. American Petroleum Institute (API), 2009.

[6] *Advanced Wellbore Hydraulics in Advanced Drilling Well Technology by Ahmed R. and Miska S.* Society of Petroleum Engineers, 2009.

[7] *BS EN 12350-2:2009Testing fresh concrete. Slump-test*. British Standards Institution, 2009.

[8] *ASTM C 143 Standard Test Method for Slump of Hydraulic-Cement Concrete*. American Society Testing Materials (ASTM), 2011.

[9] *Standard guide for use of maxi-horizontal directional drilling for placement of polyethylene pipe or conduit under obstacles, including river crossings*. American Society Testing Materials (ASTM), 2011.

[10] *DIN 4127 Earthworks and foundation engineering - Test methods for supporting fluids used in the construction of diaphragm walls and their constituent products*. German Institute of for Standardization (DIN), 2014.

[11] Openfoam v6 user guide: 7.3 transport/rheology models, Jul 2018. URL https://cfd.direct/openfoam/user-guide/v6-transport-rheology/.

[12] ANSYS. Viscosity for non-newtonian fluids, Jul 2017. URL https://www.sharcnet.ca/Software/Ansys/18.2.2/en-us/help/flu_ug/flu_ug_sec_viscosity_non_newtonian.html#g_flu_ug_fig_nn_hb.

[13] Hyeon-Shik Baik, Dulcy M. Abraham, and Sanjiv Gokhale. A decision support system for horizontal directional drilling. *Tunnelling and Underground Space Technology*, 18(1):99–109, 2003. doi: 10.1016/s0886-7798(03)00002-6.

[14] Matthew T. Balhoff, Larry W. Lake, Paul M. Bommer, Rebecca E. Lewis, Mark J. Weber, and Jennifer M. Calderin. Rheological and yield stress measurements of non-newtonian fluids using a marsh funnel. *Journal of Petroleum Science and Engineering*, 77(3-4):393–402, 2011. doi: 10.1016/j.petrol.2011.04.008.

[15] Michael E. Baumert and Erez N. Allouche. Methods for Estimating Pipe Pullback Loads for Horizontal Directional Drilling (hdd) crossings. *Journal of Infrastructure Systems*, 8(1):12–19, 2002. doi: 10.1061/(asce)1076-0342(2002)8:1(12).

[16] Michael E. Baumert, Erez N. Allouche, and Ian D. Moore. Drilling fluid considerations in design of engineered horizontal directional drilling installations. *International Journal of Geomechanics*, 5(4):339–349, 2005. doi: 10.1061/(asce)1532-3641(2005)5:4(339).

[17] Karim Bekkour, Macaire Leyama, Adel Benchabane, and Olivier Scrivener. Time-dependent rheological behavior of bentonite suspensions: An experimental study. *Journal of Rheology*, 49(6):1329–1345, 2005. doi: 10.1122/1.2079267.

[18] A. Benslimane, K. Bekkour, P. François, and H. Bechir. Laminar and turbulent pipe flow of bentonite suspensions. *Journal of Petroleum Science and Engineering*, 139:85–93, 2016. doi: 10.1016/j.petrol.2015.12.020.

[19] Adam T. Bourgoyne. *Applied drilling engineering*. Society of Petroleum Engineers, 1991.

[20] Adrien Bouvet, Elhem Ghorbel, and Rachid Bennacer. The mini-conical slump flow test: Analysis and numerical study. *Cement and Concrete Research*, 40(10):1517–1523, 2010. doi: 10.1016/j.cemconres.2010.06.005.

[21] Liangxue Cai, Guangli Xu, Maria Anna Polak, and Mark Knight. Horizontal directional drilling pulling forces prediction methods – a critical review. *Tunnelling and Underground Space Technology*, 69:85–93, 2017. doi: 10.1016/j.tust.2017.05.026.

[22] Elisabeth Cheng and Maria Anna Polak. Theoretical model for calculating pulling loads for pipes in horizontal directional drilling. *Tunnelling and Underground Space Technology*, 22(5-6):633–643, 2007. doi: 10.1016/j.tust.2007.05.009.

[23] R. P. Chhabra and J. F. Richardson. *Non-Newtonian flow and applied rheology: engineering applications*. Butterworth-Heinemann, 2011.

[24] P. Coussot. Yield stress fluid flows: A review of experimental data. *Journal of Non-Newtonian Fluid Mechanics*, 211:31–49, 2014. doi: 10.1016/j.jnnfm.2014.05.006.

[25] M. Cremonesi, L. Ferrara, A. Frangi, and U. Perego. Simulation of the flow of fresh cement suspensions by a lagrangian finite element approach. *Journal of Non-Newtonian Fluid Mechanics*, 165(23-24):1555–1563, 2010. doi: 10.1016/j.jnnfm.2010.08.003.

[26] Saad El-Din M. Desouky. A new laminar-turbulent-transition criterion for pseudoplastic fluids. *Journal of Petroleum Science and Engineering*, 5(3):285–291, 1991. doi: 10.1016/0920-4105(91)90044-n.

[27] Hua-Shu Dou, Boo Cheong Khoo, and Her Mann Tsai. Determining the critical condition for turbulent transition in a full-developed annulus flow. *Journal of Petroleum Science and Engineering*, 73(1-2):41–47, 2010. doi: 10.1016/j.petrol.2010.05.003.

[28] Oney Erge, Evren M. Ozbayoglu, Stefan Z. Miska, Mengjiao Yu, Nicholas Takach, Arild Saasen, and Roland May. Laminar to turbulent transition of yield power law fluids in annuli. *Journal of Petroleum Science and Engineering*, 128:128–139, 2015. doi: 10.1016/j.petrol.2015.02.007.

[29] M.p Escudier and F Presti. Pipe flow of a thixotropic liquid. *Journal of Non-Newtonian Fluid Mechanics*, 62(2-3):291–306, 1996. doi: 10.1016/0377-0257(96)01417-6.

[30] Ashkan Faghih, Yaolin Yi, Alireza Bayat, and Manley Osbak. Fluidic drag estimation in horizontal directional drilling based on flow equations. *Journal of Pipeline Systems Engineering and Practice*, 6(4):04015006, 2015. doi: 10.1061/(asce)ps.1949-1204.0000200.

[31] Liberato Ferrara, Massimiliano Cremonesi, Nathan Tregger, Attilio Frangi, and Surendra P. Shah. On the identification of rheological properties of cement suspensions: Rheometry, computational fluid dynamics modeling and field test measurements. *Cement and Concrete Research*, 42(8):1134–1146, 2012. doi: 10.1016/j.cemconres.2012.05.007.

[32] K. Founargiotakis, V. C. Kelessidis, and R. Maglione. Laminar, transitional and turbulent flow of herschel-bulkley fluids in concentric annulus. *The Canadian Journal of Chemical Engineering*, 86(4):676–683, 2008. doi: 10.1002/cjce.20074.

[33] I. A. Frigaard, S. D. Howison, and I. J. Sobey. On the stability of poiseuille flow of a bingham fluid. *Journal of Fluid Mechanics*, 263(-1):133, 1994. doi: 10.1017/s0022112094004052.

[34] Ian Frigaard and Cherif Nouar. On three-dimensional linear stability of poiseuille flow of bingham fluids. *Physics of Fluids*, 15(10):2843, 2003. doi: 10.1063/1.1602451.

[35] Vinay R. Gopala and Berend G.m. Van Wachem. Volume of fluid methods for immiscible-fluid and free-surface flows. *Chemical Engineering Journal*, 141(1-3):204–221, 2008. doi: 10.1016/j.cej.2007.12.035.

[36] I.h. Gucuyener and T. Mehmetoglu. Characterization of flow regime in concentric annuli and pipes for yield-pseudoplastic fluids. *Journal of Petroleum Science and Engineering*, 16(1-3):45–60, 1996. doi: 10.1016/0920-4105(96)00025-3.

[37] Chandan Guria, Rajesh Kumar, and Prakash Mishra. Rheological analysis of drilling fluid using marsh funnel. *Journal of Petroleum Science and Engineering*, 105:62–69, 2013. doi: 10.1016/j.petrol.2013.03.027.

[38] Richard W. Hanks. The laminar-turbulent transition for flow in pipes, concentric annuli, and parallel plates. *AIChE Journal*, 9(1):45–48, 1963. doi: 10.1002/aic.690090110.

[39] Y. Hashash and J. Javier. Evaluation of horizontal directional drilling (hdd), Nov 2011. URL `https://apps.ict.illinois.edu/projects/getfile.asp?id=3052`.

[40] Hemphill, Campos, and Pilehvari. Yield-power law model more accurately predicts mud rheology, Aug 1993. URL `https://www.osti.gov/biblio/5452894`.

[41] Winslow H. Herschel and Ronald Bulkley. Konsistenzmessungen von gummi-benzollösungen. *Kolloid-Zeitschrift*, 39(4):291–300, 1926. doi: 10.1007/bf01432034.

[42] C.w Hirt and B.d Nichols. Volume of fluid (vof) method for the dynamics of free boundaries. *Journal of Computational Physics*, 39(1):201–225, 1981. doi: 10.1016/0021-9991(81)90145-5.

[43] Huey, McLeod, and K.b. Installation loading and stress analysis involved with pipelines installed by horizontal directional drilling, Aug 1996. URL `https://www.osti.gov/biblio/263399-installation-loading-stress-analysis-involved-pipelines-installed\-horizontal-directional-drilling`.

[44] C. Jayasree and Ravindra Gettu. Experimental study of the flow behaviour of superplasticized cement paste. *Materials and Structures*, 41(9):1581–1593, 2008. doi: 10.1617/s11527-008-9350-5.

[45] Vassilios C. Kelessidis, Christina Tsamantaki, and Panayiotis Dalamarinis. Effect of ph and electrolyte on the rheology of aqueous wyoming bentonite dispersions. *Applied Clay Science*, 38(1-2):86–96, 2007. doi: 10.1016/j.clay.2007.01.011.

[46] Vassilios C. Kelessidis, Panagiotis Dalamarinis, and Roberto Maglione. Experimental study and predictions of pressure losses of fluids modeled as herschel–bulkley in concentric and eccentric annuli in laminar, transitional and turbulent flows. *Journal of Petroleum Science and Engineering*, 77(3-4):305–312, 2011. doi: 10.1016/j.petrol.2011.04.004.

[47] Chang Lin, Obada Kayali, Evgeny V. Morozov, and David J. Sharp. Development of self-compacting strain-hardening cementitious composites by varying fly ash content. *Construction and Building Materials*, 149:103–110, 2017. doi: 10.1016/j.conbuildmat.2017.05.051.

[48] S. Marquez Damian. Description and utilization of interfoam multiphase solver, Jul 2012. URL `http://infofich.unl.edu.ar/upload/3be0e16065026527477b4b948c4caa7523c8ea52.pdf`.

[49] Mohammad Najafi. *Trenchless Technology: Planning, Equipment, and Methods*. McGraw-Hill, 2013.

[50] V.h. Nguyen, S. Rémond, J.l. Gallias, J.p. Bigas, and P. Muller. Flow of herschel–bulkley fluids through the marsh cone. *Journal of Non-Newtonian Fluid Mechanics*, 139(1-2):128–134, 2006. doi: 10.1016/j.jnnfm.2006.07.009.

[51] C. Nouar. Numerical and experimental investigation of thermal convection for thermodependent herschel-bulkley fluid in an annular duct with rotating inner cylinder. *Progress and Trends in Rheology V*, page 297–298, 1998. doi: 10.1007/978-3-642-51062-5_138.

[52] C. Nouar and M. Lebouche. Thermal convection for a thermodependent herschel-bulkley fluid in an annular duct. *Heat and Mass Transfer*, pages 257–267, 1996. doi: 10.1007/978-3-642-51062-5_138.

[53] OpenCFD. Openfoam® documentation. URL `https://www.openfoam.com/documentation/`.

[54] J. T. Park, R. J. Mannheimer, T. A. Grimley, and T. B. Morrow. Pipe flow measurements of a transparent non-newtonian slurry. *Journal of Fluids Engineering*, 111(3):331, 1989. doi: 10.1115/1.3243648.

[55] S.V. Patankar and D.B. Spalding. A calculation procedure for heat, mass and momentum transfer in three-dimensional parabolic flows. *Numerical Prediction of Flow, Heat Transfer, Turbulence and Combustion*, page 54–73, 1983. doi: 10.1016/b978-0-08-030937-8.50013-1.

[56] Maria Anna Polak and Dennis Chu. Pulling loads for polyethylene pipes in horizontal directional drilling: Theoretical modeling and parametric study. *Journal of Infrastructure Systems*, 11(2):142–150, 2005. doi: 10.1061/(asce)1076-0342(2005)11:2(142).

[57] Maria Anna Polak and Afdal Lasheen. Mechanical modelling for pipes in horizontal directional drilling. *Tunnelling and Underground Space Technology*, 16:47–55, 2001. doi: 10.1016/s0886-7798(02)00020-2.

[58] Montazar Rabiei, Yaolin Yi, Alizera Bayat, Roger Cheng, and Manley Osbak. Estimation of Hydrokinetic Pressure and Fluidic Drag Changes during Pipe Installations via HDD based on identifying Slurry Flow Pattern change within a Borehole. *Journal of Pipeline System Engineering Practice*, 8(4).

[59] Montazar Rabiei, Yaolin Yi, Alireza Bayat, and Roger Cheng. General method for pullback force estimation for polyethylene pipes in horizontal directional drilling. *Journal of Pipeline Systems Engineering and Practice*, 7(3):04016004, 2016. doi: 10.1061/(asce)ps.1949-1204.0000230.

[60] Montazar Rabiei, Yaolin Yi, Alireza Bayat, Roger Cheng, and Manley Osbak. Fluidic drag estimation in horizontal directional drilling using finite volume method. *Journal of Pipeline Engineering*, 15(4): 04015006, 2016. doi: 10.1061/(asce)ps.1949-1204.0000200.

[61] Montazar Rabiei, Yaolin Yi, Alireza Bayat, Roger Cheng, and Manley Osbak. Estimation of hydrokinetic pressure and fluidic drag changes during pipe installations via hdd based on identifying slurry-flow pattern change within a borehole. *Journal of Pipeline Systems Engineering and Practice*, 8(4):04017020, 2017. doi: 10.1061/(asce)ps.1949-1204.0000285.

[62] F. Raees, van der Heul D.R., and C. Vuik. Evaluation of the interface-capturing algorithm of openfoam for the simulation of incompressible immiscible two-phase flow. *Reports of the Department of Applied Mathematical Analysis*, 2011.

[63] N. Roussel, C. Stefani, and R. Leroy. From mini-cone test to abrams cone test: measurement of cement-based materials yield stress using slump tests. *Cement and Concrete Research*, 35(5):817–822, 2005. doi: 10.1016/j.cemconres.2004.07.032.

[64] Nicolas Roussel and Robert Le Roy. The marsh cone: a test or a rheological apparatus? *Cement and Concrete Research*, 35(5):823–830, 2005. doi: 10.1016/j.cemconres.2004.08.019.

[65] N. W. Ryan and M. M. Johnson. Transistion from laminar to turbulent flow in pipes. *AIChE Journal*, 5(4): 433–435, 1959. doi: 10.1002/aic.690050407.

[66] Biao Shu, Baosong Ma, and Haitao Lan. Cuttings transport mechanism in a large-diameter hdd borehole. *Journal of Pipeline Systems Engineering and Practice*, 6(4):04014017, 2015. doi: 10.1061/(asce)ps.1949-1204.0000190.

[67] Paul Thomas. Slatter. *Transitional and turbulent flow of non-Newtonian slurries in pipes*. 1995.

[68] A.M. Talmon and M. Huisman. Fall velocity of particles in shear flow of drilling fluids. *Tunnelling and Underground Space Technology*, 20(2):193–201, 2005. doi: 10.1016/j.tust.2004.07.001.

[69] Pa Wedding and Dl Kantro. Influence of water-reducing admixtures on properties of cement paste—a miniature slump test. *Cement, Concrete and Aggregates*, 2(2):95, 1980. doi: 10.1520/cca10190j.

[70] Norman M. Wereley. Nondimensional analysis of electrorheological and magnetorheological dampers using a herschel-bulkley constitutive model. *Aerospace*, 2003. doi: 10.1115/imece2003-43310.

[71] C. J. Yang, W. D. Zhu, W. H. Zhang, X. H. Zhu, and G. X. Ren. Determination of pipe pullback loads in horizontal directional drilling using an advanced computational dynamic model. *Journal of Engineering Mechanics*, 140(8):04014060, 2014. doi: 10.1061/(asce)em.1943-7889.0000749.

[72] Huamin Zhou. *Computer modeling for injection molding: simulation, optimization, and control*. Wiley, 2013.